Experimental prospects for detecting the quantum nature of spacetime

by

Paulina Corona Ugalde

A thesis
presented to the University of Waterloo
in fulfillment of the
thesis requirement for the degree of
Doctor of Philosophy
in
Physics

Waterloo, Ontario, Canada, 2017

© Paulina Corona Ugalde 2017

Examining Committee Membership

The following members served on the examination committee for this thesis. The decision of the examination committee is by majority vote.

Supervisor	**Robert B. Mann** Professor, Department of Physics and Astronomy, University of Waterloo
External Examiner	**Juan León** Profesor, Instituto de Física Fundamental, Universidad Complutense de Madrid
Internal Member	**Adrian Lupascu** Associate Professor, Department of Physics and Astronomy, Institute for Quantum Computing, University of Waterloo
Internal-external Member	**Achim Kempf** Professor, Department of Applied Mathematics, University of Waterloo
Committee Member	**Roger Melko** Associate Professor, Department of Physics and Astronomy, University of Waterloo Associate Faculty, Perimeter Institute for Theoretical Physics

This thesis consists of material all of which I authored or co-authored: see Statement of Contributions included in the thesis. This is a true copy of the thesis, including any required final revisions, as accepted by my examiners.

I understand that my thesis may be made electronically available to the public.

Statement of contributions

Chapter 4 of this thesis consists of material from Reference [1], co-authored with Eduardo Martín-Martínez, Robert B. Mann and Christopher Wilson.

Chapters 5 and 6 consists of material from References [2, 3], co-authored with Natacha Altamirano, Robert B. Mann and Magdalena Zych.

Abstract

This thesis is concerned with advancing the confrontation between relativistic quantum information (RQI) and experiment. We investigate the lessons that some present-day experiments can teach us about the relationship between quantum information, relativistic motion and gravitation.

First, we look at the insights we can gain within the framework of quantum field theory in curved spacetimes. Particularly, we propose a generalization of the superconducting circuit simulation of the dynamical Casimir effect where we consider relativistically moving boundary conditions following different trajectories. We study the feasibility of extending the experimental setup to reproduce richer relativistic trajectories.

Next, motivated by recent efforts to describe the gravitational interaction as a classical channel arising from continuous quantum measurements, we study what types of dynamics can emerge from a collisional model of repeated interactions between a system and a set of ancillae. We use these results in the context of gravitational interactions and show how our general framework recovers the gravitational decoherence model of Kafri, Taylor and Milburn (KTM).

Finally, we argue that single-atom interference experiments achieving large spatial superpositions can rule out a particular realization of the KTM model where gravitational interactions act pairwise between massive particles as classical channels, approximating Newtonian pair-potential at low energies. Our findings counteract the present belief that gravity-inspired decoherence models cannot be confronted by experiment. Specifically, we find experimental indications which show that if gravity does reduce to pairwise Newtonian interactions between atoms in a non-relativistic limit, these interactions cannot be fundamentally classical.

Our work shows that state-of-the-art technology can be used as a tool to test the quantum character of spacetime and that further efforts should be spent in analyzing how current experimental setups can guide us towards building a complete theory of quantum gravity.

Acknowledgements

First and foremost I want to thank my supervisor Robert Mann for his support during the course of these years. I value the kindness that you showed me during this journey. Thank you for the time you spent guiding me through projects and patiently answering all of my questions, as well as giving me the time to explore all sort of additional interests.

I want to thank my committee members, Adrian Lupascu, Achim Kempf and Chris Wilson for their time spent listening to my presentations and providing useful feedback. I also want to thank my fellow group members and friends, who provided much fun between times of hard work, including Aida Ahmadzadegan, Natacha Altamirano, Wilson Brenna, Daniel Grimmer, Laura Henderson, Robie Hennigar, Marvellous Onuma-Kalu, Keith Ng, Allison Sachs, Alex Smith and many others. In the Physics & Astronomy department, I want to thank Judy McDonnell, you were truly a life saver in many occasions.

I am eternally indebted to my friends and mentors, Eduardo Martín Martínez and Magdalena Zych. This PhD would not have been possible without your help. Magdalena, you are an inspiration. Listening to your passion about life and physics made me want to keep exploring and learning. Eduardo, I cannot thank you enough for motivating me and encouraging me to always persevere (and for sharing your enthusiasm for science, for funny internet videos and for Spanish history and regional accents).

During my time in Canada I have had the fortune of meeting amazing people, who have become great friends, including Andrzej Banburski, Linqing Chen, Nayeli Rodriguez Briones, Todd Sierens and Nosiphiwo Zwane. I value your friendship immensely.

Special thanks to Judy and Alan Moore, for welcoming me into their house and teaching me so much about life. Thanks for becoming my family far away from home. I cherish in my heart the time I spent with you in Australia. To Lauren, discovering your friendship during the last years has been a true gift. To Ale, Mariana and Tefi, thank you for being friends that are more like family. Knowing that we can always count on each other is one of the best things in my life. To Pablo, for sharing life by my side, I am proud of the good man you have become. I am sure you will achieve everything that you set your eyes upon.

I am grateful to all my family, specially my grandparents. Being away from you has been tremendously hard, but every day I dedicate my work to you. I am forever thankful to my parents, to whom I dedicate this thesis. Mom and dad, everything that I have achieved has been possible thanks to your infinite love and hard work. Thank you for teaching me to always stand up for my beliefs, to be compassionate and to chase my dreams.

And finally, to Pedro, there are no words to thank you enough. Your unwavering love, support and understanding motivate me to become a better version of myself. Life is so much brighter by your side!

Dedication

To my mom and dad, who are always there for me.

Table of Contents

List of Tables

List of Figures

Chapter 1

Introduction

1.1 Motivation

Despite their respective individual success, the two pillars of modern physics, general relativity and quantum theory have not been yet made fully compatible. Each theory independently yields predictions that have been tested with high precision, but the question remains as to how to understand the two of them in the same framework, or how to formulate a quantum theory of gravity.

For example, one can think of quantum superpositions of macroscopic objects in different positions. Although in principle predicted by quantum theory, we have not yet fully realized them in experiments. Despite the fast paced progress in experimental control of large quantum systems, the state-of-the-art of such experiments is at the stage where only superpositions of a molecule exceeding a mass of $10,000$ amu that combines 810 atoms into one particle have been achieved [7].

On the other hand, general relativity, which has provided accurate predictions used in a breath of fields from cosmology and astronomy [8] to technology [9], has revealed itself insufficient to account for phenomena such as black hole radiation [10, 11] or the description of the very early stages of the Universe [12].

The work presented in this thesis attempts to make progress in a relatively new direction in the field of relativistic quantum information (RQI). RQI is an emerging and rapidly growing field that studies how to transmit and process information taking into account not only quantum but also relativistic aspects of physical systems. It also attempts to answer the question of how gravity affects quantum systems. We can think of RQI as the theory that lies at the intersection of Quantum Theory, General Relativity and Information

Theory. By studying the relationship between these fields, it can provide useful tools for understanding the nature of spacetime.

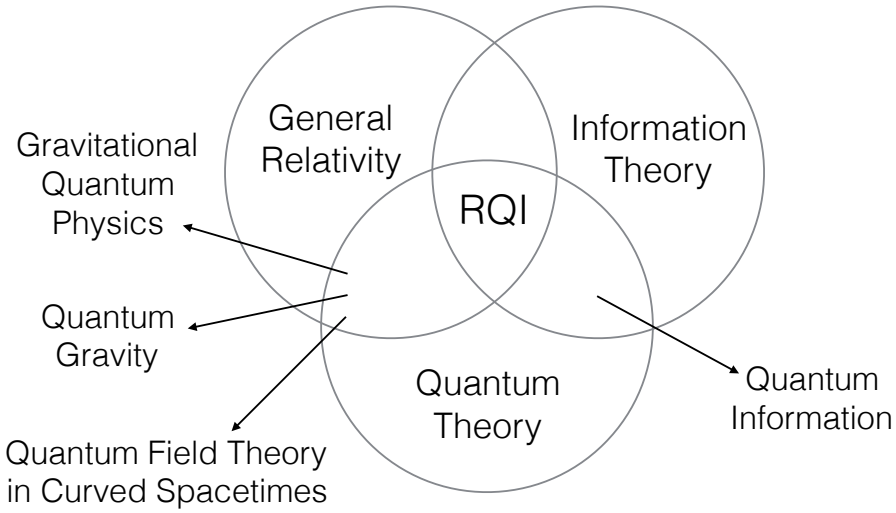

Figure 1.1: RQI lies at the intersection of General Relativity, Information Theory and Quantum Theory.

The figure above illustrates where the field of RQI lies. The study of quantum field theory (QFT) in curved spacetimes lies at the intersection of quantum theory and general relativity. Its focus is on understanding the quantization of fields in classical gravitational backgrounds. One of the problems encountered when trying to get a quantum gravity theory is the different footing of space and time in both theories. In quantum mechanics time is treated as a parameter whereas space is an observable, contrary to the equal footing they both receive in general relativity. Even though QFT in curved spacetimes is not a full quantum gravity theory, its formalism already incorporates quantum theory and general relativity and is enough to provide explanations to some effects that are not attainable with just general relativity [12]. For example, it predicts that what an inertial observer registers as the vacuum, a uniformly accelerated observer will measure a thermal bath of particles at a temperature proportional to its acceleration. This is the Unruh effect [13] and it arises as a consequence of the notion of particle not being universal, a concept that will be explained later in this thesis.

At this intersection also lies the field of gravitational quantum physics, where the focus of study is on trying to understand the effects of gravity on quantum systems. Some of the questions in this field pertain to how systems in quantum superposition gravitate and how gravity collapses quantum states [14, 15, 16, 17]. It also delves into trying to understand the notion of time [18, 19] and even proposes some models that treat gravity as fundamentally classical [14, 15, 20, 21, 22, 23, 24, 25, 26].

At the intersection of quantum mechanics and information theory, lies the field of quantum information. Its principal aim is to understand how to store, process and transmit information using quantum systems with the aim of developing new technologies and achieving tasks currently impossible with classical systems. For example, while a usual computer stores its information in bits, a quantum computer stores the information in quantum bits called qubits, which can be in a superposition of different states and can therefore allow for more efficient algorithms than its classical counterpart for certain problems[27, 28]. Much of the efforts in this field are devoted to the study of gate design, error correction, cryptographic tools, quantum key distribution and the study of entanglement to mention just a few [27, 29]. It is important to emphasize that quantum information usually considers inertial observers, living in a flat spacetime and moving with non relativistic speeds.

RQI is at the intersection of them all. It provides tools for comprehending the quantum nature of gravity by understanding how the methods of quantum information are modified when put into the framework of quantum field theory and also how quantum mechanics is affected by considering general relativistic effects. The field has made significant contributions to shed light into these questions. For example, early studies in the field led to the realization that entanglement is an observer dependent property: accelerated observers find that entanglement degrades with acceleration[30, 31]. It was soon recognized that considering quantum information protocols with observers in the presence of gravity, accelerating or moving with relativistic speeds leads to new phenomena that could be exploited to improve such protocols [32, 33, 34].

The field of RQI has rapidly grown over the past years, with many research groups making significant contributions to the field. Among them are investigations such as the study of entanglement and entropy between non inertial observers sharing modes of a quantum field [30, 31, 35], the fate of entanglement of quantum fields in expanding spacetimes [36, 37], gravitational collapses [38] and in the presence of black holes [39, 40, 41, 42].

In late years we have seen the development of techniques based on the study of the light-matter interaction in relativistic regimes through the use of particle detectors to probe quantum fields for finite times while undergoing relativistic trajectories or standing in curved spacetimes [43, 44, 45, 46, 47], the entanglement of moving cavities in non inertial frames [48, 49, 50] and the consequences all these considerations have in different

quantum information protocols such as teleportation [51, 52, 53], quantum communication [54, 55, 56, 57], design of quantum gates through relativistic motion [34, 58, 59], key distribution [56, 60], entanglement harvesting [61, 62] or metrology [63, 64, 65, 66] among many others. It has also seen contributions in more foundational studies, from models of gravitational decoherence [67, 68], to the study of time dilation [69, 70, 71, 72, 73] and the equivalence principle in quantum systems [72, 74, 75].

The field has matured to a point where the community is devoting considerable efforts to experimentally test its theoretical predictions. For example, there has been several experimental proposals to test gravitational effects on interferometric experiments [70, 76]. There are also recent works where circuit quantum electrodynamics (c-QED) setups have or could be successful in simulating and observing new physical effects proposed by RQI models. Unruh suggested that Hawking radiation could be observed in a condensed matter system consisting of sound waves in a fluid with spatially varying velocities, whose equation of motion can be written in terms of a metric corresponding to that of a non rotating Black Hole [77]. Consequently, building a system where the propagation velocity can be modulated leads to an analogue simulator where the Hawking radiation could be observed. An experiment using a c-QED system has been proposed [78], where by modulating an external flux on an array of superconducting quantum interfering devices (SQUIDs), a spatially varying velocity in the system is achieved. Another example relevant to this thesis is the observation of the dynamical Casimir effect (DCE) in a c-QED setup [4, 79, 80]. The DCE states that a moving boundary leads to the creation of particles out of the vacuum. Key to the observation of this effect is to have a moving boundary with very high accelerations. By controlling an external flux through a SQUID, a strong driving of a boundary capable of producing particle creation was experimentally achieved recently.

This thesis is divided into two parts. The first part describes the first theoretical analysis of exploiting the dynamical Casimir effect to search for particular signatures for various relativistic motions. The second part is concerned with understanding how decoherence can affect processes in RQI that might become manifest in experiments. We apply this analysis to the gravitational force and show how in fact experiment can severely constrain such approaches.

1.2 Organization

The aim of the first part of the thesis is to present the analysis of the behaviour of oscillatory boundaries in the context of c-QED. As discussed above, superconducting circuits offer an ideal testbed for the implementation of this kind of experiment. This idea is reinforced by

the fact that the Unruh effect is strongly connected with the dynamical Casimir effect. As such, we propose a modification of the settings where the latter is simulated [4, 79, 80] to study particle creation due to effectively relativistic non inertial trajectories of boundary conditions beyond the simple sinusoidal trajectories analyzed in previous works.

Part 1 of this theses is divided into three chapters. The aim of the first two chapters is to provide with the basic background and tools necessary for the understanding of the results presented in the third chapter.

In Chapter 2 we present a brief review of scalar quantum field theory, with an emphasis on the concepts relevant to this work. Chapter 3 covers the ingredients on superconducting quantum circuits required to understand the experimental setup we will work with. Making use of the material presented in these two chapters, Chapter 4 is dedicated to present our main results on the simulation of relativistic trajectories using a c-QED setup.

We then switch gears and move on to Part 2. Motivated by recent efforts to model gravitational interactions as a classical channel arising from continuous measurements, the second part of this thesis is devoted to the presentation of a general study of the types of dynamics emergent from an open systems model of repeated interactions, followed by an application to systems interacting gravitationally. We also discuss some of the consequences these models would have on different experimental setups as a way to test them.

Part 2 of this thesis is divided into two chapters. They are presented in chronological order of publication. Consequently, the second chapter builds up on work presented on the previous chapter, but an effort was made so that each can be read independently without much referencing.

In Chapter 5 we present our work on a general model of continuous interactions, including the different regimes of emergent dynamics. In Chapter 6 we apply the framework developed in the previous chapter to present a model for gravitational interactions, together with its experimental implications.

We finish by presenting in Chapter 7 some future directions of our work.

Part I

The observation of the Unruh effect, either directly or in analogue systems, is one of the experimental cornerstones of quantum field theory in curved spacetimes and relativistic quantum information. Since field quantization schemes associated with inertial and accelerated observers are not equivalent [81], observers uniformly accelerating in what inertial observers regard as a vacuum will detect a thermal bath of particles [13]. The temperature T of this thermal bath is predicted to be proportional to the magnitude a of the proper acceleration of the detector.

Yet generalizations of this effect to other (nonequilibrium) regimes, such as nonuniformly accelerated trajectories [82, 83] and short times are not completely understood, even from a theoretical point of view [44, 45, 47, 79, 84]. Recently it has been shown [45] that within optical cavities in (1+1)-dimensions an accelerated detector equilibrates to a thermal state whose temperature is proportional to its acceleration. Provided the detector is allowed enough interaction time, this effect holds independently of the cavity boundary conditions [84], though for sufficiently short timescales the temperature decreases with acceleration in certain parameter regimes [44].

In the classic Unruh Effect a detector with constant acceleration a in an inertial vacuum measures thermal radiation at the Unruh temperature T_U

$$k_{\text{B}} T_U = \frac{\hbar a}{2\pi c} \tag{1.1}$$

Amongst the problems one encounters when trying to experimentally detect this effect, the two main ones are (a) an inability to eternally accelerate anything (hence uniformity of acceleration cannot always hold) and (b) in practical terms, difficulty in accelerating a physical detector, such as a 2-level atom, with sufficient control. For these reasons, it would be extremely useful to have a quantum simulation of these phenomena. However its implementation requires some care.

The first problem involves overcoming the idealization of uniformity of acceleration by considering generalizations to nonuniformly accelerating trajectories. Under general conditions, a particle detector undergoing a general non-inertial trajectory will register a coloured noise that turns thermal only under the limiting conditions of uniform acceleration [85]. The natural setting to consider is oscillatory motion, which is more convenient for experimental implementations and extremely interesting from a theoretical point of view. A recent analysis of detectors undergoing various kinds of oscillatory motion [47] found that in general such detectors responded to the vacuum fluctuations of a quantum field and experienced a constant effective temperature at late times in these out of equilibrium conditions. Three kinds of oscillatory motion – sinusoidal motion, sinusoidal acceleration and alternating uniform acceleration – were considered, and the effective temperature for

each was found to depend more strongly on the geometry of the worldline than on the instantaneous proper acceleration. The behaviour of their steady state temperature was seen to be more similar to each other than to that of the Unruh temperature of an idealized uniformly accelerated detector provided the time scale of the detector's response was longer than the period of the oscillatory motion.

The second problem, that of the difficulty of (relativistically) accelerating a detector (even under the restriction to oscillatory motion) can be addressed by considering an inertial detector and a moving reflective boundary (or mirror). For a mirror that uniformly accelerates at late times, the detector experiences the same thermal radiation as predicted in the original Unruh effect. In spite of considerable theoretical support for the Unruh effect, as yet it lacks direct experimental proof. Experimental explorations of relativistic particle creation from the vacuum [4, 79, 80] are therefore particularly interesting.

The aim of the first part of this thesis is to present our contribution to the understanding of these problems by analyzing the feasibility of simulating different relativistic motions of a boundary using a slight modification of the setup previously used to simulate the dynamical Casimir effect [4, 79, 80] and to compute their photon emission spectrum. We dedicate the first two chapters (Chapter 2 and Chapter 3) to provide a general background on both quantum field theory and superconducting quantum circuits, to the extent needed for an understanding of our work, which we present in Chapter 4.

The material presented in Chapter 4 derives from [1], in collaboration with Eduardo Martín-Martínez, Robert B. Mann and Christopher Wilson.

Chapter 2

Scalar quantum field theory

Quantum Field Theory (QFT) is one of the most widely used frameworks in modern physics. It is most popular for its success in adequately describing elementary particles and their interactions, but its tools are essential to the description of physical phenomena in other fields like condensed matter physics [86] and nuclear physics [87] to mention just a few. Its application yields incredible agreement between its theoretical predictions and experimental results. QFT combines two of the cornerstone theories in physics: quantum mechanics and special relativity, but its basic objects are quantum fields instead of particles, which arise as the excited states of these quantum fields. It provides us with a set of computational methods to calculate the results of particle interactions. For a comprehensive presentation on QFT, see for example [88, 89].

In this thesis we will only make use of the most basic quantum field in a $(1+1)$ dimensional flat spacetime: a free scalar field obeying the Klein-Gordon equation. We will study the consequences of considering non-inertial frames of reference for this field. Although the real world is $(3+1)$ dimensional, much of the basic physics can be understood from an analysis in one spatial dimension. In particular, a scalar field with a planar moving boundary effectively becomes a problem in $(1+1)$ dimensions.

The organization of this chapter is as follows: In Section 2.1 we present the basic scheme of the quantization of a scalar field in $(1+1)$ dimensional flat spacetime, followed by a review of the Unruh effect in Section 2.2 and the dynamical Casimir effect in Section 2.3. We finish by presenting in Section 2.4 the calculation of particular parameters of relativistic trajectories that will be used in this work.

2.1 Field quantization

We start by considering a scalar field in $(1+1)$ dimensional Minkowski spacetime with metric signature $\eta_{\mu\nu} = \mathrm{diag}(+1, -1)$ whose equation of motion follows from the following action (in units where $\hbar = c = k_{\mathrm{B}} = 1$)

$$\mathcal{S} = \frac{1}{2}\int dxdt\left((\partial_t\phi)^2 - (\partial_x\phi)^2 - m^2\phi\right) \tag{2.1}$$

with Lagrangian density

$$\mathcal{L} = \frac{1}{2}\left((\partial_t\phi)^2 - (\partial_x\phi)^2 - m^2\phi\right) \tag{2.2}$$

From this Lagrangian, we obtain the equation of motion for the scalar field, the so called Klein-Gordon equation

$$\left(\Box + m^2\right)\phi(x,t) = 0 \tag{2.3}$$

where $\Box = \partial_t^2 - \partial_x^2$. To quantize the theory we promote the field ϕ and its canonically conjugate momenta $\pi = \frac{\partial\mathcal{L}}{\partial(\partial_t\phi)} = \partial_t\phi$ to quantum operators $\hat{\phi}$, $\hat{\pi}$ obeying the equal time commutation relations

$$\begin{aligned}\left[\hat{\phi}(x,t), \hat{\pi}(x',t)\right] &= i\delta(x-x') \\ \left[\hat{\phi}(x,t), \hat{\phi}(x',t)\right] &= [\hat{\pi}(x,t), \hat{\pi}(x',t)] = 0\end{aligned} \tag{2.4}$$

We can expand the field operators in terms of a set of mode functions $u_k(x,t)$, $u_k^*(x,t)$ so that

$$\hat{\phi}(x,t) = \int dk\left[u_k(x,t)\hat{a}_k^- + u_k^*(x,t)\hat{a}_k^+\right] \tag{2.5}$$

From the equation of motion (2.3) the mode functions $u_k(x,t)$ obey the equation

$$(\Box + m^2)u_k(x,t) = 0 \tag{2.6}$$

We demand that this set of modes forms a complete orthonormal basis with respect to the inner product defined as

$$(f,g) = i\int dx\,(f^*\partial_t g - \partial_t f^* g) \tag{2.7}$$

which is preserved under Klein-Gordon evolution. Therefore, we demand that the modes obey

$$\begin{aligned}(u_k, u_{k'}) &= \delta(k-k') \\ (u_k^*, u_{k'}^*) &= -\delta(k-k') \\ (u_k, u_{k'}^*) &= 0\end{aligned} \tag{2.8}$$

The time independent operators $\hat{a}_k^{\pm}$ inherit from Equation (2.4) the commutation relations

$$\begin{aligned}\left[\hat{a}_k^-, \hat{a}_{k'}^+\right] &= \delta(k'-k) \\ \left[\hat{a}_k^-, \hat{a}_{k'}^-\right] &= \left[\hat{a}_k^+, \hat{a}_{k'}^+\right] = 0\end{aligned} \tag{2.9}$$

We can use the creation and annihilation operators $\hat{a}_k^+$ and $\hat{a}_k^-$ respectively to construct a Fock basis for the Hilbert space. As usual, the vacuum state is defined as the state that is annihilated by all annihilation operators $\hat{a}_k^-$

$$\hat{a}_k^- |\, 0\rangle = 0 \tag{2.10}$$

We can construct the state $|\, n_1, n_2, ...\rangle$, with occupation number n_α for the mode k_α, by applying creation operators on the vacuum state as follows

$$|\, n_1, n_2, ...\rangle = \prod_\alpha \frac{(\hat{a}_{k_\alpha}^+)^{n_\alpha}}{\sqrt{n_\alpha!}} |\, 0\rangle \tag{2.11}$$

This state corresponds to the quantum state with n_1 particles with momentum k_1, n_2 particles with momentum k_2 and so on. The basis of the Hilbert space consists of the set of quantum states with all possible occupation numbers n_α for each momentum k_α.

Now we turn our attention to the mode functions. One set of solutions to the equation of motion (2.3) is given by the delocalized plane waves

$$u_k(x,t) \propto e^{i(kx-\omega_k t)}$$

where $\omega_k^2 = k^2 + m^2$. From Equations (2.8), a normalized set of modes is given by

$$u_k(x,t) = \frac{1}{\sqrt{4\pi\omega_k}} e^{i(kx-\omega_k t)} \tag{2.12}$$

These modes satisfy the relation

$$\frac{du_k(x,t)}{dt} = -i\omega u_k(x,t) \tag{2.13}$$

and are called positive frequency modes. The $u_k^*(x,t)$ modes are called negative frequency modes. Each choice of modes defines a particular set of operators $\hat{a}_k^+, \hat{a}_k^-$ as $\hat{a}_k^+ = -(u_k^*, \hat{\phi})$ and $\hat{a}_k^- = (u_k, \hat{\phi})$ and consequently a particular Fock basis. Notice from Equations (2.10), (2.11) that the notion of particle is defined by the positive frequency modes. Let us analyze the particular basis defined by the choice of modes in Equation (2.12).

By performing a Legendre transformation of the Lagrangian in Equation (2.2), the quantized Hamiltonian is found to be given by

$$\hat{\mathcal{H}} = \frac{1}{2}\int dx \left((\partial_t\hat{\phi})^2 + (\partial_x\hat{\phi})^2 + m^2\hat{\phi}\right) \tag{2.14}$$

By substituting Equation (2.12) into Equations (2.5) and (2.14), the Hamiltonian above can be written as

$$\hat{\mathcal{H}} = \int dk\omega_k \left(\hat{N}_k + \frac{1}{2}\delta(0)\right) \tag{2.15}$$

where $\delta(0)$ accounts for the infinite spatial volume. The last term is a sum over all modes of the zero point energies, and therefore, diverges with the volume of the system. However, for our purposes, we only care about energy differences and in flat spacetime we can ignore this infinite constant. Here, $\hat{N}_k = \hat{a}_k^+\hat{a}_k^-$ is the number operator of mode k. Therefore, this set of modes diagonalizes the Hamiltonian.

The states in Equation (2.11) defined with respect to the particular choice of mode basis in (2.12) are eigenstates of the Hamiltonian and are therefore stationary states with definite energy and the corresponding vacuum state is the state of minimum energy. Let us now choose a different set of orthonormal modes $v_{k'}$ in terms of which we can expand the field operator. This choice defines a new set of operators $\hat{b}_{k'}^{\pm}$, which can be used to construct a different Fock basis.

The set of modes $u_k, v_{k'}$ are related through a linear transformation, called a Bogolyubov transformation

$$v_{k'} = \int dk(\alpha_{k'k}u_k + \beta_{k'k}u_k^*) \tag{2.16}$$

The coefficients $\alpha_{k'k}, \beta_{k'k}$ are called the Bogolyubov coefficients. Using Equation (2.7), these coefficients are given by

$$\begin{aligned} \alpha_{k'k} &= (v_{k'}, u_k) \\ \beta_{k'k} &= -(v_{k'}, u_k^*) \end{aligned} \tag{2.17}$$

The operators $\hat{a}_k^{\pm}$ and $\hat{b}_{k'}^{\pm}$ are then related by a transformation

$$\hat{b}_{k'}^- = \int dk \left(\alpha_{k'k}^* \hat{a}_k^- - \beta_{k'k} \hat{a}_k^+\right) \tag{2.18}$$

$$\hat{a}_k^- = \int dk' \left(\alpha_{k'k} \hat{b}_{k'}^- + \beta_{k'k}^* \hat{b}_{k'}^+\right) \tag{2.19}$$

with normalization conditions

$$\begin{aligned} \int dk \left(\alpha_{k'k} \alpha_{k''k}^* - \beta_{k'k} \beta_{k''k}^*\right) &= \delta\left(k' - k''\right) \\ \int dk \left(\alpha_{k'k} \beta_{k''k} - \beta_{k'k} \alpha_{k''k}\right) &= 0 \end{aligned} \tag{2.20}$$

The vacuum states $|\, 0_a\rangle$ and $|\, 0_b\rangle$ defined by $\hat{a}_k^-$ and $\hat{b}_k^-$ respectively are different. From Equation (2.18), we can see that if the Bogolyubov coefficients $\beta_{kk'}$ are nonzero, the vacuum state $|\, 0_a\rangle$ is no longer annihilated by the annihilation operators $\hat{b}_{k'}^-$, so the notion of vacuum changes and consequently, from Equation (2.11), the notion of particle will also change. Indeed, the number of b-particles in the vacuum state $|\, 0_a\rangle$ is

$$\langle \hat{N}_b \rangle = \langle 0_a \,| b_{k'}^+ b_{k'}^- |\, 0_a \rangle = \int dk |\beta_{kk'}|^2 \delta(0) \tag{2.21}$$

The mean density of b-particles is then

$$n_b = \frac{\langle \hat{N}_b \rangle}{\delta(0)} = \int dk |\beta_{kk'}|^2 \tag{2.22}$$

For inertial observers, connected by a Lorentz transformation, the coefficient $\beta_{kk'}$ vanishes and different inertial observers agree on the particle content. For non-inertial observers, non-static or curved spacetimes, the $\beta_{k'k}$ Bogolyubov coefficients might not vanish and the notion of particle is not universal, depending strongly on the observer.

We illustrate this by considering two particular cases, one in which the observer is undergoing uniform acceleration, giving rise to the Unruh effect, and one in which the field is terminated by a moving boundary, giving rise to the dynamical Casimir effect.

2.2 Unruh effect

An accelerated observer will have a different notion of particle content than its inertial counterpart. To show this, let us start by considering an observer whose proper time is τ moving with a trajectory $x^\mu(\tau) = (t(\tau), x(\tau))$. If $t(\tau) = \frac{1}{\alpha}\sinh(\alpha\tau)$ and $x(\tau) = \frac{1}{\alpha}\cosh(\alpha\tau)$, the observer has a constant proper acceleration α and is therefore a uniformly accelerated observer.

This trajectory motivates us to introduce Rindler coordinates, an appropriate set of coordinates used to describe uniformly accelerated observers, defined as

$$\begin{aligned} t &= \frac{1}{a} e^{a\xi} \sinh(a\eta) \\ x &= \frac{1}{a} e^{a\xi} \cosh(a\eta) \end{aligned} \tag{2.23}$$

The range of these coordinates is $-\infty < \eta, \xi < +\infty$ and they cover the right-hand wedge $x > |t|$, as can be seen from Figure 2.1. The left-hand wedge is covered with another Rindler coordinate system, differing from the one defined in (2.23) by an overall minus sign. Both wedges, called Rindler wedges, are causally disconnected.

Observers with constant $\xi = \xi_0$, called Rindler observers, have proper time $e^{a\xi_0}\eta$ and proper acceleration $ae^{-a\xi_0}$. In the inertial coordinates (t, x), the trajectory of these observers is a hyperbola $x^2 - t^2 = a^{-2}e^{2a\xi_0}$ as illustrated in Figure 2.1. Rindler observers with $\xi = 0$ have a proper time η and proper acceleration a. Lines of constant η correspond to straight lines.

In Rindler coordinates, the metric takes the form

$$ds^2 = e^{2a\xi}\left(d\eta^2 - d\xi^2\right) \tag{2.24}$$

For a massless scalar field, the Klein-Gordon equation is now given by

$$\left(\partial_\eta^2 - \partial_\xi^2\right)\phi = 0 \tag{2.25}$$

and following a procedure analogous to the one presented in Section 2.1, the normalized positive frequency modes for the right and left wedges respectively are

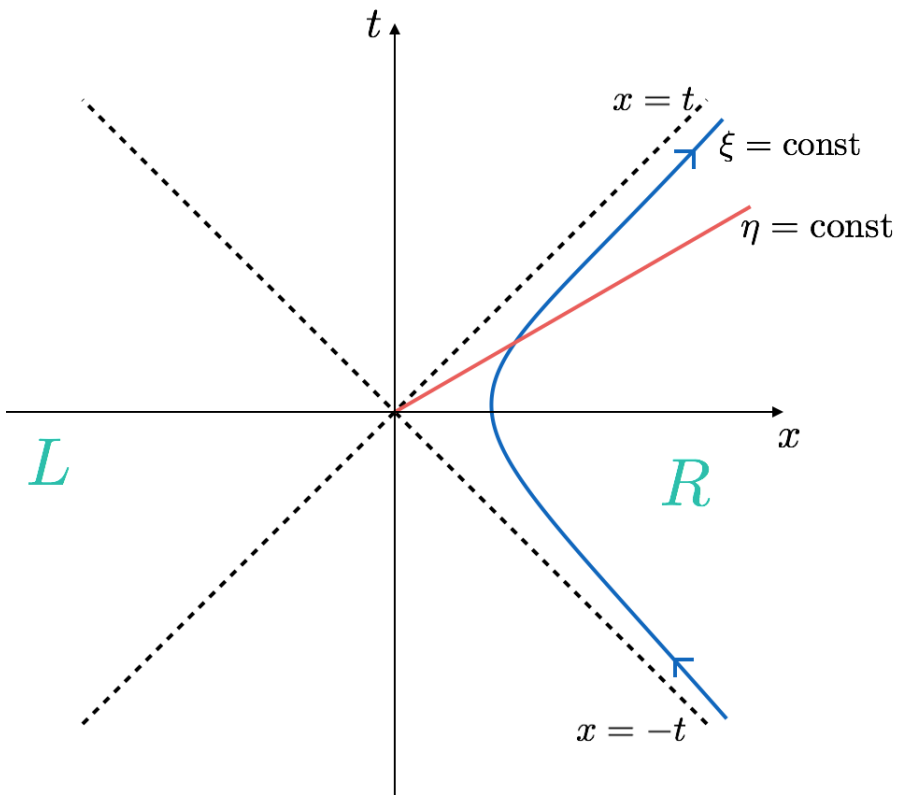

Figure 2.1: Minkowski space, illustrating the left (L) and right (R) Rindler wedges. The trajectory of uniformly accelerated observers corresponds to lines of constant ξ (shown in blue). Lines of constant η correspond to straight lines (shown in red).

$$v^R_{k'}(\xi,\eta) = \frac{1}{\sqrt{4\pi\omega_{k'}}} e^{i(k'\xi-\omega_{k'}\eta)}$$
$$v^L_{k'}(\xi,\eta) = \frac{1}{\sqrt{4\pi\omega_{k'}}} e^{i(k'\xi+\omega_{k'}\eta)} \tag{2.26}$$

with $\omega_{k'} = |k'|$ and where the superscript R, L is to indicate that the mode corresponds to the right and left wedges respectively. These so called Rindler modes (together with its conjugates) form a complete mode basis in terms of which we can expand the quantum field

$$\hat{\phi} = \int dk' \left(v^R_{k'} \hat{b}^R_{k'} + v^{R*}_{k'} \hat{b}^{R\dagger}_{k'} + v^L_{k'} \hat{b}^L_{k'} + v^{L*}_{k'} \hat{b}^{L\dagger}_{k'} \right) \tag{2.27}$$

where $\hat{b}^R_{k'}$ and $\hat{b}^L_{k'}$ are the annihilation operators associated to the right and left Rindler modes respectively and that define the Rindler vacuum $|0_R\rangle$ as

$$\hat{b}^R_{k'}|0_R\rangle = \hat{b}^L_{k'}|0_R\rangle = 0 \tag{2.28}$$

for all k'.

The Bogolyubov coefficients $\beta^R_{k'k} = -(v^R_{k'}, u_k)$ and $\beta^L_{k'k} = -(v^L_{k'}, u_k)$ are nonzero and from Equations (2.18), (2.19), the Rindler vacuum $|\,0_R\rangle$ (which is the vaccum seen by a Rindler observer) is not the same as the Minkowski vaccum $|\,0_M\rangle$ (which is the vacuum seen by an inertial observer). An explicit calculation of these coefficients, together with Equation (2.22) yields that the number of particles in mode k' seen by a Rindler observer is given by

$$n_{k'} = \left(e^{\frac{2\pi\omega_{k'}}{a}} - 1 \right)^{-1} \tag{2.29}$$

which corresponds to a Bose-Einstein distribution with temperature

$$T_U = \frac{a}{2\pi} \tag{2.30}$$

where T_U is the so-called Unruh temperature. We conclude that an accelerated observer will detect a thermal distribution of particles at a temperature proportional to its acceleration, as opposed to the zero temperature vacuum that an inertial observer measures [13].

2.3 Dynamical Casimir effect

We consider a massless scalar field in (1+1) dimensions obeying the Klein-Gordon equation (2.3) and terminated by a mirror that follows a trajectory $x = z(t)$ for $t > 0$ and $x = 0$ for $t \leq 0$. In particular, we demand that the field vanishes at the mirror's surface. The field is therefore subject to a moving boundary condition

$$\phi(z(t), t) = 0 \tag{2.31}$$

for $t > 0$.

The general solution to the wave equation is

$$\phi(x, t) = f(t + x) + g(t - x) \tag{2.32}$$

In order to obey the boundary condition (2.31), the functions f and g cannot be chosen freely. Indeed, by choosing the function f, the function g has to be such that

$$g(t - z(t)) = -f(t + z(t)) \tag{2.33}$$

to guarantee that the field vanishes at the boundary.

We can alternatively work in the null coordinates (u, v), where $u = t - x$ and $v = t + x$ with line element $ds^2 = -dudv$. The wave equation in these coordinates is then

$$\frac{\partial}{\partial u}\frac{\partial}{\partial v}\phi(u, v) = 0 \tag{2.34}$$

which has the general solution

$$\phi(u, v) = f(v) + g(u) \tag{2.35}$$

The trajectory in the (u, v) coordinates is now $v = p(u)$, so for the field to vanish at the moving boundary, the relation between the functions f and g in the null coordinates is

$$g(u) = -f(p(u)) \tag{2.36}$$

Notice that at the boundary $u = t - z(t)$ so u can be written purely as a function of t. We can therefore find a function τ such that at the boundary $t = \tau(u)$ in which case $u = \tau(u) - z(\tau(u))$. With this, we can rewrite Equation (2.33) as

$$g(u) = -f(u + 2z(\tau(u))) \tag{2.37}$$

and the solution to the wave equation obeying the boundary condition is

$$\phi(u,v) = f(v) - f(p(u)) \tag{2.38}$$

where using (2.36) and (2.37) we identify $p(u) = u + 2z(\tau(u))$. Alternatively, from the definition of $\tau(u) = u + z(\tau(u))$ we can also write the solution (2.38) as

$$\phi(u,v) = f(v) - f(2\tau(u) - u) \tag{2.39}$$

We consider the particular case where the mode functions are plane waves moving to the left that hit the moving boundary. Following the prescription developed in Section 2.1, the quantum field can be expanded as

$$\hat{\phi}(u,v) = \int dk \left[u_k(u,v)\hat{a}_k^- + u_k^*(u,v)\hat{a}_k^+\right] \tag{2.40}$$

and the normalized modes $u_k(u,v)$ in the light coordinates (u,v) are given by

$$u_k = \frac{1}{\sqrt{4\pi\omega_k}}\left(e^{-i\omega_k v} - e^{-i\omega_k(2\tau(u)-u)}\right) \tag{2.41}$$

where $\omega_k = |k|$

For $t \leq 0$, $\tau(u) = u$ and the modes are

$$u_k = \frac{2i\sin(\omega_k x)}{\sqrt{4\pi\omega_k}} e^{-i\omega_k t} \tag{2.42}$$

which are positive frequency modes with respect to Minkowski time t, so the presence of the mirror does not create any particles. However, when the mirror is accelerated, there will be a sudden change of the mode functions from (2.42) to (2.41). It is this mismatch that causes the creation of particles: the vacuum defined by the operators associated with the mode functions (2.42) for $t \leq 0$ is no longer the vacuum associated with the mode functions (2.41) for $t > 0$ and an inertial observer carrying a detector will detect particles when the mirror begins to accelerate [90].

2.4 Relativistic trajectories

In this section we show how to calculate the proper time and the proper acceleration of a given trajectory in the laboratory frame, which will be used in the simulated trajectories presented in Chapter 4. We work with a metric signature $\eta_{\mu\nu} = \text{diag}(-1,+1)$.

Consider a moving object in a $(1+1)$ dimensional flat spacetime. The path of this object relative to the laboratory frame of reference is described by

$$x^\mu = (t, z(t)) \tag{2.43}$$

where $z(t)$ describes the trajectory as a function of the rest frame time t. The 4-velocity u^μ is

$$u^\mu = \frac{dx^\mu}{d\tau} = \left(\frac{dt}{d\tau}, \frac{dz}{dt}\frac{dt}{d\tau}\right) = \frac{dt}{d\tau}\left(1, \frac{dz}{dt}\right) \tag{2.44}$$

where τ is the proper time of the object and the 4-acceleration a^μ is

$$a^\mu = \frac{du^\mu}{d\tau} = \left(\frac{d^2t}{d\tau^2}, \frac{d^2z}{dt^2}\left(\frac{dt}{d\tau}\right)^2 + \frac{dz}{dt}\frac{d^2t}{d\tau^2}\right) \tag{2.45}$$

Since the velocity satisfies the relation $u^\mu u_\mu = -1$ then

$$\left(\frac{dt}{d\tau}\right)^2 = \left[1 - \left(\frac{dz}{dt}\right)^2\right]^{-1} \tag{2.46}$$

which can be used to find the proper time τ as a function of the coordinate time t. We use this relation to find the term $\frac{d^2t}{d\tau^2}$ present in (2.45) to write the acceleration in terms of the trajectory $z(t)$ as

$$a^\mu = \frac{d^2z}{dt^2}\left[1 - \left(\frac{dz}{dt}\right)^2\right]^{-2}\left(\frac{dz}{dt}, 1\right) \tag{2.47}$$

The proper acceleration $a = \sqrt{a^\mu a_\mu}$ is therefore

$$a = \left|\frac{d^2z}{dt^2}\right|\left[1 - \left(\frac{dz}{dt}\right)^2\right]^{-\frac{3}{2}} \tag{2.48}$$

We will make use of Equations (2.46) and (2.48) later on in Chapter 4.

Chapter 3

Superconducting quantum circuits

Recently, quantum effects are being exploited to create quantum integrated circuits that exhibit novel properties making use of well-established integrated circuit technologies [91, 92, 93].

Superconducting electronic circuits take advantage of macroscopic quantum coherence effects [94]. In a normal conductor the charge carriers are electrons, each of which exhibits quantum phenomena. To obtain the macroscopic behaviour, the average over the microscopic states of the electrons is taken and the observation of quantum effects becomes impossible. In a superconductor the charge carriers are bound pairs of electrons called Cooper pairs [95]. These Cooper pairs are bosons that condense into a macroscopic quantum state. Consequently, in a superconductor it is the collective degrees of freedom of the system that display quantum effects, allowing for their observation even in large circuits.

Due to the macroscopicity of the components of a superconducting electronic circuit, coupling between them is easy, providing both an advantage for their ease of manipulation and a disadvantage since its hard to isolate them from environmental noise. As in any quantum system, high coherence is desirable. In order to minimize decoherence it is necessary to operate at ultra low temperatures so that thermal noise is suppressed. The superconductivity ensures that the resistance of the material is zero, so that there are no energy losses due to the transmission of the signal through the system, minimizing dissipation [94].

The aim of this chapter is to present some of the basic ingredients of quantum integrated circuits. The organization of this chapter is as follows: In Section 3.1 we present an important element of superconducting quantum circuits, the Josephson Junction. We then introduce a method for obtaining the equations of motion of an integrated circuit in Section

3.2 followed by the procedure to get their quantum mechanical description in Section 3.3. We finish by presenting in Section 3.4 the experimental setup that we use in our work.

3.1 Josephson junction

One of the elements of quantum integrated circuits utilized in the experimental setup with which we work is the Josephson junction [96] (which we will sometimes abbreviate as JJ). It is formed by a structure that consists of two superconductors separated by a barrier. The physics of these elements is determined by the equations of motion for the current and the voltage across the JJ. To derive these equations we need the Hamiltonian of the system. Contrary to normal conductors where the charge carriers are free electrons, in superconducting materials the charge carriers are pairs of bound electrons called Cooper pairs. When the two superconductors forming the Josephson junction are brought together, tunnelling of electrons takes place. Using second order perturbation theory, this tunnelling process couples states with different numbers of Cooper pairs, giving an effective Hamiltonian of the form [97]

$$\hat{\mathcal{H}}_J = -E_J \cos\hat{\phi} + \frac{E_C}{2}\hat{n}^2 \tag{3.1}$$

where ϕ is a parameter that labels the eigenstates. In the first term, E_J is the Josephson energy, which can be written in terms of the resistance of the conductor in the normal state and the energy gap of the material by using the Ambegaokar-Baratoff relation [98]. In the second term, $E_C = \frac{(2e)^2}{C}$ is the charging energy. The Cooper pair number $\hat{n}$ can be written in the phase representation as

$$\hat{n} = -i\frac{\partial}{\partial\hat{\phi}} \tag{3.2}$$

We can now derive the current $\hat{I}$ and the voltage $\hat{V}$ across the junction using Heisenberg equation of motion

$$\frac{d\hat{a}}{dt} = \frac{i}{\hbar}\left[\hat{\mathcal{H}}, \hat{a}\right] \tag{3.3}$$

1. Current in a Josephson Junction

– The current $\hat{I}$ is given by $\hat{I} = 2e\frac{d\hat{n}}{dt}$, so using (3.2) and (3.3)

$$\begin{aligned}\hat{I} &= \frac{-2eE_J i}{\hbar}\left[\cos\hat{\phi}, \hat{n}\right] \\ &= \frac{-2eE_J i}{\hbar}\left[\cos\hat{\phi}, -i\frac{\partial}{\partial\hat{\phi}}\right] \\ &= \frac{-2eE_J}{\hbar}\sin\hat{\phi} \end{aligned} \tag{3.4}$$

By defining the critical current I_c as

$$I_c = \frac{-2eE_J}{\hbar} \tag{3.5}$$

we can write the current as

$$\hat{I} = I_c \sin\hat{\phi} \tag{3.6}$$

2. Voltage across a Josephson Junction

– We again use (3.2) and (3.3) to get

$$\begin{aligned}\frac{d\hat{\phi}}{dt} &= \frac{E_C i}{2\hbar}\left[-\frac{\partial^2}{\partial\hat{\phi}^2}, \hat{\phi}\right] \\ &= \frac{-E_C i}{\hbar}\frac{\partial}{\partial\hat{\phi}} \\ &= \frac{E_C}{\hbar}\hat{n} \\ &= \frac{2|e|}{\hbar}\hat{V} \end{aligned} \tag{3.7}$$

so the voltage is

$$\hat{V} = \frac{\hbar}{2|e|}\frac{d\hat{\phi}}{dt} \tag{3.8}$$

Equations (3.6) and (3.8) are known as the Josephson relations. The phase parameter ϕ in these relations is related to the total magnetic flux by

$$\phi = -2\pi\frac{\Phi}{\Phi_0} \tag{3.9}$$

with Φ_0 the flux quantum defined as $\Phi_0 \equiv \frac{h}{2|e|}$ and Φ the total magnetic flux.

Josephson Junctions act as non linear inductances in parallel with a capacitance, with $L = \frac{d\Phi}{dI}$. Indeed from Equations (3.6) and (3.9) we get

$$I = \frac{\Phi_0}{2\pi L_J} \sin\left(2\pi \frac{\Phi}{\Phi_0}\right) \tag{3.10}$$

where we defined $L_J = \frac{\Phi_0}{2\pi I_c}$. In the limit where $\Phi/\Phi_0 \ll 1$ the junction acts as a linear inductance with current $I \approx \Phi/L_J$. A common representation of a Josephson junction is presented in Figure 3.1.

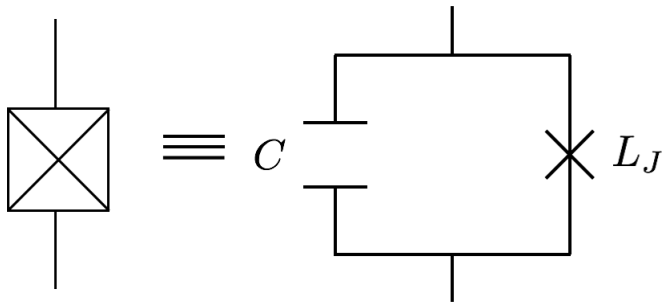

Figure 3.1: Pictorial representation of a Josephson junction as a non linear inductance.

Josephson junctions can be used to form more complex structures like superconducting quantum interference devices (SQUID) [99, 100]. This structures are formed by a superconducting loop containing Josephson junctions. Two particular examples of widely used SQUIDs are the RF-SQUID, composed of a loop with a single junction and the DC-SQUID, composed of two junctions (see [101] for a comprehensive review).

3.2 Equations of motion for integrated circuits

In this section we present a method for obtaining the equations of motion of a circuit (see [94] for a detailed description).

Given an integrated circuit, we identify a branch as a single electrical element of the circuit as illustrated in Figure 3.2 below.

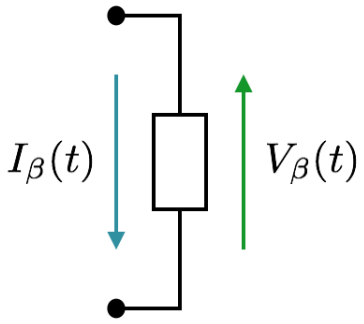

Figure 3.2: Branch of a circuit, indicating sign convention for voltage and current.

We define

$$\phi_\beta(t) = \int_{-\infty}^{t} V_\beta(t')dt' \tag{3.11}$$

$$Q_\beta(t) = \int_{-\infty}^{t} I_\beta(t')dt' \tag{3.12}$$

The set of Equations (3.11) and (3.12) define the branch variables $\phi_\beta(t)$ and $Q_\beta(t)$, called the branch flux and the branch charge respectively, as functions of the voltage $V_\beta(t)$ and the current $I_\beta(t)$ through the branch.

The analysis of a circuit involves the application of Kirchoff's laws together with the constitutive relations of its elements in order to obtain a set of equations that need to solved. The equations obtained by doing this are not all independent, since not all branch variables are independent degrees of freedom. The method of nodes provides an efficient way of analyzing a given lumped element circuit by organizing the same information as before in a clever and structured set of rules, giving the minimum number of equations needed to solve it [94]. We shall use this method, which we present next, to obtain the equations of motion of a given circuit, followed by an example to illustrate its application.

Method of nodes

1. Identify all nodes of the circuit, where a node is a point that connects two or more branches.

2. Choose a reference node to be the ground. The rest of the nodes are called active nodes.

3. Choose a spanning tree: a collection of branches that access every node and that contains no loops. This identifies the tree branch fluxes, where closure branches are left out.

4. The n node flux Φ_n is the sum of the branch fluxes along the path that connects it to the ground. Closure branches can then be expressed as differences between node fluxes.

$$\Phi_n = \sum_{\substack{\text{tree branches} \\ \beta \text{ leading} \\ \text{to n}}} \phi_\beta = \sum_b S_{nb}\phi_b \tag{3.13}$$

   where

$$S_{nb} = \begin{cases} 1 & \text{if path follows } b \text{ with proper orientation} \\ -1 & \text{if path follows } b \text{ with opposite orientation} \\ 0 & \text{if path doesn't follow } b \end{cases}$$

5. For each active node, we equate the sum of currents arriving from the inductive elements to the sum of currents going into the capacitive elements connected to that node.

6. Use the constitutive equations for the electric elements, together with the branch variables definitions (3.11) and (3.12) to express the currents in terms of the branch fluxes.

7. Use the results from step 4 to write the equations obtained from the previous step in terms of the node fluxes, finding the equations of motion of the circuit.

3.2.1 Example: LC resonator

We consider the simple example of an LC resonator. We use the Figure 3.3 below to illustrate the steps 1 to 3 of the method of nodes.

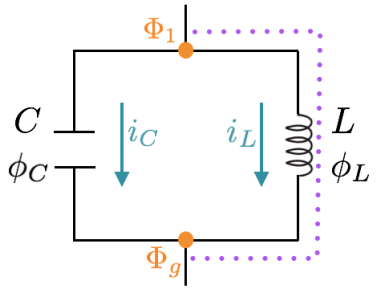

Figure 3.3: LC resonator indicating the currents i_C and i_L, the branch fluxes ϕ_C and ϕ_L, the ground node Φ_g, the node flux Φ_1, and the spanning tree as a purple dotted path.

Steps

- Steps 1-3: The spanning tree is highlighted in purple and the ground and active nodes are indicated as Φ_g and Φ_1 respectively. The tree branch flux is ϕ_L and the closure branch flux is ϕ_C.
- Step 4: the node flux Φ_1 is $\Phi_1 = \phi_L$. For this simple example, the closure branch flux is simply $\phi_C = \Phi_1$.
- Step 5: at the active node Φ_1, the currents obey the relation

$$-i_L = i_C \tag{3.14}$$

- Step 6: we write the currents through the inductor and the capacitor respectively as

$$\begin{aligned} i_L &= \frac{\phi_L}{L} \\ i_C &= \frac{dQ}{dt} = C\dot{V}_C = C\ddot{\phi}_C \end{aligned} \tag{3.15}$$

- Step 7: using Equations (3.14) and (3.15), the equation of motion for the node flux Φ_1 is

$$C\ddot{\Phi}_1 = -\frac{\Phi_1}{L} \tag{3.16}$$

Since the Josephson junction is a non linear inductance in parallel with a capacitance, we can apply the same procedure as for the LC resonator, with i_L now being given by Equation (3.10). The equation of motion is then

$$C\ddot{\Phi} = -\frac{\Phi_0}{2\pi L_J}\sin\left(2\pi\frac{\Phi}{\Phi_0}\right) \tag{3.17}$$

3.3 Hamiltonian of a circuit

Given the Lagrangian of a system, we can use the Euler-Lagrange equations to find its equations of motion. The equation of motion for the LC resonator (3.16) suggests that we can write the following Lagrangian for the system

$$\mathcal{L} = \frac{1}{2}C\dot{\Phi}^2 - \frac{1}{2L}\Phi^2 \tag{3.18}$$

where we dropped the node index. We can now define the variable conjugate to Φ as

$$Q = \frac{\partial\mathcal{L}}{\partial\dot{\Phi}} = C\dot{\Phi} \tag{3.19}$$

and use it to write the Hamiltonian as

$$\mathcal{H} = \frac{Q^2}{2C} + \frac{\Phi^2}{2L} \tag{3.20}$$

We notice this is the Hamiltonian for a simple harmonic oscillator with resonance frequency $\omega_{LC} = \frac{1}{\sqrt{LC}}$. We can quantize the system by promoting the classical variables (Φ, Q) to quantum variables $(\hat{\Phi}, \hat{Q})$ obeying the equal time canonical commutation relations

$$[\hat{\Phi}, \hat{Q}] = i\hbar \tag{3.21}$$

In the case of a Josephson junction, Equation (3.17) suggests that we can write the Lagrangian as

$$\mathcal{L} = \frac{1}{2}C\dot{\Phi}^2 - \left(\frac{\Phi_0}{2\pi}\right)^2\frac{1}{L_J}\left(1 - \cos\left(2\pi\frac{\Phi}{\Phi_0}\right)\right) \tag{3.22}$$

and Hamiltonian

$$\mathcal{H} = \frac{1}{2C}Q^2 + \left(\frac{\phi_0}{2\pi}\right)^2 \frac{1}{L_J}\left(1 - \cos\left(2\pi\frac{\Phi}{\Phi_0}\right)\right) \tag{3.23}$$

which can be written in terms of the Josephson energy as

$$\mathcal{H} = \frac{1}{2C}Q^2 + E_J\left(1 - \cos\left(2\pi\frac{\Phi}{\Phi_0}\right)\right) \tag{3.24}$$

3.4 Experimental setup

A transmission line (TL) is a structure designed to carry high frequency electromagnetic signals from one place to another with minimal losses. The size of transmission lines is a substantial fraction of the wavelength of the signal or larger [102]. A particular type of transmission line is the coplanar waveguide (CPW), which consists of three conductors printed on the same plane of a substrate and separated by a small gap, constant along the length of the line [103].

The experimental setup used to observe the dynamical Casimir effect [4, 79, 80], and used in this work, consists of a CPW terminated by a SQUID. A short fragment of a TL can be modelled as a lumped element circuit, so the line is modelled as an infinite number of lumped element circuits. In particular, we will be working with a lossless line where the resistance is zero. The equivalent circuit representation is presented in Figure 3.4.

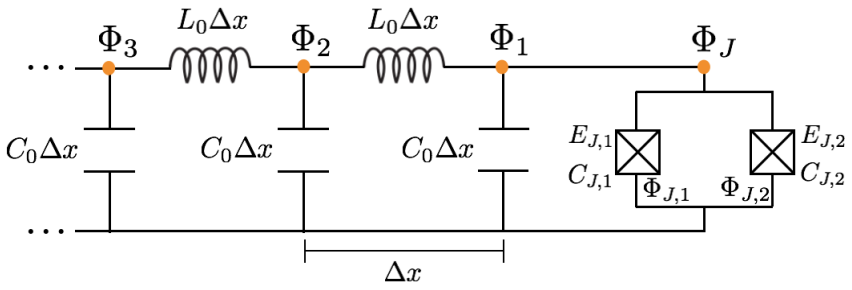

Figure 3.4: Equivalent circuit representation of the CPW setup as presented in [4], with C_0 and L_0 the capacitance and inductance per unit length. Here, Φ_i is the flux at node i and $\Phi_{J,j}$ are the fluxes at the Josephson junctions.

Using the method of nodes presented in Subsection 3.2, we calculate the Lagrangian of the system to be

$$\mathcal{L} = \frac{1}{2}\sum_{i=1}^{\infty}\left(\Delta x C_0(\dot{\Phi}_i)^2 - \frac{(\Phi_{i+1} - \Phi_i)^2}{\Delta x L_0}\right) + \sum_{j=1,2}\left[\frac{C_{J,j}}{2}(\dot{\Phi}_{J,j})^2 + E_{J,j}\cos(2\pi\frac{\Phi_{J,j}}{\Phi_0})\right] \tag{3.25}$$

where L_0 and C_0 are the respective inductance and capacitance per unit length of the CPW, $C_{J,j}$, $E_{J,j}$ and $\Phi_{J,j}$ are the capacitance, Josephson energy and flux of the j-th junction in the SQUID, and Φ_i is the dynamical flux at node i. Note that $\Phi_J = \Phi_1$.

If size of the loop of the SQUID is small enough, then $\Phi_{J,1} - \Phi_{J,2} = \Phi_{\text{ext}}$. We are considering a symmetric SQUID, so $C_{J,1} = C_{J,2} = C_J/2$ and $E_{J,1} = E_{J,2} = E_J$. The SQUID is operated in the phase regime, and it is assumed that its plasma frequency is much greater than any other frequencies in the circuit so that $\frac{\Phi_J}{\Phi_0} \ll 1$, where $\Phi_J = (\Phi_{J,1} + \Phi_{J,2})/2$ is the effective flux. The following Lagrangian is obtained

$$\mathcal{L} = \frac{1}{2}\sum_{i=1}^{\infty}\left(\Delta x C_0(\dot{\Phi}_i)^2 - \frac{(\Phi_{i+1}-\Phi_i)^2}{\Delta x L_0}\right) + \frac{1}{2}C_J\dot{\Phi}_J^2 - \frac{1}{2}\left(\frac{2\pi}{\Phi_0}\right)^2 E_J(\Phi_{\text{ext}})\Phi_J^2 \tag{3.26}$$

where $E_J(\Phi_{\text{ext}}) = 2E_J|\cos(\pi\frac{\Phi_{\text{ext}}}{\Phi_0})|$ is the tuneable Josephson energy. Note that the effective capacitance for the first node is $C_0\Delta x + C_J$ which becomes C_J in the limit of $\Delta x \to 0$.

The Hamiltonian of the system is consequently given by

$$\mathcal{H} = \frac{1}{2}\sum_{i=1}^{\infty}\left(\frac{(P_i)^2}{\Delta x C_0} + \frac{(\Phi_{i+1}-\Phi_i)^2}{\Delta x L_0}\right) + \frac{1}{2}\frac{P_1^2}{C_J} + \frac{1}{2}\left(\frac{2\pi}{\Phi_0}\right)^2 E_J(\Phi_{\text{ext}})\Phi_1^2 \tag{3.27}$$

with

$$P_i = \frac{\partial\mathcal{L}}{\partial\dot{\Phi}_i} \tag{3.28}$$

the conjugate variable to Φ_i.

The system is quantized by promoting the classical variables (Φ_i, P_i) to quantum variables $(\hat{\Phi}_i, \hat{P}_i)$ obeying the canonical commutation relations

$$\left[\hat{\Phi}_i, \hat{P}_j\right] = i\hbar\delta_{i,j} \tag{3.29}$$

We use Heinsenberg equation of motion on $\hat{P}_1$ to get

$$\begin{aligned}\dot{\hat{P}}_1 &= C_J\ddot{\Phi}_1 \\ &= -\frac{i}{\hbar}\left[\hat{P}_1, \mathcal{H}\right] \\ &= -E_J\left(\Phi_{\text{ext}}\right)\left(\frac{2\pi}{\Phi_0}\right)^2\Phi_1 - \frac{1}{L_0}\frac{(\Phi_2-\Phi_1)}{\Delta x}\end{aligned} \tag{3.30}$$

which in the continuous limit of $\Delta x \to 0$ becomes

$$C_J\ddot{\Phi}(0,t) + \left(\frac{2\pi}{\Phi_0}\right)^2 E_J(t)\Phi(0,t) + \frac{1}{L_0}\frac{\partial\Phi(x,t)}{\partial x}\bigg|_{x=0} = 0 \tag{3.31}$$

where $\Phi_i(t) \equiv \Phi(x,t)$ and $E_J(t) = E_J|\Phi_{\text{ext}}(t)|$. This equation plays the role of the boundary condition on the field in the CPW. It is noticed that this boundary can be tuned by an externally applied magnetic flux.

Furthermore, the dynamical fluxes away from the SQUID and in the continuum limit $\Delta x \to 0$ follow the Klein-Gordon equation

$$\frac{\partial^2}{\partial t^2}\Phi(x,t) - v^2\frac{\partial^2}{\partial x^2}\Phi(x,t) = 0 \tag{3.32}$$

with propagating velocity $v = 1/\sqrt{C_0 L_0}$.

Chapter 4

Dynamical Casimir effect in circuit QED for nonuniform trajectories

In this chapter, we present our results on the simulation of relativistic moving boundaries. This is achieved by utilizing the setup presented in Section 3.4 of the previous chapter, a coplanar waveguide (CPW) terminated by a superconducting quantum interference device (SQUID), which is used to simulate a trajectory described by $x = z(t)$, where t is the coordinate time in the laboratory frame.

An experimental simulation of a moving boundary naturally involves oscillatory motions. As discussed on the introduction to Part 1 of this thesis, the relativistic trajectories that we aim to simulate are the ones considered in [47], where a study of the response of a moving detector to a quantum field was presented. These trajectories are: sinusoidal motion (SM), sinusoidal acceleration (SA), and alternating uniform acceleration (AUA).

The experimental setup used for the observation of the dynamical Casimir effect [79] already simulates a sinusoidal motion, so we explore how to modify the settings to achieve more general moving boundaries. We point out that the trajectories we consider have a very similar spatial shape, so it would be interesting to analyze if even under this scenario their generated spectrums are distinguishable.

This chapter is organized as follows: We start by reviewing in Section 4.1 the different relativistic moving boundary conditions that we investigate. In Section 4.2 we compute the number of photon quanta emitted for a general trajectory and discuss how to interpret these in the context of circuit QED. In Section 4.3 we discuss the choice of input parameters, followed by a presentation of our results in Sections 4.4 and 4.5, where we compute the output number of photons for each trajectory and discuss how this differs for different relativistic trajectories. Finally, our conclusions are presented in Section 4.6.

4.1 Relativistic trajectories and moving boundaries

In this section we present the relativistic trajectories that we wish to simulate. Namely, we discuss sinusoidal motion (SM), sinusoidal acceleration (SA), and alternating uniform acceleration (AUA).

The periodic boundary motion we simulate is in one dimension, and we define its directional proper acceleration as its (positive definite) proper acceleration multiplied by the sign of the spatial component of the 4-acceleration. We denote the periodicity of the motion as ω_d, anticipating that the external driving flux that will be used to simulate these trajectories has the same natural frequency, as we will see in detail later on.

In the following, we use Equations (2.46) and (2.48) derived in Section 2.4 to calculate the proper time τ and the proper acceleration a for each trajectory, given that we know the form of the trajectory in the laboratory frame.

For each trajectory, the time averaged proper acceleration is

$$\bar{a} = \frac{\int_{\tau(t=0)}^{\tau(t=2\pi/\omega_d)} \mathrm{d}\tau\, a(\tau)}{\int_{\tau(t=0)}^{\tau(t=2\pi/\omega_d)} \mathrm{d}\tau} \tag{4.1}$$

where τ is the proper time.

4.1.1 Sinusoidal motion

Sinusoidal motion is one for which the 4-position of the boundary is given by

$$z^{\mu}_{\mathrm{SM}}(t) = (t, 0, 0, -R\cos(\omega_d t)) \tag{4.2}$$

where R is the oscillation amplitude, and ω_d is the oscillation frequency in coordinate time. In order for the motion to remain subluminal we must have $R\omega_d < 1$ in units with $c = 1$. The proper time τ of the boundary is $\tau = \omega_d^{-1} E(\omega_d t, (\frac{R\omega_d}{v})^2)$, where $E(\phi, m)$ is an elliptic integral of the second kind. The directional proper acceleration is

$$\alpha_{\mathrm{SM}}(t) = R\omega_d^2 \frac{\cos\omega_d t}{(1 - (\frac{R\omega_d}{v})^2 \sin^2\omega_d t)^{3/2}}$$

whereas the proper acceleration $a_{\mathrm{SM}}(t) = |\alpha_{\mathrm{SM}}(t)|$. Note that for $R\omega_d \ll 1$ the acceleration is proportional to the position, as expected for nonrelativistic motion. The oscillation

period is $t_p = 2\pi/\omega_d$ (or $\tau_p = \omega_d^{-1} E(2\pi, (\frac{R\omega_d}{v})^2)$ in proper-time). The time-averaged proper acceleration (over one oscillation period) is:

$$\bar{a} \;=\; \frac{v\omega_d \tanh^{-1}\left(\frac{R\omega_d}{v}\right)}{E\left(\frac{R^2\omega_d^2}{v^2}\right)}. \tag{4.3}$$

4.1.2 Sinusoidal acceleration

Sinusoidal acceleration (SA) (employed in a experimental proposal by Chen and Tajima [104], in which a particle of mass m and charge e is placed at one of the magnetic nodes of an EM standing wave with frequency ω_d and ampitud E_0) is described by the worldline

$$z^\mu_{\rm SA}(t) = \left[t, 0, 0, -\frac{v}{\omega_d}\arcsin\left(\frac{2\frac{\alpha}{v\omega_d}\cos(\omega_d t)}{\sqrt{1+4\left(\frac{\alpha}{v\omega_d}\right)^2}}\right)\right] \tag{4.4}$$

with directional proper acceleration

$$\alpha_{\rm SA}(t) = 2\alpha\cos\omega_d t$$

where $\alpha = \frac{eE_0}{m}$ has units of acceleration and the proper time of the boundary τ is related to the coordinate time t by $\tau(t) = \omega_d^{-1} F(\omega_d t, -4\alpha^2/v^2\omega_d^2)$, where $F(\phi, m)$ is the elliptic integral of the first kind. The oscillation period of this worldline is $t_p = 2\pi/\omega_d$ or a proper time period of $\tau_p = \omega_d^{-1} F(2\pi, -4\alpha^2/v^2\omega_d^2)$. The time-averaged proper acceleration reads

$$\bar{a} = \frac{v\omega_d \sinh^{-1}\left(2\frac{\alpha}{v\omega_d}\right)}{F\left(\pi/2, -4\left(\frac{\alpha}{v\omega_d}\right)^2\right)}. \tag{4.5}$$

and for low accelerations ($|\alpha| \ll v\omega_d$) and nonrelativistic velocities we obtain $z_{\rm SA} \sim z_{\rm SM}$.

4.1.3 Alternating uniform acceleration

For Alternating Uniform Acceleration (AUA) the trajectory of the boundary (parametrized in the accelerated observer's proper time) is

$$\begin{aligned} z^\mu_{\rm AUA}(\tau) = \quad & \left[\frac{v^2}{a}\left[\sinh\frac{a}{v}\left(\tau - \frac{n\tau_p}{2}\right) + 2n\sinh\frac{a\tau_p}{4v}\right], 0, 0,\right. \\ & \left.\frac{(-1)^n v^2}{a}\left[\cosh\frac{a}{v}\left(\tau - \frac{n\tau_p}{2}\right) + \{(-1)^n - 1\}\cosh\frac{a\tau_p}{4v}\right]\right] \end{aligned} \tag{4.6}$$

and so it experiences constant acceleration a that periodically alternates in sign

$$a^{\mu}_{\mathrm{AUA}}(\tau) = \left(a \sinh \frac{a}{v}\left[\tau - \frac{n\tau_p}{2}\right], 0, 0, (-1)^n a \cosh \frac{a}{v}\left[\tau - \frac{n\tau_p}{2}\right]\right). \tag{4.7}$$

where $n(\tau) \equiv \mathrm{floor}\left(\frac{2\tau}{\tau_p} + \frac{1}{2}\right)$, with $\mathrm{floor}(x)$ the largest integer less than or equal to x. We consequently have $\bar{a} = a$.

We illustrate in Figure 4.1 the position (top figure) and proper acceleration (bottom figure) as functions of time of these trajectories.

4.2 cQED setup

To simulate these boundary motions we make use of the setup [4] (illustrated in Figure 2 of [4]) and which we also presented in Figure 3.4 of Chapter 3, where a SQUID modulates the boundary condition of a Coplanar Waveguide (CPW). The CPW is at $x < 0$ and the SQUID is at $x = 0$.

Following the procedure presented in Section 3.4, the dynamical flux away from the SQUID respects the Klein-Gordon equation (see Equation (3.32))

$$\frac{\partial^2}{\partial t^2}\Phi(x,t) - v^2 \frac{\partial^2}{\partial x^2}\Phi(x,t) = 0 \tag{4.8}$$

with propagating velocity $v = 1/\sqrt{C_0 L_0}$, where C_0 and L_0 are the capacitance and inductance per unit length of the CPW.

The equation of motion at the boundary (see Equation (3.31)) is

$$\begin{aligned} 0 &= C_J \ddot{\Phi}(0,t) + \left(\frac{2\pi}{\Phi_0}\right)^2 E_J(t)\Phi(0,t) + \frac{1}{L_0}\frac{\partial \Phi(x,t)}{\partial x}\bigg|_{x=0} \\ &\simeq \Phi(0,t) + \frac{1}{L_0 E_J(t)}\left(\frac{\Phi_0}{2\pi}\right)^2 \frac{\partial \Phi(x,t)}{\partial x}\bigg|_{x=0} \end{aligned} \tag{4.9}$$

where $\Phi_0 = \frac{h}{2e}$ is the magnetic flux quantum, C_J is the capacitance of the symmetric SQUID, which has a small enough loop (so that self-inductance is neglected) and operates in the phase regime, and $E_J(t) = E_J(\Phi_{\mathrm{ext}}(t))$ is the tunable Josephson energy whose arbitrary time dependence can be given by controlling Φ_{ext}, the external flux threading through the SQUID. The second equality follows under the assumption that the SQUID plasma frequency is much larger than any other frequencies in the circuit. This boundary

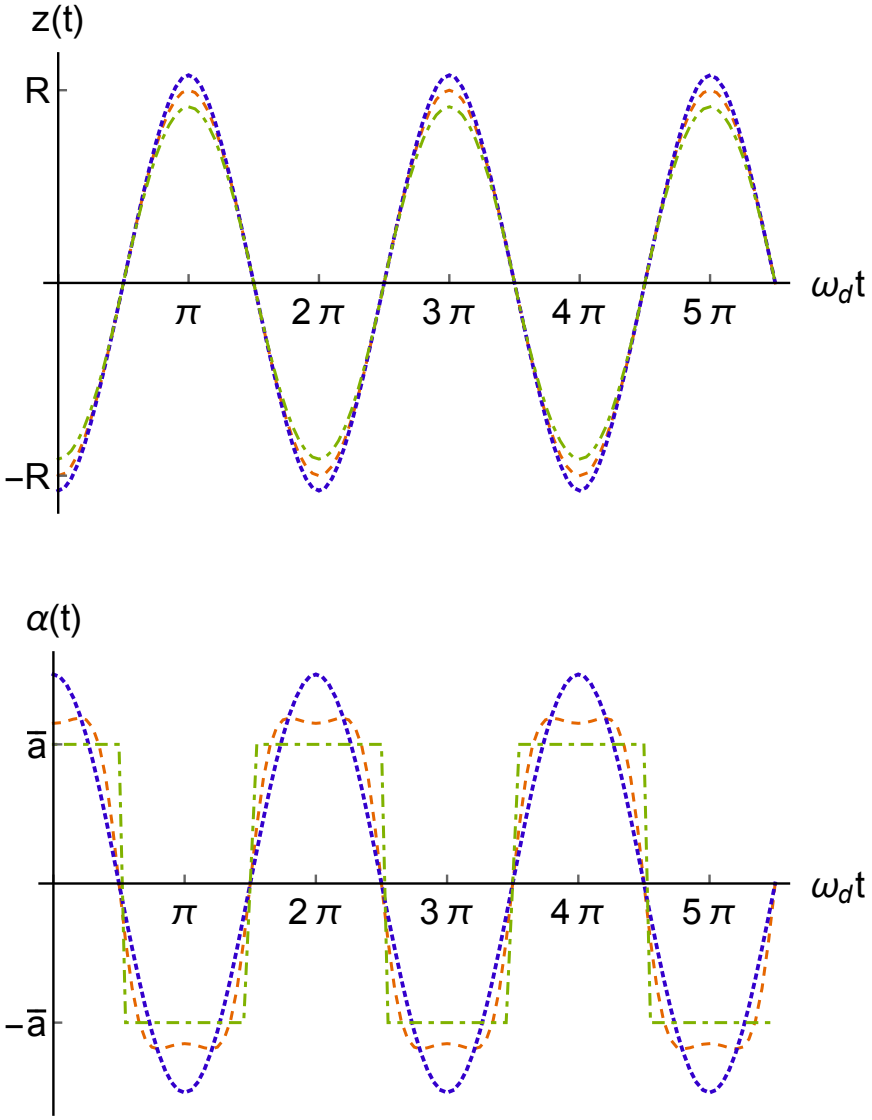

Figure 4.1: (Top) Trajectory's position as a function of time. (Bottom) Trajectory's directional acceleration as a function of time. In both cases the trajectories are distinguished as follows: Sinusoidal motion (red dashed), Sinusoidal Acceleration (blue dotted), Alternating Uniform Acceleration (green dot-dashed). The average acceleration for all trajectories is $\bar{a} = 1.2 \times 10^{19} \mathrm{m/s^{-2}}$ and the driving frequency is $\omega_d/2\pi = 28$ GHz.

can be tuned by the externally applied magnetic flux. All this assumptions and conditions are being recalled from Section 3.4.

Remember that for a field terminated by a moving mirror, we would have the boundary condition

$$\phi(t, Z(t)) = 0 \tag{4.10}$$

where $Z(t)$ is some prescribed trajectory.

Note that the above equation can be written in the approximate form

$$\phi(t,x)\Big|_{x=0} + (Z_0 - z(t))\frac{\partial\phi(t,x)}{\partial x}\Big|_{x=Z_0} = 0 \tag{4.11}$$

upon expanding Equation (4.10) about the origin, where $Z(t) = Z_0 - z(t)$ with $z(t) \ll Z_0$. Equation (4.9) plays the role of the boundary condition on the flux field in the CPW, and is designed to simulate the boundary condition (4.11). We remark that the boundary condition (4.9) does not exactly correspond to a Dirichlet condition, and instead is similar to it only in an approximate way. In principle identifying this simulation with the original perfect-mirror Dirichlet boundary condition employed in the classic literature on the dynamical Casimir effect [90, 105, 106] can be problematic. This is because the condition (4.9) well approximates a pure Dirichlet condition at a moving boundary only when $|dz(t)/dt| \ll c$ [107].

In our case this is not a concern for two reasons. First, the dynamical Casimir effect does not require strict use of a Dirichlet condition; indeed it occurs for a general set of time dependent boundary conditions near relativistic regimes [108]. Second, the boundary condition (4.11) (which is faithfully approximated by (4.9) for field frequencies much smaller than the SQUID plasma frequency [109]) produces the same particle spectrum (at leading order) as the pure Dirichlet condition. Writing $V = \omega t + k_\omega x$ and $U = \omega t - k_\omega x$, the full solution to (4.8) that respects (4.10) is given by

$$\phi(t,x) = f(V) - f(p_+(U)) + g(U) - g(p_-(V)) \tag{4.12}$$

where $\omega t \pm k_\omega z_\pm(t) = p_\pm(\omega t \mp k_\omega z_\pm(t))$ in the case of two boundaries with trajectories $V = p_+(U)$ and $U = p_-(V)$, respectively determined in terms of the prescribed boundary motions $x = z_\pm(t)$. We shall set $f(V) = 0$ as there is neither a left boundary nor incoming right-propagating signals, and write $z_-(t) = z(t)$.

The general method for interpreting this equation (for left-moving modes that are reflected from the boundary) is to write (4.12) as

$$\Phi(x,t) = \sqrt{\frac{\hbar Z_0}{4\pi}}\int_0^\infty \frac{d\omega}{\sqrt{\omega}}\left(a_{\text{in}}(\omega)e^{-i(-k_\omega x+\omega t)} + a_{\text{out}}(\omega)e^{-i(k_\omega x+\omega t)} + \text{H.c}\right) \tag{4.13}$$

where $Z_0 = \sqrt{L_0/C_0}$ is the characteristic impedance and $k_\omega = |\omega|/v$ is the wave vector. The subscripts *out* and *in* in the operators stand for the direction in which the signals are propagating, with $a_{\text{in}}(\omega) = \int dU g(U) e^{-i\omega U}$ and we interpret $a_{\text{out}}(\omega) = \int dV g(p_-(V)) e^{i\omega V}$. Rather than directly computing this latter integral, we shall obtain $a_{\text{out}}(\omega)$ by requiring the field (4.13) to satisfy the boundary condition (4.9). After a Fourier transformation this yields

$$\begin{aligned} 0 = \left(\frac{2\pi}{\Phi_0}\right)^2 \int_{-\infty}^{\infty} d\omega g(\omega,\omega')[\Theta(\omega)(a_\omega^{\text{in}} + a_\omega^{\text{out}}) + \Theta(-\omega)(a_{-\omega}^{\text{in}} + a_{-\omega}^{\text{out}})^\dagger] \\ -\omega'^2 C_J(a_{\omega'}^{\text{in}} + a_{\omega'}^{\text{out}}) + i\frac{k_{\omega'}}{L_0}(a_{\omega'}^{\text{in}} - a_{\omega'}^{\text{out}}) \end{aligned} \tag{4.14}$$

where

$$g(\omega,\omega') = \frac{1}{2\pi}\sqrt{\frac{|\omega'|}{|\omega|}} \int_{-\infty}^{\infty} \mathrm{d}t\, E_J(t) e^{-i(\omega-\omega')t} \tag{4.15}$$

Consider an arbitrary driving motion $E_J(t)$ with Fourier decomposition

$$E_J(t) = \frac{a_0}{2} + \sum_n a_n \cos(\omega_d n t) + \sum_n b_n \sin(\omega_d n t) \tag{4.16}$$

Writing the trigonometric functions as complex exponentials, we get

$$\begin{aligned} g(\omega,\omega') &= \sqrt{\frac{|\omega'|}{|\omega|}}\left[\frac{a_0}{2}\delta(\omega-\omega')\right. \\ &+ \sum_n \frac{a_n}{2}(\delta(\omega-\omega'-\omega_d n) + \delta(\omega-\omega'+\omega_d n)) \\ &+ \left.\sum_n \frac{b_n}{2i}(\delta(\omega-\omega'-\omega_d n) - \delta(\omega-\omega'+\omega_d n))\right] \end{aligned} \tag{4.17}$$

and inserting (4.17) into (4.14), then gives

$$
\begin{aligned}
0 =& \left(\frac{2\pi}{\Phi_0}\right)^2 \Bigg[\frac{a_0}{2} \int_{-\infty}^{\infty} \sqrt{\frac{|\omega'|}{|\omega|}} \left[\theta(\omega)(a_\omega^{\text{in}} + a_\omega^{\text{out}}) + \theta(-\omega)(a_{-\omega}^{\text{in}} + a_{-\omega}^{\text{out}})^\dagger\right] \delta(\omega - \omega') d\omega \\
&+ \sum_n \frac{a_n}{2} \int_{-\infty}^{\infty} \sqrt{\frac{|\omega'|}{|\omega|}} \left[\theta(\omega)(a_\omega^{\text{in}} + a_\omega^{\text{out}}) + \theta(-\omega)(a_{-\omega}^{\text{in}} + a_{-\omega}^{\text{out}})^\dagger\right] \times \\
&\qquad (\delta(\omega - \omega' - \omega_d n) + \delta(\omega - \omega' + \omega_d n)) d\omega \\
&+ \sum_n \frac{b_n}{2i} \int_{-\infty}^{\infty} \sqrt{\frac{|\omega'|}{|\omega|}} \left[\theta(\omega)(a_\omega^{\text{in}} + a_\omega^{\text{out}}) + \theta(-\omega)(a_{-\omega}^{\text{in}} + a_{-\omega}^{\text{out}})^\dagger\right] \times \\
&\qquad (\delta(\omega - \omega' - \omega_d n) - \delta(\omega - \omega' + \omega_d n)) d\omega \Bigg] \\
&- \omega'^2 C_J (a_{\omega'}^{\text{in}} + a_{\omega'}^{\text{out}}) + i \frac{k_{\omega'}}{L_0} (a_{\omega'}^{\text{in}} - a_{\omega'}^{\text{out}})
\end{aligned} \tag{4.18}
$$

which after integrating becomes

$$
\begin{aligned}
0 \;=\; & \left(\frac{2\pi}{\Phi_0}\right)^2 \Bigg[\frac{a_0}{2} \left[\theta(\omega')(a_{\omega'}^{\text{in}} + a_{\omega'}^{\text{out}}) + \theta(-\omega')(a_{-\omega'}^{\text{in}} + a_{-\omega'}^{\text{out}})^\dagger\right] \\
&+ \sum_n \frac{a_n}{2} \Bigg(\sqrt{\frac{|\omega'|}{|\omega' + \omega_d n|}} \left[\theta(\omega' + \omega_d n)(a_{\omega' + \omega_d n}^{\text{in}} + a_{\omega' + \omega_d n}^{\text{out}}) \right. \\
&\qquad \left. + \theta(-\omega' - \omega_d n)(a_{-\omega' - \omega_d n}^{\text{in}} + a_{-\omega' - \omega_d n}^{\text{out}})^\dagger\right] \\
&\qquad + \sqrt{\frac{|\omega'|}{|\omega' - \omega_d n|}} \left[\theta(\omega' - \omega_d n)(a_{\omega' - \omega_d n}^{\text{in}} + a_{\omega' - \omega_d n}^{\text{out}}) \right. \\
&\qquad \left. + \theta(-\omega' + \omega_d n)(a_{-\omega' + \omega_d n}^{\text{in}} + a_{-\omega' + \omega_d n}^{\text{out}})^\dagger\right] \Bigg) \\
&+ \sum_n \frac{b_n}{2i} \Bigg(\sqrt{\frac{|\omega'|}{|\omega' + \omega_d n|}} \left[\theta(\omega' + \omega_d n)(a_{\omega' + \omega_d n}^{\text{in}} + a_{\omega' + \omega_d n}^{\text{out}}) \right. \\
&\qquad \left. + \theta(-\omega' - \omega_d n)(a_{-\omega' - \omega_d n}^{\text{in}} + a_{-\omega' - \omega_d n}^{\text{out}})^\dagger\right] \\
&\qquad - \sqrt{\frac{|\omega'|}{|\omega' - \omega_d n|}} \left[\theta(\omega' - \omega_d n)(a_{\omega' - \omega_d n}^{\text{in}} + a_{\omega' - \omega_d n}^{\text{out}}) \right. \\
&\qquad \left. + \theta(-\omega' + \omega_d n)(a_{-\omega' + \omega_d n}^{\text{in}} + a_{-\omega' + \omega_d n}^{\text{out}})^\dagger\right] \Bigg) \Bigg] \\
&- \omega'^2 C_J (a_{\omega'}^{\text{in}} + a_{\omega'}^{\text{out}}) + i \frac{k_{\omega'}}{L_0} (a_{\omega'}^{\text{in}} - a_{\omega'}^{\text{out}})
\end{aligned} \tag{4.19}
$$

Assuming $\omega' > 0$ then $\theta(-\omega') = 0$ and $\theta(-\omega' - \omega_d n) = 0$. Also, we assume the SQUID plasma frequency is large ($|\omega|^2 C_J \ll 1$) so that we neglect the term with C_J and find

$$\begin{aligned}
0 &= a^{\rm in}_\omega(1 + ik_\omega L^0_{\rm eff}) + a^{\rm out}_\omega(1 - ik_\omega L^0_{\rm eff}) \\
&+ \sum_n \frac{a_n}{a_0}\left(\sqrt{\frac{\omega}{\omega - n\omega_d}}\theta(\omega - n\omega_d)(a^{\rm in}_{\omega - n\omega_d} + a^{\rm out}_{\omega - n\omega_d})\right. \\
&\qquad + \sqrt{\frac{\omega}{n\omega_d - \omega}}\theta(n\omega_d - \omega)(a^{\rm in}_{n\omega_d - \omega} + a^{\rm out}_{n\omega_d - \omega})^\dagger \\
&\qquad \left. + \sqrt{\frac{\omega}{\omega + n\omega_d}}(a^{\rm in}_{\omega + n\omega_d} + a^{\rm out}_{\omega + n\omega_d})\right) \\
&+ \sum_n \frac{b_n}{a_0 i}\left(-\sqrt{\frac{\omega}{\omega - n\omega_d}}\theta(\omega - n\omega_d)(a^{\rm in}_{\omega - n\omega_d} + a^{\rm out}_{\omega - n\omega_d})\right. \\
&\qquad - \sqrt{\frac{\omega}{n\omega_d - \omega}}\theta(n\omega_d - \omega)(a^{\rm in}_{n\omega_d - \omega} + a^{\rm out}_{n\omega_d - \omega})^\dagger \\
&\qquad \left. + \sqrt{\frac{\omega}{\omega + n\omega_d}}(a^{\rm in}_{\omega + n\omega_d} + a^{\rm out}_{\omega + n\omega_d})\right)
\end{aligned} \tag{4.20}$$

where

$$L^0_{\rm eff} = \left(\frac{\Phi_0}{2\pi}\right)^2 \frac{1}{L_0}\left(\frac{2}{a_0}\right) \tag{4.21}$$

and we have set $\omega' \to \omega$.

Equation (4.20) is the general relation determining $a^{\rm out}_\omega$ in terms of $a^{\rm in}_\omega$ for an arbitrary driving force. We can solve this equation perturbatively by writing

$$a^{\rm out}_\alpha = a^{\rm out}_{\alpha 0} + \sum_n a^{\rm out}_{\alpha n}\frac{a_n}{a_0} + \sum_n b^{\rm out}_{\alpha n}\frac{b_n}{i a_0} + O(2) \tag{4.22}$$

where we require $\frac{a_n}{a_0} \ll 1$ and $\frac{b_n}{a_0} \ll 1$ and where $a^{\rm out}_{\alpha n}$, $b^{\rm out}_{\alpha n}$ are the coefficients in the perturbation series that we will determine. Here $O(2)$ means second order in a_n/a_0 and b_n/a_0 With this, the 0th order term is

$$0 = a^{\rm in}_\omega(1 + ik_\omega L^0_{\rm eff}) + a^{\rm out}_{\omega 0}(1 - ik_\omega L^0_{\rm eff}) \tag{4.23}$$

yielding

$$a^{\rm out}_{\omega 0} = -\frac{1 + ik_\omega L^0_{\rm eff}}{1 - ik_\omega L^0_{\rm eff}} a^{\rm in}_\omega = R(\omega) a^{\rm in}_\omega \tag{4.24}$$

Using (4.24) and upon imposing the requirement that $k_\omega L^0_{\rm eff} \ll 1$ ($R(\omega) \approx -e^{2ik_\omega L^0_{\rm eff}}$), which gives an upper bound on frequencies where our treatment is valid, the 1st order term is

$$\begin{aligned} a^{\rm out}_{\omega n} = \frac{2iL^0_{\rm eff}}{v}\Big[&\sqrt{\omega}\sqrt{\omega - n\omega_d}\theta(\omega - n\omega_d)e^{i(k_\omega + k_{\omega - n\omega_d})L^0_{\rm eff}}a^{\rm in}_{\omega - n\omega_d} \\ &-\sqrt{\omega}\sqrt{n\omega_d - \omega}\theta(n\omega_d - \omega)e^{i(k_\omega - k_{n\omega_d - \omega})L^0_{\rm eff}}a^{in\dagger}_{n\omega_d - \omega} \\ &+\sqrt{\omega}\sqrt{\omega + n\omega_d}e^{i(k_\omega + k_{\omega + n\omega_d})L^0_{\rm eff}}a^{\rm in}_{\omega + n\omega_d}\Big] \end{aligned} \tag{4.25}$$

and similarly

$$\begin{aligned} b^{\rm out}_{\omega n} = \frac{2iL^0_{\rm eff}}{v}\Big[&-\sqrt{\omega}\sqrt{\omega - n\omega_d}\theta(\omega - n\omega_d)e^{i(k_\omega + k_{\omega - n\omega_d})L^0_{\rm eff}}a^{\rm in}_{\omega - n\omega_d} \\ &+\sqrt{\omega}\sqrt{n\omega_d - \omega}\theta(n\omega_d - \omega)e^{i(k_\omega - k_{n\omega_d - \omega})L^0_{\rm eff}}a^{in\dagger}_{n\omega_d - \omega} \\ &+\sqrt{\omega}\sqrt{\omega + n\omega_d}e^{i(k_\omega + k_{\omega + n\omega_d})L^0_{\rm eff}}a^{\rm in}_{\omega + n\omega_d}\Big] \end{aligned} \tag{4.26}$$

where we substituted $k_\alpha = \frac{|\alpha|}{v}$

Substituting Equations (4.24), (4.25) and (4.26) into (4.22), we finally get

$$\begin{aligned} a^{\rm out}_\omega &= R(\omega)a^{\rm in}_\omega \\ &+ \sum_n \Bigg(\left[\frac{a_n}{a_0}P(\omega, \omega - n\omega_d) - i\frac{b_n}{a_0}P^*(\omega, \omega - n\omega_d)\right] e^{i(k_\omega + k_{\omega - n\omega_d})L^0_{\rm eff}}a^{\rm in}_{\omega - n\omega_d} \\ &\quad + \left[\frac{a_n}{a_0}P^*(\omega, n\omega_d - \omega) - i\frac{b_n}{a_0}P(\omega, n\omega_d - \omega)\right] e^{i(k_\omega - k_{n\omega_d - \omega})L^0_{\rm eff}}a^{in\dagger}_{n\omega_d - \omega} \\ &\quad + \left[\frac{a_n}{a_0}P(\omega, \omega + n\omega_d) - i\frac{b_n}{a_0}P(\omega, \omega + n\omega_d)\right] e^{i(k_\omega + k_{\omega + n\omega_d})L^0_{\rm eff}}a^{\rm in}_{\omega + n\omega_d}\Bigg) \end{aligned} \tag{4.27}$$

where we have defined

$$P(\omega', \omega'') = \frac{2iL^0_{\rm eff}}{v}\sqrt{\omega'}\sqrt{\omega''}\theta(\omega')\theta(\omega'') \tag{4.28}$$

If the initial photon population of the field is given by that of a thermal bath of temperature T: $\bar{n}^{\rm in}_\omega = (\exp(\hbar\omega/k_{\rm B}T) - 1)^{-1}$, then

$$\begin{aligned} \bar{n}^{\rm out}_\omega = |R(\omega)|^2\bar{n}^{\rm in}_\omega + \frac{4(L^0_{\rm eff})^2}{v^2}\sum_n \Bigg[&\omega(|\omega - n\omega_d|)\left|\frac{a_n}{a_0} + i\frac{b_n}{a_0}\right|^2 \bar{n}^{\rm in}_{|\omega - n\omega_d|} \\ &+\omega(n\omega_d - \omega)\left|\frac{a_n}{a_0} + i\frac{b_n}{a_0}\right|^2 \Theta(n\omega_d - \omega) + \omega(\omega + n\omega_d)\left|\frac{a_n}{a_0} - i\frac{b_n}{a_0}\right|^2 \bar{n}^{\rm in}_{\omega + n\omega_d}\Bigg] \end{aligned} \tag{4.29}$$

Requiring that $k_{\rm B}T \ll \hbar\omega_d$, we neglect terms containing the small factor $\bar{n}^{\rm in}_{\omega+n\omega_d}$, finally obtaining

$$\begin{aligned}\bar{n}^{\rm out}_{\omega} &= |R(\omega)|^2\bar{n}^{\rm in}_{\omega} \\ &+ \frac{4(L^0_{\rm eff})^2}{v^2|a_0|^2}\sum_n\left[|a_n+ib_n|^2\left(\omega|\omega-n\omega_d|\bar{n}^{\rm in}_{|\omega-n\omega_d|}+\omega(n\omega_d-\omega)\Theta(n\omega_d-\omega)\right)\right] \quad (4.30)\end{aligned}$$

and upon using

$$\begin{aligned}E_J(t) &= \frac{a_0}{2}+\sum_n a_n\cos(\omega_d n t)+\sum_n b_n\sin(\omega_d n t) \\ &= E^0_J+\delta E_J(t) \quad (4.31)\end{aligned}$$

we compute an effective length

$$L_{\rm eff} = \left(\frac{\Phi_0}{2\pi}\right)^2\frac{1}{E_J(t)}\frac{1}{L_0} = \left(\frac{\Phi_0}{2\pi}\right)^2\frac{1}{E^0_J+\delta E_J(t)}\frac{1}{L_0} \approx L^0_{\rm eff}-\delta L_{\rm eff} \quad (4.32)$$

with

$$\delta L_{\rm eff} = L^0_{\rm eff}\left(\frac{\delta E_J(t)}{E^0_J}\right) \quad (4.33)$$

If we want to simulate a trajectory with a position given by $x = Z(t)$, then upon comparison with (4.11) we obtain

$$z(t) = \delta L_{\rm eff} \Rightarrow \delta E_J(t) = \frac{E^0_J}{L^0_{\rm eff}}z(t) \quad (4.34)$$

and given $z(t)$ and its Fourier coefficients $\{\tilde{a}_0, \tilde{a}_m, \tilde{b}_m\}$ we find

$$\begin{aligned}\tilde{a}_0 &= 0 \\ \tilde{a}_m &= \frac{4}{a_0^2L_0}\left(\frac{\Phi_0}{2\pi}\right)^2 a_m \\ \tilde{b}_m &= \frac{4}{a_0^2L_0}\left(\frac{\Phi_0}{2\pi}\right)^2 b_m \quad (4.35)\end{aligned}$$

Recall that the external driving field as a function of the external flux is given by $E_J(t) = 2E_J|\cos\left(\frac{\pi\Phi_{\rm ext}(t)}{\Phi_0}\right)|$. Consequently

$$\Phi_{\rm ext}(t) = \frac{\Phi_0}{\pi}\cos^{-1}\left(\frac{E_J(t)}{2E_J}\right) \quad (4.36)$$

so the external flux as a function of the desired trajectory is

$$\Phi_{\text{ext}}(t) = \frac{\Phi_0}{\pi} \cos^{-1}\left(\frac{E_J^0}{2E_J}\left(1 + \frac{z(t)}{L_{\text{eff}}^0}\right)\right) \tag{4.37}$$

The last expression provides us with the time dependent externally applied flux required to obtain the trajectory $z(t)$ to be simulated.

4.3 Parameters for relativistic trajectories

In this section we suggest physically relevant parameters for the relativistic trajectories SM, SA, and AUA (described in Section 4.1) and compute the number of photons produced for each. From Equations (4.2), (4.4) and (4.6), we see that each trajectory has a characteristic acceleration parameter (generically denoted A) that will roughly determine the scale of the proper acceleration. Respectively A is $R\omega_d^2$ for SM, α for SA and a for AUA.

The time averaged proper acceleration for each trajectory is calculated using Equation (4.1), as presented in Section 4.1. We reproduce these in Table 4.1 for convenience. We notice that $\bar{a}$ is a monotonically increasing function of the accelerating parameter A for fixed frequency. For fixed A and varying frequency, $\bar{a}$ is monotonically increasing for SM and monotonically decreasing for SA.

	SM	SA	AUA
$\bar{a}$	$\frac{v\omega_d \tanh^{-1}\left(\frac{R\omega_d}{v}\right)}{E\left(\frac{R^2\omega_d^2}{v^2}\right)}$	$\frac{v\omega_d \sinh^{-1}\left(2\frac{\alpha}{v\omega_d}\right)}{F\left(\frac{\pi}{2},-4\left(\frac{\alpha}{v\omega_d}\right)^2\right)}$	a

Table 4.1: Time averaged proper accelerations for the three trajectories studied. $F(\phi, m)$ and $E(\phi, m)$ are elliptic integrals of the first and second kind respectively.

As an estimator of how relativistic the trajectory is we can compare $\bar{a}t$ with the effective speed of light v. If $\bar{a}t \lesssim v$ the trajectory would be significantly relativistic. For a realistic propagation velocity of photons in the waveguide of $v = \frac{2}{5}c = .4c$ [4], this means that $\bar{a}t = \frac{\bar{a}2\pi}{\omega_d} \approx \frac{2}{5}c$ or $\bar{a}\frac{2\pi}{\omega_d}\frac{5}{2c} \approx 1$, so if $\frac{\omega_d}{2\pi} \sim O(10^{10})$ Hz, then $\bar{a} \sim O(10^{17})$ $\mathrm{m\,s^{-2}}$. We remark that by ω, ω_d we mean angular frequencies, that is $2\pi\nu$, where ν is the linear frequency.

The values of the parameters employed in [4] are summarized in Table 4.2. These parameters yield a proper acceleration for the sinusoidal motion simulated in [4] of $\bar{a} =$

$9.054 \times 10^{17}\ \mathrm{m\,s^{-2}}$, then $\bar{a}\frac{2\pi}{\omega_d}\frac{5}{2c} = 0.419$. For this acceleration and the oscillation period considered, neither the SA nor AUA trajectories will yield any significant difference with the simple sinusoidal motion as we will see in Section 4.5.

	SM
$\frac{\omega_d}{2\pi}$	18 GHz
$E_J^0 = \frac{a_0}{2}$	$1.3E_J$
a_1	$\frac{\left(\frac{a_0}{2}\right)}{4}$
E_J	$I_c\left(\frac{\phi_0}{2\pi}\right)$
I_c	$1.25\,\mu$A
C_J	90 fF
v	$.4c$
$Z0$	$55\,\Omega$
$\omega_s/2\pi$	37.3 GHz

Table 4.2: Parameters used in [4].

In order to obtain significant differences between the SM and the other two trajectories we need to work with larger $\bar{a}$ so as to reach speeds that are closer to the effective speed of light, and thus have larger contributions from higher than first order Fourier coefficients in (4.16). We are constrained by the fact that the speed of the wall cannot be faster than the speed of light. Both the SA and AUA trajectories already incorporate this constraint by construction, but in the case of sinusoidal motion, not every value of the characteristic acceleration parameter is possible. In this case we will have the constraint

$$R\omega_d < v \tag{4.38}$$

This means that for a maximum driving frequency of $\frac{\omega_d}{2\pi} = 40$ GHz, and $v = .4c$, then $R < .4775$mm.

We therefore impose three requirements in choosing our parameters. First, we set $\bar{a}(A, \omega_d) = 20 \times 10^{18}\ \mathrm{m\,s^{-2}}$ and fix the same driving frequency ω_d for the trajectories. Next we select the characteristic acceleration parameter A and driving frequency ω_d such that we retain the higher order contributions for the SA and AUA trajectories while ensuring that $\frac{E_J^0}{E_J} > 0.1$. Finally, we maximize the quantity $\frac{\bar{a}(A,\omega_d)}{\omega_d}$ so as to maximally amplify the contribution of the motions. The first criterion provides a point of comparison between trajectories, the second gives a region on the plane (A,ω_d) in which we can perform the

experiment, and the third selects the parameters in which the trajectory is 'maximally relativistic' given the other constraints.

We find these criteria imply that $\alpha = 13.725 \times 10^{18}\ \mathrm{m\,s^{-2}}$ for the SA motion and $a = 20 \times 10^{18}\ \mathrm{m\,s^{-2}}$ for the AUA motion and a driving frequency of $\frac{\omega_d}{2\pi} = 14.6$ GHz for both trajectories. For the SM, in order to keep the driving frequency less than the plasma frequency and still achieve an average acceleration of $20 \times 10^{18}\ \mathrm{m\,s^{-2}}$ we would need $R \geq .398$mm, and the greater the R, the smaller the required driving frequency. Due to Equation (4.38), $R < .4775$mm, and to achieve the desired acceleration the minimum driving frequency is $\frac{\omega_d}{2\pi} = 31.7$ GHz. This driving frequency is much bigger than the frequency needed for SA and AUA. For this reason we shall first consider these two cases, presenting the analogous results for the sinusoidal case at the end of this work with the parameters used in [4] (presented in Table 4.2).

We summarize in Table 4.3 the experimentally controlled parameters for the cases we subsequently analyze, unless otherwise specified.

	SA	AUA
$\bar{a}$	$20 \times 10^{18}\mathrm{m\,s^{-2}}$	$20 \times 10^{18}\mathrm{m\,s^{-2}}$
A	$\alpha = 13.725 \times 10^{18}\ \mathrm{m\,s^{-2}}$	$a = 20 \times 10^{18}\ \mathrm{m\,s^{-2}}$
$\omega_d/2\pi$	14.6 GHz	14.6 GHz
$E_J^0 = \frac{a_0}{2}$	$0.1002E_J$	$0.1006E_J$
a_1	$\frac{\left(\frac{a_0}{2}\right)}{4}$	$\frac{\left(\frac{a_0}{2}\right)}{4}$
E_J	$I_c\left(\frac{\phi_0}{2\pi}\right)$	$I_c\left(\frac{\phi_0}{2\pi}\right)$
I_c	$1.25\,\mu$A	$1.25\,\mu$A
C_J	90 fF	90 fF
v	$.4c$	$.4c$
$Z0$	$55\,\Omega$	$55\,\Omega$
$\omega_s/2\pi$	37.3 GHz	37.3 GHz

Table 4.3: Parameters used for each trajectory.

4.4 Results

With the parameters presented in Table 4.3, the Fourier coefficients for the SA and AUA trajectories are non vanishing but are quickly suppressed as n increases. We present them

in Figure 4.2. In both cases we find that we get an exponential suppression, and so can safely consider only the first 3 Fourier coefficients.

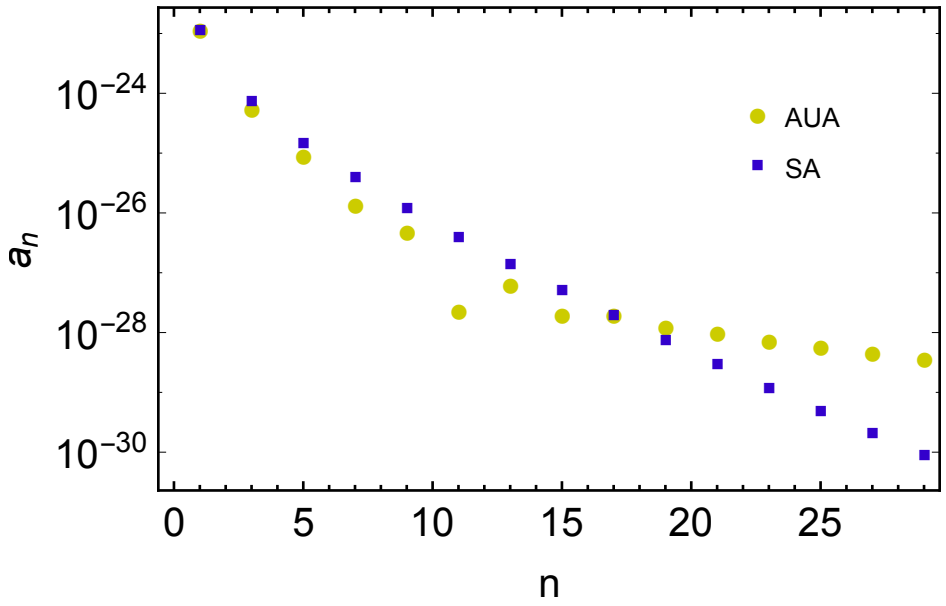

Figure 4.2: Fourier coefficients of the SA trajectory (blue squares) and AUA trajectory (green circles).

Using Equation (4.30) we can calculate the output number of photons as a function of the frequency ω and of the driving frequency ω_d. Fixing the driving frequency as in Table 4.3, we calculate $n_{\text{out}}(\omega)$ for different external temperatures. In Figure 4.3, we illustrate results for various values of the temperature of the thermal bath for each motion. We see that second order contributions are in principle detectable, as depicted in the insets.

In Figures 4.4 and 4.5 we calculate $n_{\text{out}}(\omega)$ (for two different fixed driving frequencies) and $n_{\text{out}}(\omega_d)$ (for two different fixed frequencies) respectively for two different temperatures of the thermal bath. For comparison purposes, we present both trajectories together. We can see that even though small, there is a difference in the statistics for different trajectories.

We see from Figures 4.4 and 4.5 that the different relativistic motions are indeed distinguishable from their spectrum, with the distinction becoming more pronounced at larger values of ω_d. The maximum of the curve in figure 4.4 occurs at values $\omega = n\omega_d/2$. An analytic expression for determining the maxima of the curves in Figure 4.5 can be given in terms of elliptic functions; we shall not reproduce it here.

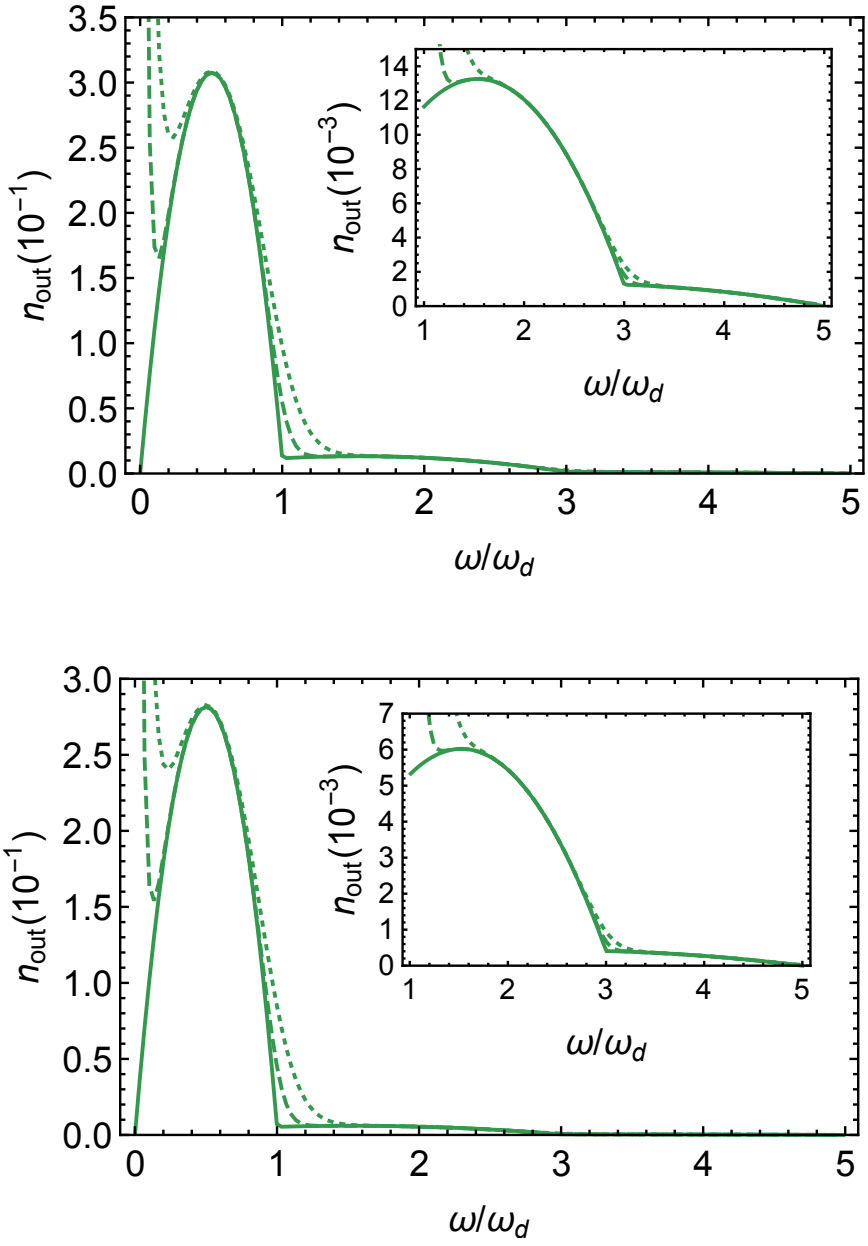

Figure 4.3: Plots comparing n_{out} at differing thermal bath temperatures $T = 0$K (solid), $T = 25$ mK(dashed) and $T = 50$ mK(dotted) and fixed $\omega_d/2\pi = 14.6$GHz as a function of ω/ω_d for SA trajectory (top) and AUA trajectory (bottom). The average acceleration for both trajectories is $\bar{a} = 20 \times 10^{18}$ m s^{-2}. The insets show detail for the second maximum.

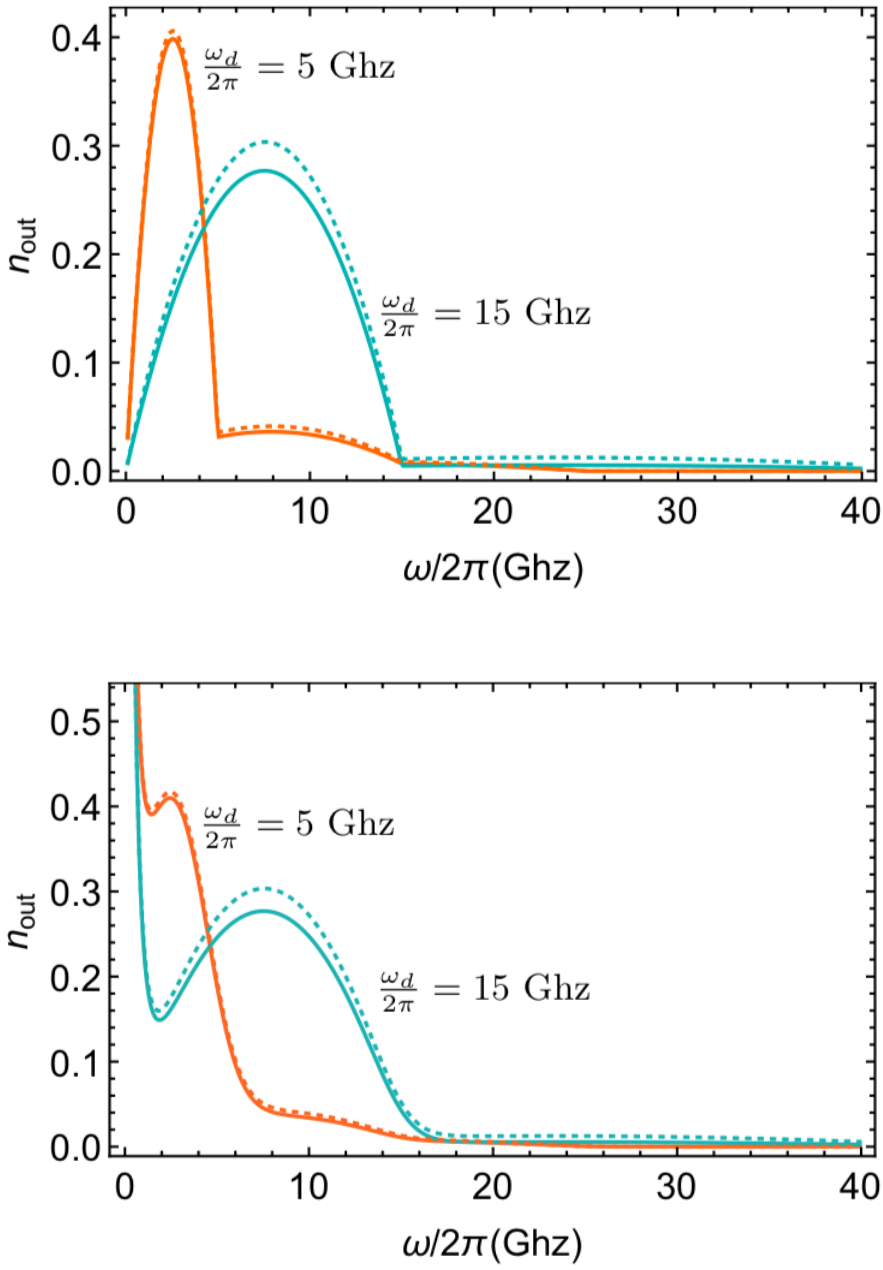

Figure 4.4: Output number of photons for varying frequency ω and fixed driving frequencies ω_d as indicated in the figure. The solid lines correspond to AUA trajectory and the dashed lines to SA trajectory, where both have the same average acceleration $\bar{a} = 20 \times 10^{18}$ m s^{-2} for $\omega_d/2\pi = 15$ GHz and $\bar{a} = 21.9 \times 10^{18}$ m s^{-2} for $\omega_d/2\pi = 5$ GHz, and for T=0 K (top) and T=25 mK (bottom), where T is the temperature of the thermal bath.

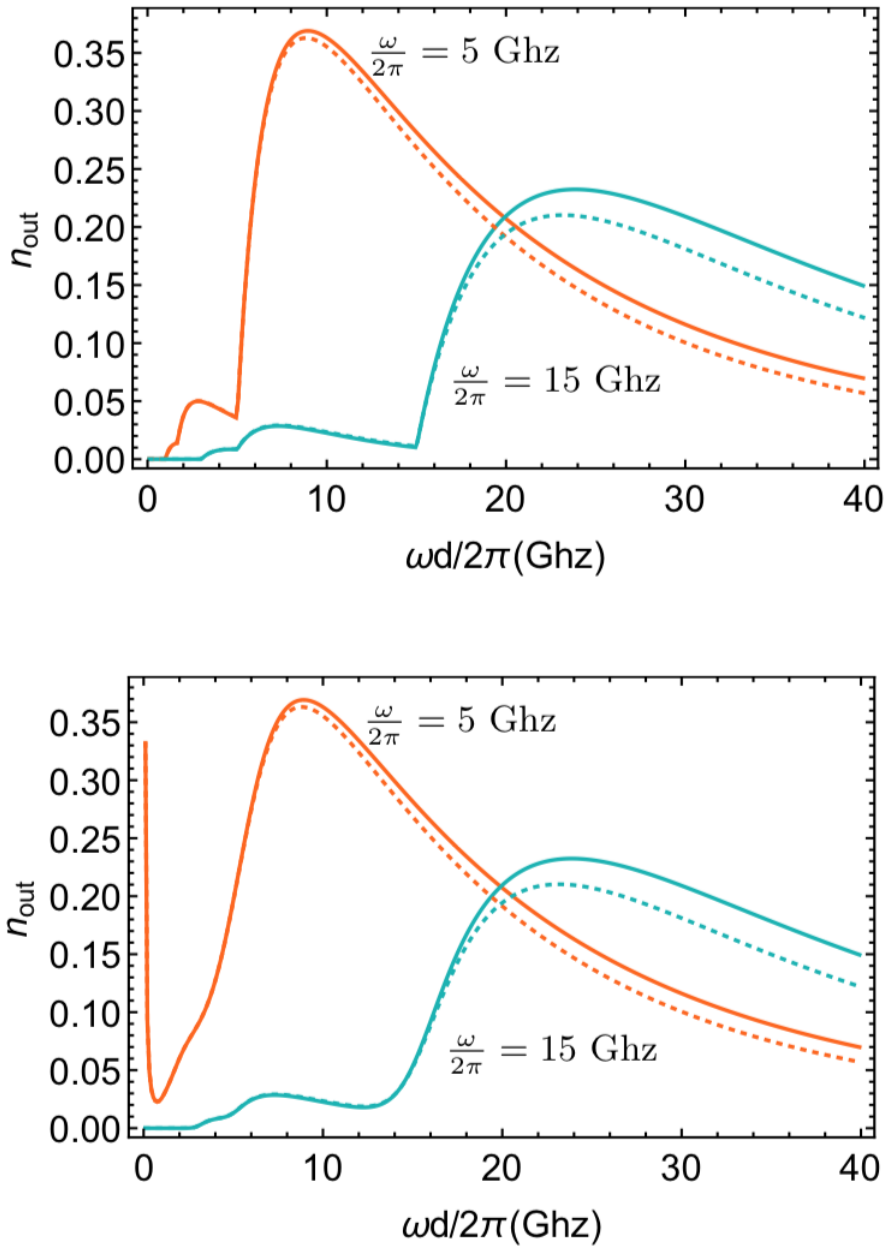

Figure 4.5: Output number of photons for varying driving frequency ω_d and fixed frequencies ω as indicated in the figure. The solid lines correspond to AUA trajectory and the dashed lines to SA trajectory, where both have the same average acceleration $\bar{a} = 20 \times 10^{18}$ $\mathrm{m\,s^{-2}}$ and for T=0 K (top) and T=25 mK (bottom), where T is the temperature of the thermal bath.

Finally we compute the output number of photons as a function of $\bar{a}$. Note that for AUA, the average acceleration is only a function of the acceleration parameter while for both SM and SA, due to the relativistic nature of the trajectories, the average proper acceleration depends nontrivially on the characteristic acceleration parameter and the driving frequency (periodicity of the motion).

Consequently there are two ways of having a variation in the acceleration. We can either fix the characteristic acceleration parameter and vary the driving frequency ω_d or we can fix the driving frequency ω_d and vary the characteristic acceleration parameter. We will consider the case where we vary the acceleration by varying the acceleration parameter A, since this is the variable that carries the units of acceleration. The result is presented in Figure 4.6, where we set the driving frequency to $\frac{\omega_d}{2\pi} = 14.6$ GHz. We notice that the output number of particles is an increasing monotonic function of the average acceleration.

4.5 Sinusoidal motion and the dynamical Casimir effect

Turning now to the SM case, this is essentially the same as that considered in the dynamical Casimir effect [79, 80, 4]. To order $R\omega_d$ we are unable to produce any distinctly relativistic effects for this motion as discussed in Section 4.3. As such, the DCE provides a cross-check on our approach. We set all the parameters to be the same as specified in [4] (presented in Table 4.2). These parameters give an effective length $L^0_{\text{eff}} = .44$ mm and a modulation $R = \delta L_{\text{eff}} = .11$ mm. With these parameters, we obtain the output number of photons calculated in [4].

To compare the three trajectories, we set the driving frequency for SA and AUA to be the same as the Sinusoidal case and we modulate the acceleration parameter such that the average acceleration is the same for the three of them, which is $\bar{a} = 9.054 \times 10^{17}\ \text{m}\,\text{s}^{-2}$ as in [4]. In Figure 4.7 we present the result for $n_{\text{out}}(\omega)$ as a function of $\frac{\omega}{\omega_d}$ and in Figure 4.8 for n_{out} as a function of $\bar{a}$. We notice that for this relatively small value of the acceleration, the output photon spectra for SA and SM is very similar, whereas the spectra for AUA is smaller. We also notice that the additional Fourier coefficients make noticeable changes in the output spectra only for higher values of the acceleration, as indicated in Figure 4.3 and in contrast to Figure 4.7.

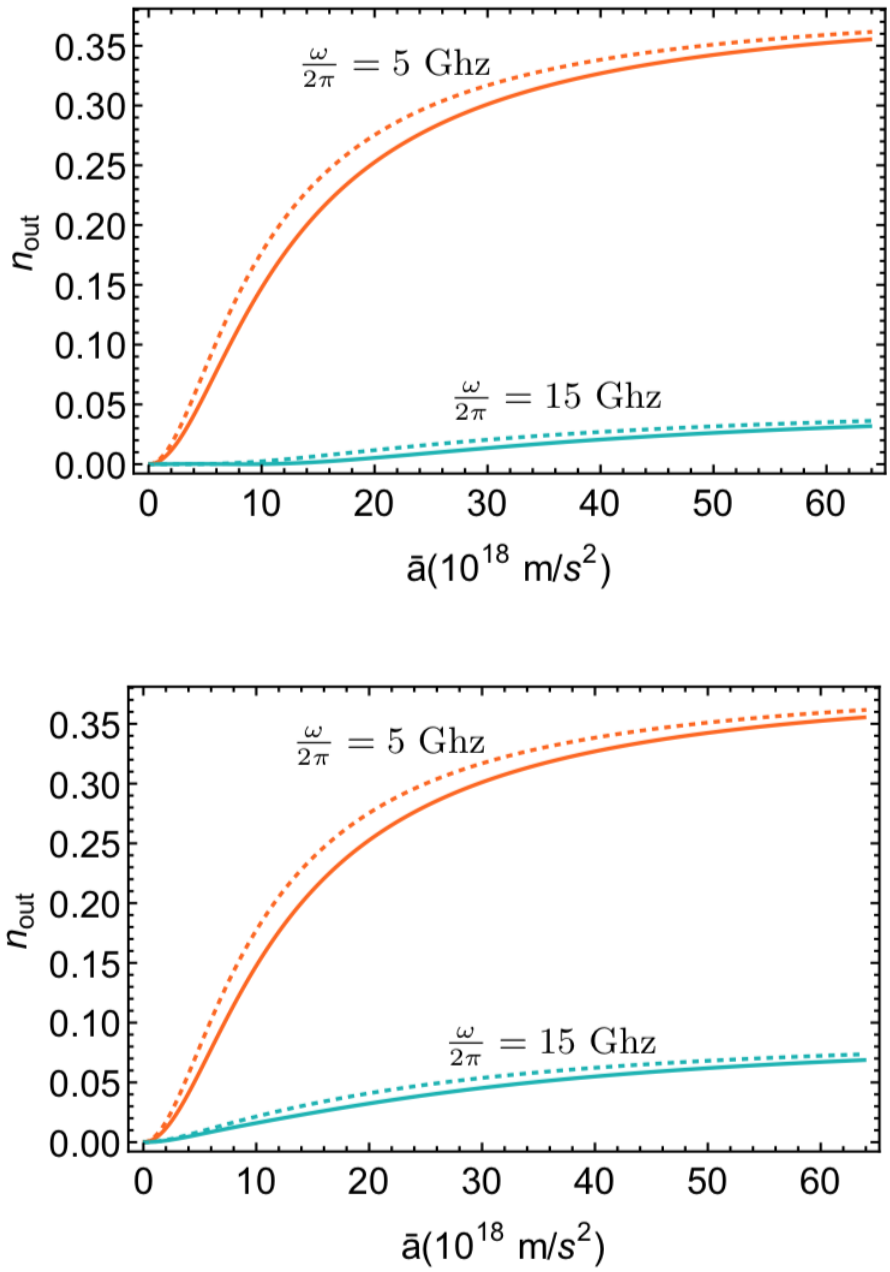

Figure 4.6: Output number of photons for varying $\bar{a}$ for fixed driving frequency $\omega_d/2\pi =$ 14.6GHz and varying the characteristic acceleration parameter A for different frequencies ω as indicated in the plots, where the solid lines correspond to AUA trajectory and the dashed lines to SA trajectory, at T=0 mK (top) and T=25 mK (bottom), where T is the temperature of the thermal bath.

4.6 Conclusions

We have seen that the dynamical Casimir effect yields different particle creation distributions depending on the trajectory of the moving boundary condition. Despite the limitations concerning the Dirichlet boundary condition inherent to the cQED implementation that we point out in this work, we have shown that a simulation of this effect in a superconducting circuit can distinguish different particle creation spectra due to different kinds of relativistic oscillatory motion (all of them yielding very similar periodic boundary trajectories as shown in Figure 4.1).

To relate our results to the phenomenology of the Unruh effect we can associate the average number of observed particles created by the time-dependence of the boundaries to a temperature estimator. This can be done by relating the observed output flux density to n_{out} in the same way as in [4]. Doing so yields a temperature estimator proportional to the average number of created particles $T \propto \hbar\omega n_{\text{out}}/k_{\text{B}}$. This temperature estimator could be compared with the temperature perceived by an accelerated Unruh-DeWitt detector following the same trajectories we impose in our moving boundaries.

These results may be helpful in shedding some light on a long debated question: How much can the dynamical Casimir effect be discussed in terms of the same physical phenomena behind the Unruh effect as seen by a freely accelerating particle detector? One might argue that all moving boundary condition effects are basically manifestations of the DCE, and as such this should also be the case of an accelerated atom. However the point of this study is the acceleration of the moving boundary conditions, and whether or not this picks up new features of the type expected from the Unruh effect for particle detectors with the same trajectories as studied in [47]. As we can see from our results, the temperature estimator does not really follow the simple behaviour of the response of particle detectors predicted in [47], which may be suggesting that, beyond constant acceleration, the DCE may not be so easy to relate to the Unruh effect, possibly because of these nonequilibrium effects showing up in very different ways for particle detectors and accelerating mirrors.

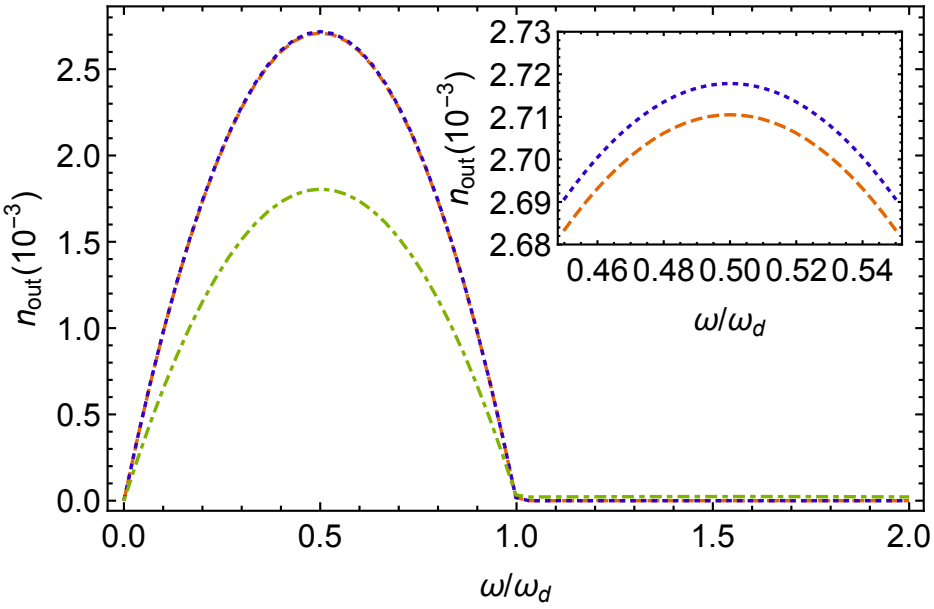

Figure 4.7: Plot comparing n_{out} at a thermal bath temperature of $T = 0$K and fixed $\omega_d/2\pi = 18$GHz as a function of ω/ω_d for Sinusoidal trajectory (red dashed), SA trajectory (blue dotted) and AUA trajectory (green dot-dashed). The average acceleration for all the motions is $\bar{a} = 9.054 \times 10^{17}\ \mathrm{m\,s^{-2}}$. The inset shows detail for the difference between Sinusoidal and SA.

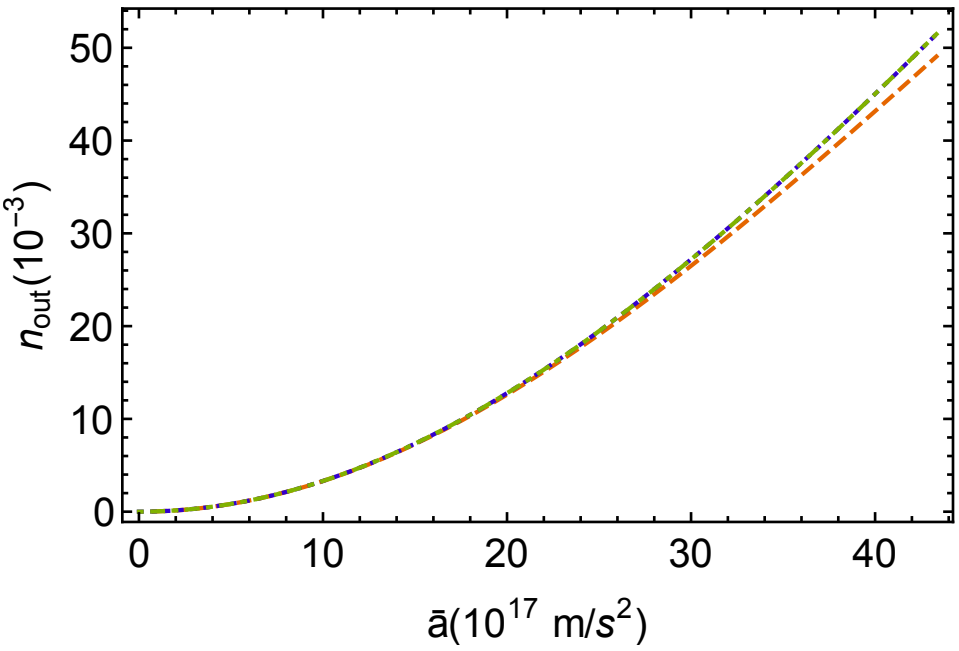

Figure 4.8: Plot comparing n_{out} at a thermal bath temperature of $T = 0$K and fixed frequency $\omega/2\pi = 9$GHz as a function of $\bar{a}$ where we fix $\omega_d/2\pi = 18$GHz for Sinusoidal trajectory (red dashed), SA trajectory (blue dotted) and AUA trajectory (green dot-dashed).

Part II

There is currently firm experimental evidence that macroscopic systems interact gravitationally [110]. On the other hand, quantum phenomena such as the superposition principle is exhibited by many systems [111, 112, 113, 114, 115, 116, 117, 118]. However there is a lack of direct observation of quantum gravitational phenomena [119] and at present there is no fully satisfactory consistent theory of quantum gravity [120].

These concerns have led to the question of whether gravity remains classical at a fundamental level, giving rise to a host of gravity-inspired modifications to quantum mechanics models built on the hypothesis of fundamentally classical gravity [14, 15, 20, 21, 22, 23, 24, 25, 26]. Such models include mechanisms that collapse the wavefunction of sufficiently massive objects to avoid non-classical states of the gravitational field at macroscopic scales, where classicality is understood as the lack of coherent spatial superposition [15, 121, 122, 123].

Recently a continuous measurement with feedback model was proposed where repeated interactions between two systems with a set of common ancillae results in an effective long range interaction between them [67, 68, 124]. This emerging force is accompanied by dissipation terms that ensure that the resulting dynamics are classical, where classicality here is understood as the inability of the resulting interaction to increase entanglement between the systems.

The application of this model to gravity by Kafri, Taylor and Milburn (KTM) [67, 68] aims to enforce classicality of gravitational interactions and predicts decoherence in the position basis of the CM of systems that interact gravitationally, with a decoherence rate of just the right amount so that the emergent interactions cannot increase entanglement between pairs of masses. So far the model produces an approximately Newtonian potential, which raises a series of questions like: What are the assumptions of the model? Can such assumptions be generalized? Is it possible to attain any kind of dynamics? Can we generate an exact Newtonian potential? How are the interactions and the decoherence rates related?

Motivated by these questions, we dedicate Chapter 5 to present our study on the type of dynamics that can emerge from a quantum collisional model where a system undergoes repeated interactions with a Markovian environment [2]. We quantify the decoherence that arises with the induced potential and show that for local linear interactions this decoherence is lower bounded. We also discuss how, by admitting more general interactions, a larger class of effective evolutions can emerge with arbitrarily low decoherence. While there are many studies of collisional models of an open system [125, 126, 127, 128, 129, 130], our focus is on the nature of the emergent interactions and its relation to decoherence.

Using the tools developed in our simple model of repeated interactions, in Chapter 6 we examine the assumptions and conditions that give rise to the KTM model described

above. We furthermore generalize the model to composite systems and show that recent single-atom interferometric experiments achieving large spatial superpositions [5, 6] present strong evidence against the KTM model. Since the lower bound of the KTM decoherence rate lies at the border that differentiates theories where the gravitational interaction of low energy particles is classical or quantum, our results are highly relevant to the understanding of the nature of gravitation, suggesting that gravity cannot be described as pairwise local classical channels connecting massive particles.

The material presented in Chapters 5 and 6 derives from [2] and [3] respectively, in collaboration with Natacha Altamirano, Robert B. Mann and Magdalena Zych.

Chapter 5

Continuous quantum measurements

The study of a system involves the study of its dynamics. Classical systems are deterministic in the sense that their physical description at a given time is well defined and unique. This is not true for quantum systems, where the system can be in a *coherent* quantum superposition of multiple states at the same time. The dynamics of a quantum system are dictated by Heisenberg equation and the system is said to evolve *unitarily*. However, when a system is opened to the outside world, the system undergoes interactions with the environment –i.e. other systems whose dynamics we want to neglect– which subjects the system to *decoherence*. This is because the joint system-environment forms a closed system and together they undergo unitary evolution; but after tracing out the latter, the final state of the system may not be given by a unitary transformation of its initial state [27, 131, 132].

Much effort has been devoted to the study of open quantum systems (see for example [125, 126, 127, 128, 133]). For instance, in the quantum information processing community, the interactions of a quantum system with its environment introduce unwanted noise. It is of central importance to understand these noise processes for building quantum information processing systems [134, 135].

In this chapter, we present our study on continuous measurements of a quantum system with a set of ancillae and the consequence these interactions have on its dynamics. The organization of this chapter is as follows: in Section 5.1 we give a brief presentation of quantum measurements discussing both projective measurements in 5.1.1 and general measurements in 5.1.2. We then present in Section 5.2 an open dynamics model of repeated interactions between a system and a set of independent ancillae. By considering different model parameters, such as state preparation, choice of the operators acting on the joint system and the interaction strengths, we obtain different limits for the dynamics

of the quantum system, from effective unitary in 5.2.1 to finite decoherence in 5.2.2. In Section 5.3 we generalize the model to a sequence of repeated interactions. We show how to recover unitary dynamics in 5.3.1 and how coherent-feedback of the quantum system can emerge in 5.3.2. In Section 5.4, by considering subsystems interacting with a set of common ancillae, we find the conditions under which effective interaction terms between them can arise, accompanied by dissipation whose lower bound we calculate. Finally, we present some discussion and conclusions in Section 5.5

5.1 Single shot measurements

The traditional presentation of quantum measurement is that of a projective measurement, in which the state of the system after the measurement *collapses* to one of the eigenstates of the observable that is measured [136]. The modern concept of quantum measurement dispenses with this description: a measurement is described as a quantum operation on the state of the system, with outcomes distributed according to a "Positive-Operator-Valued-Measure" (POVM) [137]. In the following, we give a brief presentation of both concepts (see e.g. [27, 138] for a comprehensive presentation).

5.1.1 Projective measurements

We start by presenting projective measurements. Suppose we want to measure an observable A. The spectral theorem allows us to write the associated operator $\hat{A}$ as

$$\hat{A} = \sum_a a\hat{\Pi}_a \tag{5.1}$$

where $\hat{\Pi}_a = \sum_i |\, a, i\rangle\langle a, i\,|$ – with $|\, a, i\rangle$ the basis for the Hilbert space of the system such that $\hat{A}|\, a, i\rangle = a|\, a, i\rangle$ – form a set of orthogonal projectors where $\hat{\Pi}_a\hat{\Pi}_{a'} = \delta_{a,a'}\hat{\Pi}_a$. Note that for convenience we have assumed a discrete spectrum. If the eigenvalues of $\hat{A}$ are non-degenerate, then $\hat{\Pi}_a = |\, a\rangle\langle a\,|$. When a measurement of A is performed, the result is one of the eigenvalues of $\hat{A}$. If the state of the system $\mathcal{S}$ is described by the density matrix ρ_s, the normalized state of the system after a time T, during which we measured A and obtained result a, is given by

$$\rho_s(t+T) = \frac{\hat{\Pi}_a\rho_s(t)\hat{\Pi}_a}{\mathrm{Tr}\left[\hat{\Pi}_a\rho_s(t)\right]} \tag{5.2}$$

We call this the *conditional* state of the system, where the system is *projected* into a subspace of the total Hilbert space.

We can also measure A and ignore the measurement outcome. In this case the state of the system is

$$\rho_s(t+T) = \sum_a \hat{\Pi}_a \rho_s(t) \hat{\Pi}_a \tag{5.3}$$

and we call it the *unconditional* state of the system, which is generally a mixed state.

The above description of quantum measurement is also called von Neumann measurement and it is the traditional first presentation of a quantum measurement [136].

5.1.2 General measurements

Realistically, the measurement of an observable of a system is not described by a projective measurement. A more accurate description of a measurement involves an interaction between the system and its environment [27, 138]. We can think of this process as having a closed system that is opened and subject to measurement. The environment consists of all systems interacting with the system whose observable we want to measure. We illustrate this process in the quantum circuit diagram presented in Figure 5.1.

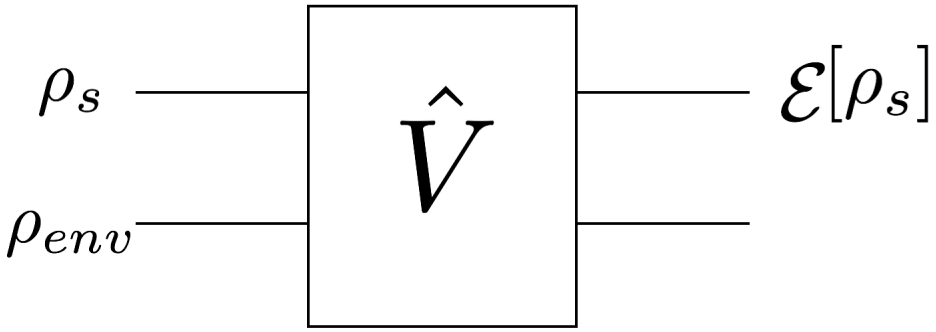

Figure 5.1: Quantum circuit diagram illustrating a quantum operation $\mathcal{E}$ on the state of the system ρ_s via a unitary interaction $\hat{V}$ with an environment ρ_{env}.

In Figure 5.1, $\mathcal{E}$ is a quantum operation over the initial state of the system $\mathcal{S}$ and ρ_s, ρ_{env} are the density matrices of the system and the environment respectively. Note that we assume that they start in an initially uncorrelated state.

There are an infinite number of degrees of freedom that one could consider for the environment. We employ a cutoff and consider the environment to consist of a second quantum system, which we call a meter or ancilla ($\rho_{env} \equiv \rho_m$). The joint state of the system and the meter at time t is described by the density matrix ρ_{sm}. We want to analyze the state of the system after it interacts with the meter during a finite time T after which the latter is projectively measured. We will consider the same two scenarios we considered before: one in which we look at the measurement result and one in which we don't.

The joint system evolves under the Hamiltonian $\hat{\mathcal{H}}_{sm}$ so the state of the joint system after an interaction time T is

$$\rho_{sm}(t+T) = \hat{V}(T)\rho_{sm}(t)\hat{V}^\dagger(T) \tag{5.4}$$

where

$$\hat{V}(T) = \mathcal{T}\exp\left(-\frac{i}{\hbar}\int_t^{t+T} \mathcal{H}_{sm}(t)dt \right) \tag{5.5}$$

We assume that at time t the system and the meter are initially uncorrelated, so $\rho_{sm}(t) = \rho_s(t)\rho_m(t)$, where $\rho_s(t)$, $\rho_m(t)$ are the state of the system and the meter respectively at time t. The unnormalized state of the joint system after measuring an observable R of the meter and getting a result r is

$$\rho_{sm}(t+T) = |\, r\rangle\langle r\,|\hat{V}(T)\rho_s(t)\rho_m(t)\hat{V}^\dagger(T)|\, r\rangle\langle r\,| \tag{5.6}$$

where we performed an operation $\mathbb{1}_s \otimes \hat{\Pi}_r = \mathbb{1}_s \otimes |\, r\rangle\langle r\,|$ over the state of the joint system at time $t+T$, with $\{|\, r\rangle\}$ an orthonormal basis for the Hilbert space of the meter. For simplicity we have assumed non-degenerate eigenvalues of the operator $\hat{R}$ associated with the observable R. Assuming the ancilla is in a pure state $\rho_m(t) = |\, \phi_m(t)\rangle\langle\phi_m(t)\,|$, Equation (5.6) is then

$$\rho_{sm}(t+T) = |\, r\rangle\langle r\,|\hat{V}(T)|\, \phi_m(t)\rangle\rho_s(t)\langle\phi_m(t)\,|\hat{V}^\dagger(T)|\, r\rangle\langle r\,| \tag{5.7}$$

We define the operators $\hat{M}_r = \langle r\,|\hat{V}(T)|\, \phi_m(t)\rangle$. These are operators acting on the system and whose properties we will analyze later. With this definition, the normalized state of the joint system is

$$\rho_{sm}(t+T) \quad = \frac{|\, r\rangle\langle r\,|\hat{M}_r\rho_s(t)\hat{M}_r^\dagger}{P_r} \tag{5.8}$$

where the probability of the measurement result being r after measuring the observable R is $P_r = \mathrm{Tr}\left([|\, r\rangle\langle r\,| \otimes \mathbb{1}_s]\, \hat{V}(T)\rho_s(t)\rho_m(t)\hat{V}^\dagger(T) \right) = \mathrm{Tr}_{\mathcal{S}}\left(\hat{M}_r^\dagger\hat{M}_r\rho_s(t) \right)$, with $\mathrm{Tr}_{\mathcal{S}}$ the partial trace over the system.

Tracing (5.8) over the state of the meter, we get the state of the system,

$$\rho_s^{(r)}(t+T) \quad = \frac{\hat{M}_r \rho_s(t) \hat{M}_r^\dagger}{\mathrm{Tr}_{\mathcal{S}} \left(\hat{M}_r^\dagger \hat{M}_r \rho_s(t) \right)} \tag{5.9}$$

We call (5.9) the *conditional* state of the system, since it is conditioned on obtaining measurement result r for the meter. If we discard the measurement result, the *unconditional* state of the system is

$$\rho_s(t+T) = \sum_r \hat{M}_r \rho_s(t) \hat{M}_r^\dagger \tag{5.10}$$

In order to preserve the trace, the system operators $\hat{M}_r$ must obey the the relation

$$\sum_r \hat{M}_r^\dagger \hat{M}_r = \mathbb{1} \tag{5.11}$$

We define the new operators $\hat{E}_r = \hat{M}_r^\dagger \hat{M}_r$, which from (5.11), obey the completeness relation $\sum_r \hat{E}_r = \mathbb{1}$. We notice that the probability of the measurement outcomes are determined by these new operators, since $P_r = \mathrm{Tr}_{\mathcal{S}} \left(\hat{E}_r \rho_s(t) \right)$. The complete set $\{\hat{E}_r\}$ is known as the "Positive-Operator-Valued-Measure" (POVM). To gain some intuition on this abstract formulation of quantum measurements, we proceed by presenting an example.

Example

In this example, we take the meter to be a measuring apparatus with a needle whose position x is the observable we will measure. For simplicity, we assume that the free evolution of the system and the meter are trivial and that they interact via the following Hamiltonian

$$\hat{\mathcal{H}}_{sm} = g(t) \hat{S} \otimes \hat{P} \tag{5.12}$$

where $g(t)$ is the interaction strength. Here $\hat{S}$ is an operator on the system and $\hat{P}$ is the momentum operator of the needle. The joint state thus evolves under

$$\hat{V} = \exp\left(-\frac{i}{\hbar} \bar{g} \hat{S} \otimes \hat{P} \right) \tag{5.13}$$

where under the assumption that $g(t)$ is continuous and differentiable over the interaction period $(t, t+T)$, we used the mean value theorem to define $\bar{g} := \frac{1}{T} \int_t^{t+T} g(t) dt$.

We can write the state of the meter in the position basis as

$$|\,\phi_m\rangle = \int \phi(x)|\,x\rangle dx \tag{5.14}$$

We consider the special case of a Gaussian meter, i.e. one in which the wavefunction $\phi(x)$ is a Gaussian function with mean μ and variance σ^2 such that

$$\phi(x) = \frac{1}{(2\pi\sigma^2)^{1/4}}\exp\left(-\frac{(x-\mu)^2}{4\sigma^2}\right) \tag{5.15}$$

The system operators $\hat{M}_r$ are given by

$$\begin{aligned}\hat{M}_r &= \langle x_r\,|e^{-\frac{i}{\hbar}\bar{g}\hat{S}\otimes\hat{P}}|\,\phi_m\rangle \\ &= \langle x_r - \bar{g}\hat{S}\,|\phi_m\rangle\end{aligned} \tag{5.16}$$

which can also be written as $\hat{M}_r = \phi(x_r - \bar{g}\hat{S})$. Considering $\mu = 0$ for simplicity, they become

$$\hat{M}_r = \frac{1}{(2\pi\sigma^2)^{1/4}}\exp\left(-\frac{(x_r-\bar{g}\hat{S})^2}{4\sigma^2}\right) \tag{5.17}$$

To understand their effect on the system, we assume the state of the system is pure and we write it in the basis of the $\hat{S}$ operator as

$$|\,\psi_s\rangle = \sum_i \psi_i|\,s_i\rangle \tag{5.18}$$

where $\hat{S}|\,s_i\rangle = s_i|\,s_i\rangle$. The conditional state of the system is

$$\hat{M}_r|\,\psi_s\rangle = \frac{1}{(2\pi\sigma^2)^{1/4}}\sum_i \exp\left(-\frac{(x_r-\bar{g}s_i)^2}{4\sigma^2}\right)\psi_i|\,s_i\rangle \tag{5.19}$$

and after the measurement, the needle is now in state $|\,x_r\rangle$ with probability

$$P_r = \frac{1}{(2\pi\sigma^2)^{1/2}}\sum_i |\psi_i|^2\exp\left(-\frac{(x_r-\bar{g}s_i)^2}{2\sigma^2}\right) \tag{5.20}$$

Denoting the variance of the eigenvalues as σ_S^2, if $\sigma^2 \gg \sigma_S^2$, the above probability distribution becomes a normal distribution centred at $\bar{g}\sum_i |\psi_i|^2 s_i$, which is proportional to the average of the eigenvalues of $\hat{S}$ and the change in the state of the system is negligible in

this limit. Therefore, you gain partial access to the state of the system without significantly perturbing it. In the limiting case where $\sigma^2 \to \infty$, the system is not perturbed but there is also no information gain.

The process described in this example, with gaussian distributions where the standard deviation is larger than the difference between the eigenvalues of the system, is what is known as a weak measurement [139].

5.2 Continuous measurements: general model

With the single-shot weak measurement method we gain some information about the system without disturbing it too much. Can we do many of these measurements to keep gaining information about the system? What is the effect on its state? Motivated by these questions, we study the types of dynamics that can emerge from a simple model of continuous interactions. The setup is as follows: we consider a system $\mathcal{S}$ and a set of n identically prepared ancillae $\mathcal{M}_r$, $r = 1, ..., n$. Note that from now on, we talk about *ancillas* as opposed to *meters* to emphasize the generality of the model, but their physical meaning is the same. Initially, the system is uncorrelated with the ancillae, couples to the first one for a time τ, decouples, then couples to the second one for time τ, decouples, and so on. This process repeats n times, one time for each ancilla, as illustrated in Figure 5.2 and can be thought of as a sequence of n of the single-shot measurements described above. This is equivalent to a collisional model [125, 126, 127, 128] of an open system, modelling interaction with a Markovian environment with relaxation time τ. During an r^{th} cycle the joint system $\mathcal{S} \otimes \mathcal{M}_r$ evolves under the Hamiltonian

$$\hat{\mathcal{H}}_{sm_r} = \hat{\mathcal{H}}_0 + g_r(t)\hat{\mathcal{H}}_I = \hat{S}_0 + \hat{M}_0 + g_r(t)\hat{S} \otimes \hat{M}\,, \tag{5.21}$$

where $\hat{S}_0$ acts only on the system, $\hat{M}_0$ acts only on the ancilla and $g_r(t)$ is the interaction strength, which is the same for each cycle ($g_r(t) = g_{r+1}(t + \tau)$). To simplify notation, we call $\hat{\mathcal{H}}_0 := \hat{S}_0 + \hat{M}_0$ the free Hamiltonian, containing only the free evolution of the subsystems and $\mathcal{H}_I := \hat{S} \otimes \hat{M}$ the interaction Hamiltonian. The latter is identical at each cycle: the same operators $\hat{S}$ and $\hat{M}$ act on $\mathcal{S}$ and $\mathcal{M}_r$ for each r. After the r^{th} interaction the joint state of the system and the respective ancilla is

$$\rho_{sm_r}(t_{r+1}) = \hat{U}_r(\tau)\rho_{sm_r}(t_r)\hat{U}_r^\dagger(\tau)\,, \tag{5.22}$$

where

$$\hat{U}_r(\tau) = \mathcal{T}\text{exp}\left(-\frac{i}{\hbar}\int_{t_r}^{t_r+\tau} \mathcal{H}_{sm_r}(t)dt \right). \tag{5.23}$$

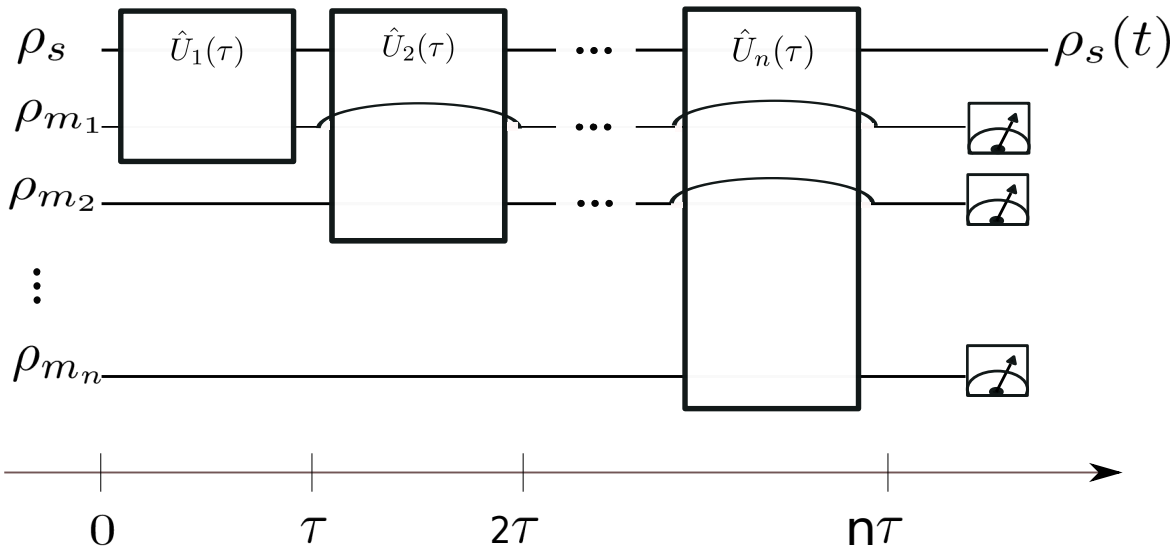

Figure 5.2: Quantum circuit illustrating time evolution of a system $\mathcal{S}$ undergoing repeated interactions with n ancillae. ρ_s is the initial state of the system and ρ_{m_i}, $i = 1, ..., n$ – of the i^{th} ancilla. During each step the system and the respective ancilla interact during a time τ, after which they decouple and the ancilla is discarded. This process is equivalent to performing n repeated single-shot measurements of the system, each one with a fresh meter. For identical ρ_{m_i}, the ancillae are also equivalent to a Markovian environment with relaxation time τ. In the limit $\tau \to 0$ the process describes a continuous quantum measurement of the system, or a memoryless collisional model of the system's environment.

We are interested in studying the dynamics of the system ρ_s in the limit of continuous interactions. We thus want the interaction time during each cycle to be vanishingly small while keeping a finite duration of the total interaction time. We achieve this by taking the limit:

$$n \to \infty, \quad \tau \to 0, \quad \text{such that} \lim_{n\to\infty, \tau\to 0} n\tau = T, \tag{5.24}$$

where T is the fixed finite total interaction time. In the context of single-shot measurements, this translates into doing infinitely many measurements of the observable $\hat{S}$ on the system, infinitely often, during a finite time interval T. From an open systems interpretation, this describes a memoryless environment.

We assume that the ancillae are identically prepared, so the final state of the system is described by n iterations of a superoperator $\mathcal{V}(\tau)[\rho_s] := \mathrm{Tr}_{\mathcal{M}}\{\hat{U}(\tau)(\rho_s \otimes \rho_m)\hat{U}^\dagger(\tau)\}$, where $\mathrm{Tr}_{\mathcal{M}}$ denotes the partial trace over the ancilla degrees of freedom, and ρ_m is the initial

state of the ancilla. The final state of the system after a time T is then

$$\rho_s(T) = \mathcal{E}[\rho_s(0)] = \lim_{n\to\infty} \mathcal{V}^n\left(\frac{T}{n}\right)[\rho_s(0)]\,, \tag{5.25}$$

This quantum operation is generally not unitary. The resulting dynamics in the continuous limit gives rise to a Markovian master equation, which we derive next.

If the interaction strength $g_r(t)$ is continuous and differentiable in the interval $(t_r, t_r+\tau)$ we can use the mean value theorem to get

$$\int_{t_r}^{t_{r+1}} \hat{\mathcal{H}}_{sm}\, dt = (\hat{\mathcal{H}}_0 + \bar{g}\hat{\mathcal{H}}_I)\tau, \tag{5.26}$$

where $\bar{g} = \frac{1}{\tau}\int_{t_r}^{t_r+\tau} g_r(t)\, dt$.

Under certain restrictions on the interaction strength $g_r(t)$, described in Appendix A, the density matrix of the system at time t_r can be written as

$$\rho_s(t_r) = \left(\hat{I} + \sum_{m=1}^{\infty} \mathcal{P}_m\right)[\rho_s(t_{r-1})]\,, \tag{5.27}$$

where $\mathcal{P}_m$ is the super-operator consisting of m commutators:

$$\mathcal{P}_m[\rho_s(t_r)] = \frac{1}{m!}\left(-\frac{i\tau}{\hbar}\right)^m \langle[\hat{\mathcal{H}}, [\hat{\mathcal{H}}, [..., [\hat{\mathcal{H}}, \rho_s(t_{r-1})]]]]\rangle_{\mathcal{M}_r}, \tag{5.28}$$

where $\hat{\mathcal{H}} := \hat{\mathcal{H}}_0 + \bar{g}\hat{\mathcal{H}}_I$. Here, $\langle A\rangle_{\mathcal{M}_r}$ denotes the trace over the degrees of freedom of the r^{th}-ancilla. Note that Equation (5.27) applies in particular for switching functions that are symmetric in time and applies to recent gravitational decoherence models [24, 67, 68], where we aim to apply results of this work.

We expand Equation (5.27) using Equation (5.28) to get

$$\begin{aligned}
\rho_s(t_n) &= \rho_s(t_{n-1}) - \frac{i}{\hbar}\tau[\hat{S}_0 + \bar{g}\langle\hat{M}\rangle\hat{S}, \rho_s(t_{n-1})] + \frac{i\tau^2}{2\hbar^2}\bar{g}\langle i[\hat{M}, \hat{M}_0]\rangle[\hat{S}, \rho_s(t_{n-1})] \\
&- \frac{\tau^2}{2\hbar^2}\Big([\hat{S}_0, [\hat{S}_0, \rho_s(t_{n-1})]] + \bar{g}\langle\hat{M}\rangle[\hat{S}, [\hat{S}_0, \rho_s(t_{n-1})]] + \bar{g}\langle\hat{M}\rangle[\hat{S}_0, [\hat{S}, \rho_s(t_{n-1})]]\Big) \\
&- \frac{\tau^2}{2\hbar^2}\bar{g}^2\langle\hat{M}^2\rangle[\hat{S}, [\hat{S}, \rho_s(t_{n-1})]] + \cdots
\end{aligned} \tag{5.29}$$

where $\langle \hat{M}^k \rangle \equiv \mathrm{Tr}_{\mathcal{M}}\{\hat{M}^k \rho_m\}$ for $k \in \mathbb{N}$. The equation of motion for the system at time T is obtained by taking the limit

$$\dot{\rho}_s(T) = \lim_{\tau \to 0, n \to \infty} \frac{\rho_s(t_n) - \rho_s(t_{n-1})}{\tau} \tag{5.30}$$

Equations (5.29) and (5.30) define a general quantum master equation for a system that undergoes repeated interactions with a set of identically prepared ancillae. We note that the coefficients of the commutators of the operators acting on the system consist of products of expectation values of operators acting on the ancillae and powers of the time interval τ and of the interaction strength $\bar{g}$. Consequently different types of dynamics for the system emerge, depending on the preparation of the ancillae, the operators acting on them, and the interaction strength $g(t)$. In what follows we present two particular limits of the emergent dynamics: effective unitarity and finite decoherence.

5.2.1 Effective unitarity

The evolution of a system is unitary if the dynamics follow the Heisenberg equation

$$\dot{\rho} = -\frac{i}{\hbar}[\hat{H}, \rho] \tag{5.31}$$

where $\hat{H}$ is a Hermitian operator. From Equation (5.29), one can see that if higher order terms $\propto \tau^k$ for $k \geq 2$ are small in comparison to the first order term, then the evolution is effectively unitary. This can be expressed as

$$\lim_{\tau \to 0} \frac{\tau^k \bar{g}^k \langle \hat{M}^k \rangle}{\tau \bar{g} \langle \hat{M} \rangle} = 0 \ , \quad k = 2, 3, \cdots \tag{5.32}$$

The terms that contain at least one $\hat{S}_0$ or $\hat{M}_0$ are multiplied by a factor $\tau^k \bar{g}^{k'}$ with $k' < k$. In the limit $\tau \to 0$, these terms are small compared to lower order ones, which are multiplied by $\tau^{k'} \bar{g}^{k'}$, and the limiting behaviour is met.

Under the conditions in Equation (5.32), the master equation becomes

$$\dot{\rho}_s = -\frac{i}{\hbar}[\hat{S}_0 + \Xi \hat{S}, \rho_s], \tag{5.33}$$

where we defined

$$\Xi := \lim_{\tau \to 0} \bar{g} \langle \hat{M} \rangle. \tag{5.34}$$

and the evolution of the system is approximately unitary. Then, by controlling the preparation of the ancilla and its coupling to the system, different potentials $\Xi\hat{S}$ can be generated. This result is commensurate with the one presented in [129].

We highlight that in the weak interaction regime, where $\lim_{\tau\to 0}\tau\bar{g} = 0$ and for fixed moments $\langle\hat{M}^k\rangle$, the master equation immediately follows Equation (5.33).

In the strong interaction regime, where $\lim_{\tau\to 0}\tau\bar{g} = C$ with $C = 1$ for simplicity, the conditions in Equation (5.32) become

$$\lim_{\tau\to 0}\langle\hat{M}^k\rangle/\langle\hat{M}\rangle \to 0 \tag{5.35}$$

and to ensure that Ξ stays finite, we need a τ-dependent state preparation of the ancillae. For example, we can choose an instantaneous interaction between the system and the ancilla, where the interaction strength is a delta function in time, such that $\bar{g} = \frac{1}{\tau}$ and therefore $\lim_{\tau\to 0}\tau\bar{g} = 1$. To keep Ξ finite, $\langle\hat{M}\rangle$ has to be $\propto \tau$, with its higher moments obeying Equation (5.35). An example of a suitable choice is an ancilla with a Gaussian distribution over the eigenvalues of $\hat{M}$ with a τ-dependent mean and variance given by $\mu\tau$ and $(\sigma\tau)^2$ respectively, with μ and σ constants. In this case, $\langle\hat{M}\rangle = \mu\tau$ and $\langle\hat{M}^k\rangle \propto \tau^k$, so the limit in Equation (5.35) vanishes and $\Xi = \mu$. This choice gives an effective unitary evolution for the system, subject to a potential $\mu\hat{S}$.

5.2.2 Finite decoherence

We now analyze the limit of finite decoherence, in the case where in Equation (5.29) only terms up to second order remain relevant. Together with Ξ defined in Equation (5.34), we define the constants

$$\begin{aligned}\Gamma &:= \lim_{\tau\to 0}\tau\bar{g}^2\langle\hat{M}^2\rangle \\ \tilde{M} &:= \lim_{\tau\to 0}\frac{\tau\bar{g}\langle i[\hat{M},\hat{M}_0]\rangle}{2\hbar}\end{aligned} \tag{5.36}$$

and assume all higher order terms vanish in the considered limit.

Using Equations (5.29), (5.30),(5.34) and (5.36), the master equation is

$$\dot{\rho}(t) = -\frac{i}{\hbar}[\hat{S}_0 + (\Xi - \tilde{M})\hat{S}, \rho] - \frac{\Gamma}{2\hbar^2}[\hat{S},[\hat{S},\rho]], \tag{5.37}$$

We can see that in addition to Ξ, a new term $\tilde{M}$ contributes to the unitary part of the evolution, provided that the commutator $[\hat{M},\hat{M}_0]$ doesn't vanish. The new double commutator $\propto \Gamma$ gives rise to decoherence of the system. Notice that this master equation has the form of the usual Born-Markov master equation [131].

An example where this can be achieved in the weak interaction regime ($\lim_{\tau\to 0}\tau\bar{g}=0$), is a Gaussian meter with fixed $\langle\hat{M}\rangle=\Xi/\bar{g}$ and with a τ-dependent second order moment $\langle M^k\rangle=\Gamma/\tau$. In the strong interaction regime ($\lim_{\tau\to 0}\tau\bar{g}=1$), a suitable choice is given by a Gaussian meter with τ-dependent mean $\Xi\tau$ and τ-dependent variance $\sigma^2=\Gamma\tau-(\Xi\tau)^2$.

Example

Let us present a concrete example. We work in the strong interaction regime ($\bar{g}=1/\tau$) and take $\hat{M}$ to be the momentum operator over the ancillae ($\hat{M}=\hat{p}_m$). For simplicity, we assume trivial free evolution for the ancillae ($\hat{M}_0=0$) and consider that these are prepared in a Gaussian state $|\,\phi\rangle$ with wave function

$$\phi(x)=\langle x|\,\phi\rangle=\frac{1}{(2\pi\sigma^2)^{1/4}}\exp\left(-\frac{(x-\mu)^2}{4\sigma^2}\right) \tag{5.38}$$

that is, a Gaussian ancilla with mean μ and variance σ^2. In this case we have

$$\begin{aligned}\langle\hat{M}\rangle&=\langle\hat{p}_m\rangle=0\\ \langle\hat{M}^2\rangle&=\langle\hat{p}_m^2\rangle=\frac{\hbar^2}{4\sigma^2}\end{aligned} \tag{5.39}$$

We substitute this in Equations (5.34) and (5.36) to get

$$\begin{aligned}\Xi&=0\\ \tilde{M}&=0\\ \Gamma&=\lim_{\tau\to 0}\frac{1}{\tau}\frac{\hbar^2}{4\sigma^2}\end{aligned} \tag{5.40}$$

In order to keep Γ finite, the variance has to be such that $\lim_{\tau\to 0}\tau\sigma^2=D$, with D a constant. This gives a master equation

$$\dot{\rho}(t)=-\frac{i}{\hbar}[\hat{S}_0,\rho]-\frac{1}{8D}[\hat{S},[\hat{S},\rho]], \tag{5.41}$$

In the context of quantum measurements, this is equivalent to considering a Gaussian meter with a τ-dependent variance that gets infinitely broad in the continuous limit. The resulting system dynamics exhibit finite decoherence, due to noise introduced by the measurements, but with no modifications to the unitary part. If we choose $\hat{S}=\hat{x}$, our Equation (5.41) reduces to a continuous position measurement derived in ref. [140].

5.3 Generalization to multiple observables

We now generalize the previous model to the case where an interaction is composed of p sub-interactions, each of duration $\tau' = \tau/p$. In the context of measurements, this corresponds to measuring multiple observables of the system. An illustration of this extension is presented in Figure 5.3.

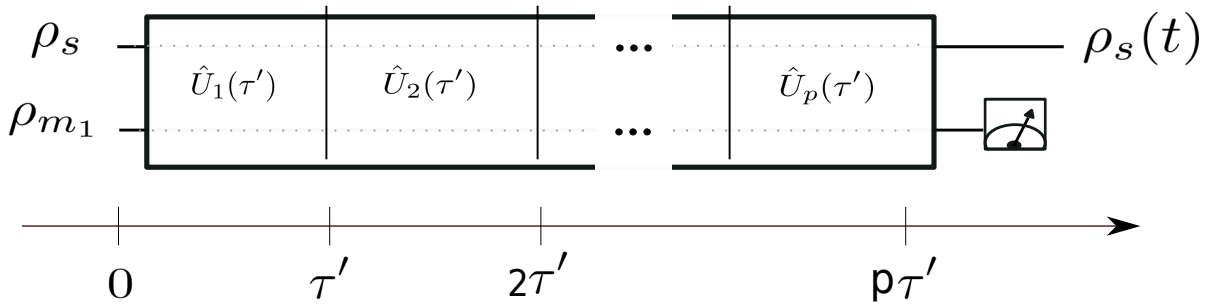

Figure 5.3: Quantum circuit diagram illustrating the first cycle, composed of p sub-cycles, of the interaction between a system $\mathcal{S}$ and an ancilla. At the end of the cycle, the ancilla is discarded. The process is repeated n times, each with a fresh ancilla.

Analogously to the previous section, the r^{th} cycle evolves under the Hamiltonian

$$\hat{\mathcal{H}}^{(p)}_{sm_r} = \hat{\mathcal{H}}_0 + \sum_{i=1}^{p} g_i(t)\hat{\mathcal{H}}^I_i \tag{5.42}$$

where $g_i(t)$ is the interaction strength of the i^{th} sub-cycle. The free Hamiltonian $\hat{\mathcal{H}}_0$ is defined as before and the interaction Hamiltonian of the i^{th} sub-cycle is $\hat{\mathcal{H}}^I_i = \hat{S}_i \otimes \hat{M}_i$, where S_i and $\hat{M}_i$, $i = 1, ..., p$ act only on the system $\mathcal{S}$ and on the r^{th} ancilla respectively. The density matrix of the joint system at time t_{r+1} is given by

$$\rho_{sm}(t_{r+1}) = \prod_{i=p}^{1} \hat{U}_i(\tau')\rho_{sm}(t_r) \prod_{i=1}^{p} \hat{U}^\dagger_i(\tau')\,, \tag{5.43}$$

where

$$U_i(\tau') = \mathcal{T}\exp\left(-\frac{i}{\hbar}\int_{t_r}^{t_r+\tau'} (\hat{\mathcal{H}}_0 + g_i(t)\hat{\mathcal{H}}^I_i)dt\right) \tag{5.44}$$

As before, we assume the switching function $g_i(t)$ is continuous in its support, the i^{th} sub-cycle of length τ', and use the mean value theorem to get $\bar{g}_i = \frac{1}{\tau'}\int_0^{\tau'} g_i(t)dt$. We expand

Equation (5.43) at time t_n in powers of τ and trace over the ancillae degrees of freedom to get

$$\begin{aligned}\rho(t_n) &= \rho - \sum_{i=1}^{p}\Bigg\{\frac{i}{\hbar}\tau'[\hat{S}_0 + \bar{g}_i\langle\hat{M}_i\rangle\hat{S}_i, \rho] - \frac{\tau'^2}{2\hbar^2}\sum_{j=1}^{i}(2-\delta_{ij})\Bigg[[\hat{S}_0,[\hat{S}_0,\rho]] \\ &+ \bar{g}_j\langle\hat{M}_j\rangle[\hat{S}_0,[\hat{S}_j,\rho]] + \bar{g}_i\langle\hat{M}_i\rangle[\hat{S}_i,[\hat{S}_0,\rho]] + \bar{g}_i\langle[\hat{M}_i,\hat{M}_0]\rangle[\hat{S}_i,\rho] \\ &+ \frac{\bar{g}_i\bar{g}_j}{2}\Big(\langle[\hat{M}_i,\hat{M}_j]\rangle[\hat{S}_i,\hat{S}_j\rho+\rho\hat{S}_j] + \langle\{\hat{M}_i,\hat{M}_j\}\rangle[\hat{S}_i,[\hat{S}_j,\rho]]\Big)\Bigg]\Bigg\} + \cdots \quad (5.45)\end{aligned}$$

where we defined $\rho \equiv \rho(t_{n-1})$.

Equation (5.45) is a generalization of Equation (5.29) to a series of p repeated interactions from which we obtain the equation of motion of the system $\mathcal{S}$ at time T.

5.3.1 Effective unitarity

The conditions for effective unitarity given in Equation (5.32) directly generalize to the multiple observables scenario. The master equation is now given by

$$\dot{\rho}(t) = -\frac{i}{\hbar}[\hat{S}_0 + \frac{1}{p}\sum_{i=1}^{p}\Xi_i\hat{S}_i, \rho(t)], \quad (5.46)$$

where

$$\Xi_i := \lim_{\tau'\to 0}\bar{g}_i\langle\hat{M}_i\rangle. \quad (5.47)$$

The system evolves effectively unitary and is subject to an average potential $\frac{1}{p}\sum_{i=1}^{p}\Xi_i\hat{S}_i$.

Just as in the single observable case, in the weak interaction regime, effective unitarity is a generic feature of the system's dynamics. In the strong interaction regime, effective unitarity can be achieved by having a τ-dependent state preparation of the ancillae.

5.3.2 Feedback

We now consider the conditions under which in Equation (5.45) only terms up to second order contribute to the system dynamics. Together with Ξ_i in Equation (5.47), we define

$$\begin{aligned}\Gamma_{ij} &:= \lim_{\tau'\to 0}\frac{1}{4}\tau'\bar{g}_i\bar{g}_j\langle\{\hat{M}_i,\hat{M}_j\}\rangle \\ \tilde{M}_{ij} &:= \lim_{\tau'\to 0}\frac{1}{4\hbar}\tau'\bar{g}_i\bar{g}_j\langle i[\hat{M}_i,\hat{M}_j]\rangle \quad (5.48)\end{aligned}$$

and assume that all higher order terms vanish in the considered limit. To better illustrate the emergence of feedback-control of the system, we analyze the particular case of two sequential interactions ($p = 2$). From Equations (5.30) and (5.45) (with $\tau = 2\tau'$), the master equation is

$$\begin{aligned}\dot{\rho}(t) &= -\frac{i}{\hbar}[\hat{S}_0 + (\frac{1}{2}\Xi_1 - \tilde{M}_{10})\hat{S}_1 + (\frac{1}{2}\Xi_2 - 3\tilde{M}_{20})\hat{S}_2, \rho] - \frac{i}{\hbar}\tilde{M}_{12}[\hat{S}_2, \hat{S}_1\rho + \rho\hat{S}_1] \\ &- \frac{1}{2\hbar^2}\sum_{i=1,2}\Gamma_{ii}[\hat{S}_i, [\hat{S}_i, \rho]] - \frac{1}{\hbar^2}\Gamma_{12}[\hat{S}_2, [\hat{S}_1, \rho]]) \end{aligned} \tag{5.49}$$

where in defining $\tilde{M}_{10}, \tilde{M}_{20}$ we introduced the convention $\bar{g}_0 \equiv 1$.

Similar to the case of one interaction, in this case terms $\propto \tilde{M}_{i0}$ contribute to the unitary dynamics if the commutators $[\hat{M}_i, \hat{M}_0]$ don't vanish. The double commutators $\propto \Gamma_{ij}$ give rise to decoherence of the system at a finite rate. We notice that there is a new term $\propto \tilde{M}_{12}$ that didn't appear before. This term can contribute to the unitary part of the system dynamics, and in particular, it can allow for the feedback-control of the system.

After the first interaction of the system and the ancilla via a Hamiltonian $\hat{S}_i \otimes \hat{M}_i$, the state of the meter is translated in the basis complementary to the eigenbasis of $\hat{M}_i$ by a magnitude that depends on the state of the system. The second interaction $\hat{S}_j \otimes \hat{M}_j$ will now transform the state of the system depending on the position of the meter, which carries a dependence on the system's $\hat{S}_i$-eigenvalue. This procedure results in an operation on the system that depends on its quantum state: a coherent-feedback [138, 141, 142, 143]. The feedback term, proportional to $\tilde{M}_{12}$, is at most of the same order as the also arising decoherence terms, proportional to Γ_{ii}. This is a consequence of the inequality

$$\langle(\bar{g}_1\hat{M}_1 - i\bar{g}_2\hat{M}_2)(\bar{g}_1\hat{M}_1 + i\bar{g}_2\hat{M}_2)\rangle \geq 0. \tag{5.50}$$

which gives a lower bound on the dissipation introduced in the system independently of the state of the ancillae, the interaction regime or the repetition rate. Note that if $\hat{M}_i$ and $\hat{M}_j$ are a canonically conjugate pair of operators, then $[\hat{M}_i, \hat{M}_j] \propto i\mathbb{I}$ and the feedback-control doesn't depend on the state of the ancillae.

Let us consider the particular case in which in Equation (5.49) we take $\hat{S}_2 \propto \hat{S}_1 + \beta\hat{O}$ for $[\hat{O}, \hat{S}_1] \neq 0$. If $\beta = 0$, the feedback over the system contributes to the unitary dynamics as a quadratic potential in $\hat{S}_1$. For $\beta \neq 0$, the feedback can take the form of a dissipative force and contributes to the decoherence of the system.

We want to highlight that the bound on dissipation coming from Equation (5.50) holds under the assumption that only measurements that are linear in the system operators can

be realized by the ancillae. If interactions of the form $\hat{V}\otimes\hat{M}$, for arbitrary system operators $\hat{V}$ are allowed, potential terms $\propto\langle\hat{M}\rangle\hat{V}$ can be induced and noise-free feedback could be realized. For example, if $\hat{S}_2 \propto \hat{S}_1^2$, a quadratic potential arises already in the effective unitarity regime.

Equation (5.49) is valid when the quantities Ξ_i, Γ_{ij}, $\tilde{M}_{ij}$ remain finite in the limit $\tau' \to 0$, while contributions from higher moments vanish. We now present an example where these conditions are satisfied.

Example

For illustrative purposes, we build up on the example presented in Section 5.2.2. We again assume trivial free evolution for the ancillae ($\hat{M}_0 = 0$) and take the first operator acting on the ancilla to be the momentum operator ($\hat{M}_1 = \hat{p}_m$) while the second operator is taken to be the position operator ($\hat{M}_2 = \hat{x}_m$). We consider that the ancillae are prepared in a state $|\,\phi\rangle$ with a Gaussian wave function as in Equation (5.38). In this case we calculate

$$\begin{aligned}
\langle\hat{M}_0\rangle &= 0\,,\\
\langle\hat{M}_1\rangle &= \langle\hat{p}_m\rangle = 0\,,\\
\langle\hat{M}_2\rangle &= \langle\hat{x}_m\rangle = \mu\\
\langle\{\hat{M}_1,\hat{M}_1\}\rangle &= 2\langle\hat{p}_m^2\rangle = \frac{\hbar^2}{2\sigma^2}\\
\langle\{\hat{M}_2,\hat{M}_2\}\rangle &= 2\langle\hat{x}_m^2\rangle = 2\left(\sigma^2+\mu^2\right)\\
\langle\{\hat{M}_1,\hat{M}_2\}\rangle &= \langle\{\hat{x}_m,\hat{p}_m\}\rangle = 0\\
\langle i[\hat{M}_1,\hat{M}_2]\rangle &= \langle i[\hat{p}_m,\hat{x}_m]\rangle = \hbar
\end{aligned} \tag{5.51}$$

Considering $\mu = 0$ for simplicity, the limits in Equation (5.48) become

$$\begin{aligned}
\Xi_i &= 0 \quad \forall i\\
\Gamma_{11} &= \lim_{\tau'\to 0}\frac{1}{8}\tau'\bar{g}_1^2\frac{\hbar^2}{\sigma^2}\\
\Gamma_{22} &= \lim_{\tau'\to 0}\frac{1}{2}\tau'\bar{g}_2^2\sigma^2\\
\tilde{M}_{12} &= \lim_{\tau'\to 0}\frac{\tau'\bar{g}_1\bar{g}_2}{4}
\end{aligned} \tag{5.52}$$

We assume that the first interaction is instantaneous, so that $\bar{g}_1 = \frac{1}{\tau'}$, and that in the second interaction $\bar{g}_2$ is fixed and finite. The non-vanishing terms are then

$$\begin{aligned}\Gamma_{11} &= \frac{\hbar^2}{8}\lim_{\tau'\to 0}\frac{1}{\tau'\sigma^2}\\ \Gamma_{22} &= \frac{\bar{g}_2^2}{2}\lim_{\tau'\to 0}\tau'\sigma^2\\ \tilde{M}_{12} &= \frac{\bar{g}_2}{4}\end{aligned} \tag{5.53}$$

In order to keep the above quantities finite, the variance has to be such that $\lim_{\tau'\to 0}\tau'\sigma^2 = D$, with D a finite constant. The variance is then a τ-dependent quantity that grows with the repetition rate. Therefore, in the continuous limit the Gaussian becomes infinitely broad. Taking $\bar{g}_2 = 1$ for simplicity, the master equation (5.49) in this example becomes

$$\begin{aligned}\dot{\rho}(t) &= -\frac{i}{\hbar}[\hat{S}_0,\rho(t)] - \frac{i}{4\hbar}[\hat{S}_2,\hat{S}_1\rho(t)+\rho(t)\hat{S}_1]\\ &- \frac{1}{16D}[\hat{S}_1,[\hat{S}_1,\rho(t)]] - \frac{D}{4\hbar^2}[\hat{S}_2,[\hat{S}_2,\rho(t)]]\,.\end{aligned} \tag{5.54}$$

In particular, if $\hat{S}_1 = 2\hat{x}_s$ so that in the first sub-cycle a measurement of the position is performed, the master equation is

$$\begin{aligned}\dot{\rho}(t) &= -\frac{i}{\hbar}[\hat{S}_0,\rho(t)] - \frac{i}{2\hbar}[\hat{S}_2,\hat{x}_s\rho(t)+\rho(t)\hat{x}_s]\\ &- \frac{1}{4D}[\hat{x}_s,[\hat{x}_s,\rho(t)]] - \frac{D}{4\hbar^2}[\hat{S}_2,[\hat{S}_2,\rho(t)]]\end{aligned} \tag{5.55}$$

This master equation was obtained in [140], where a model for a sequence of weak position measurements followed by a feedback mechanism was presented. By choosing $\hat{S}_2$ to be the position operator $\hat{x}_s$, a harmonic potential arises as feedback, with accompanying decoherence in the position basis.

5.4 Measurement-induced dynamics for composite systems

We now extend the previous model to the case of composite systems, in the simplest case where the system is bipartite. We now have n steps, each with p sub-steps, and during each sub-step the composite system interacts with an ancilla that is discarded at the end of

each step. During the i^{th} sub-step, the most general system operator acting on subsystems s_1, s_2 can be written as

$$\hat{S}_i = \sum_j c_j \hat{S}_{i,j}^{s_1} \otimes \hat{S}_{i,j}^{s_2} \,, \tag{5.56}$$

with c_j real coefficients. The operators $\hat{S}_{i,j}^{s_k}$ are operators acting on subsystem s_k, with $k = 1, 2$. We focus on the particular case where each ancilla interacts with one subsystem at a time, and does so only once per step. Under these assumptions, we can apply the model for multiple observables derived in Section 5.3 with $p = 2$. The systems operators acting on the i^{th} sub-step in Equation (5.56) are now

$$\begin{aligned} \hat{S}_1 &= \hat{S}_1^{s_1} \otimes \hat{\mathcal{I}}^{s_2} \,, \\ \hat{S}_2 &= \hat{\mathcal{I}}^{s_1} \otimes \hat{S}_2^{s_2} \,, \end{aligned} \tag{5.57}$$

where $\hat{\mathcal{I}}^{s_i}$ is the identity operator on the Hilbert space of subsystem s_i. This means that the ancilla interacts with subsystem s_1 during the first sub-step and with subsystem s_2 during the second sub-step.

The total Hamiltonian acting during the r^{th} step is

$$\hat{\mathcal{H}}^{(2)}_{s_1 s_2 m_r} = \hat{S}_0 + g_1(t)\hat{S}_1{}^{s_1} \otimes \hat{\mathcal{I}}^{s_2} \otimes \hat{M}_1 + g_2(t)\hat{\mathcal{I}}^{s_1} \otimes \hat{S}_2{}^{s_2} \otimes \hat{M}_2, \tag{5.58}$$

where the label (2) in the exponent of $\hat{\mathcal{H}}$ indicates that it is a two sub-step process, in accordance with Equation (5.42). The operators $\hat{M}_i$ act on the r^{th} ancillae in the same way as before and $g_i(t)$ is the interaction strength during the i^{th} sub-step. Notice that for simplicity, we have assumed that the ancillae have trivial free evolution (since $\hat{M}_0 \neq 0$ would give terms analogous to those discussed in Section 5.3).

The different regimes that emerge from this process are analogous to the ones discussed for the case of a single system. However the terms in the resulting master equation have a different physical interpretation. Since the operators contained in those terms act on different subsystems, they will in general cause the emergence of interactions between them. We use the master equation for a 2 sub-step process given in Equation (5.45) with the system operators of Equation (5.56) to get the master equation of the composite system

$$\begin{aligned} \dot{\rho}^{s_1,s_2}(T) &= -\frac{i}{\hbar}[\hat{S}_0 + \sum_{i=1,2}\frac{1}{2}\Xi_i \hat{S}_i^{s_i}, \rho^{s_1,s_2}] + \frac{i}{\hbar}\tilde{M}_{12}[\hat{S}_2^{s_2}, \hat{S}_1^{s_1}\rho^{s_1,s_2} + \rho^{s_1,s_2}\hat{S}_1^{s_1}] \\ &- \frac{1}{2\hbar^2}\sum_{i=1,2}\Gamma_{ii}[\hat{S}_i^{s_1}, [\hat{S}_i^{s_i}\rho^{s_1,s_2}]] - \frac{1}{\hbar^2}\Gamma_{12}[\hat{S}_2^{s_2}, [\hat{S}_1^{s_1}, \rho^{s_1,s_2}]]) \end{aligned} \tag{5.59}$$

with Ξ_i, Γ_{ij} and $\tilde{M}_{ij}$ as defined in Equations (5.47) and (5.48). Here ρ^{s_1,s_2} is the joint state of subsystems s_1 and s_2.

In analogy with the discussion presented in Section 5.3 for the single system case, the master equation (5.59) contains terms $\propto \Xi_i$ that contribute to the unitary evolution of the composite system and which can arise with negligible decoherence, terms $\propto \Gamma_{ij}$ that produce finite rate decoherence and a term $\propto \tilde{M}_{12}$, whose physical interpretation is different to the one given in the case of a single system. This term has the form

$$\propto \bar{g}_1 \bar{g}_2 \langle [\hat{M}_2, \hat{M}_1] \rangle [\hat{S}_2^{s_2}, \hat{S}_1^{s_1} \rho^{s_1,s_2} + \rho^{s_1,s_2} \hat{S}_1^{s_1}] \tag{5.60}$$

Note that in the commutator we have terms connecting different subsystems and can therefore give rise to effective interactions that can generate forces between them. Note that these forces can exist without the subsystems ever interacting directly with each other and are present just because of their interaction with common ancillae. Within the feedback interpretation, this can be thought of as an ancilla measuring system s_1 and then acting on system s_2 based on the result of the previous measurement.

We note that the above effective interactions cannot arise without inducing dissipation over the system of at least the same magnitude, in the same way that feedback is accompanied by dissipation in the case of a single sysem. In the present scenario, the lower bound on the magnitude of the induced decoherence also follows from the inequality (5.50). We emphasize that this conclusion does not hold if more general interactions are allowed. For example, if the ancillae can simultaneously interact with both subsystems, so that the system operators have the general form presented in Equation (5.56), then potential terms of the form $\sim \Xi_i \sum_j c_j \hat{S}_{i,j}^{s_1} \otimes \hat{S}_{i,j}^{s_2}$ can arise even at the effective unitarity regime, with no dissipation. Such interaction terms can even entangle the subsystems.

In the next chapter we shall present an example that makes use of the formalism developed here.

5.5 Conclusions

By considering a general model of repeated interactions of a system with ancillae in the continuous limit, we presented the conditions that give rise to different dynamics of the system. Therefore, by appropriately choosing the parameters of the model, namely ancillae state preparation, interaction strength and operators on the joint system-ancillae, the former can evolve unitarily or be subject to an effective potential with finite decoherence.

We also presented an extension of the model to the case where an interaction is composed of many different subinteractions and showed the emergence of feedback-control over

the system. Lastly, we demonstrated how interaction-free interactions between subsystems can be realized by letting the systems interact with common ancillae.

Finally, we discussed the observation that under the assumptions that only local linear interactions can be realized, the feedback and induced interactions terms are accompanied by decoherence, lower bounded by the magnitude of the emergent unitary potentials. However, if more general interactions are allowed, arbitrary potentials can arise free of decoherence.

Chapter 6

Gravity as a classical channel

We now consider the model presented in Chapter 5 in the context of gravitational interactions. Let us start by considering two masses m_1 and m_2 in equilibrium at a distance d apart along the x-axis. We define x_k to be the small displacement of the centre of mass m_k from its equilibrium position, with $x_k \ll d$. The classical Newtonian potential energy between them is $V_N = -\frac{Gm_1m_2}{d+x_2-x_1}$, which to second order in the relative displacement is

$$V_N \approx -G\frac{m_1m_2}{d}\left(1 - \frac{(x_2 - x_1)}{d} + \frac{(x_2 - x_1)^2}{d^2}\right)$$

The quantized Hamiltonian of the system is then approximated by

$$\hat{H} \approx \hat{S}_0 - G\frac{m_1m_2}{d}\left(1 - \frac{(\hat{x}_2 - \hat{x}_1)}{d} + \frac{(\hat{x}_2^2 + \hat{x}_1^2)}{d^2}\right) + 2G\frac{m_1m_2}{d^3}\hat{x}_1\hat{x}_2 \tag{6.1}$$

where $\hat{S}_0$ is the free evolution of each mass and with $\hat{x}_i$ the operator associated to the displacement of the centre of mass m_i from its equilibrium position. The potential contains local terms in $\hat{x}_1$ and $\hat{x}_2$ and an interaction term $\propto \hat{x}_1\hat{x}_2$ connecting both masses. It is natural to assume that the joint quantum system evolves under this Hamiltonian, but doing so would allow for the creation of entanglement between its parts, in contradiction to experimental results to date, where macroscopic systems behave classically. The lack of direct observation of quantum gravitational phenomena [119] has led to the speculation that gravity is fundamentally classical.

To discuss classical behaviour, we first need a notion of classicality. In [15, 121, 122, 123] the authors understand classicality as the suppression of spatial superpositions of macroscopic states whereas in [67, 68, 124], an interaction is understood to be classical if

it doesn't allow for the creation of entanglement and yet the expected classical dynamics are recovered.

To enforce such notions, different mechanisms that introduce noise into the system and that inhibit quantum effects are proposed. In [124], a condition that tests if a force emerging from a channel can generate entanglement is derived. If the condition is not met, quantum information is transmitted and the associated force is not classical in the sense that is allows for the creation of entanglement. The KTM model uses this result and provides such a mechanism [67, 68]. It postulates the existence of *gravitational* ancillae that interact continuously with two systems in a process following the one we presented in Chapter 5. An approximately Newtonian interaction between the systems emerges from the model, accompanied by lower bounded decoherence terms. Such noise terms, which arise as a consequence of the interactions between the system and the ancillae, allow for the emergence of classicality.

In this chapter, we present our work on continuous interactions in the gravitational sector. We organize it as follows: In Section 6.1 we derive the KTM model as a special case of our continuous interactions model presented in Chapter 5. In Section 6.2 we present an extension of the KTM model to systems composed of elementary subsystems. With the two models at hand, in Subsection 6.3 we consider a test mass in the presence of the Earth and derive some observational consequences of the models and we then test them agains atom interference experiments using large momentum transfer (LMT). In Section 6.4 we give an application of the model to torsion balance experiments. We end the chapter by presenting some discussion and conclusions in Section 6.5.

6.1 KTM model

In this section, we present the derivation of the KTM model. Since the aim is to obtain a gravitational interaction between the subsystems, it is natural to consider a symmetrized version of the model presented in Section 5.4 of Chapter 5, where a set of ancillae interact with two subsystems in a continuous manner. In the present case, a second ancillae is added, which interacts with s_2 in the first sub-step and with s_1 in the second sub-step. In general, we can visualize the resulting process through the circuit in Figure 6.1.

The process is as follows: we consider a bipartite system composed of subsystems s_1, s_2 which interact with a pair of ancillae m_1, m_2 (equivalently, we can think of the ancilla as a composite system with subsystems m_1, m_2). As in the previous chapter, we are looking for a continuous limit of a discrete in time protocol whose one step of duration τ is composed of two sub-steps, each of length $\tau' = \tau/2$. During the first sub-step subsystem s_1 interacts

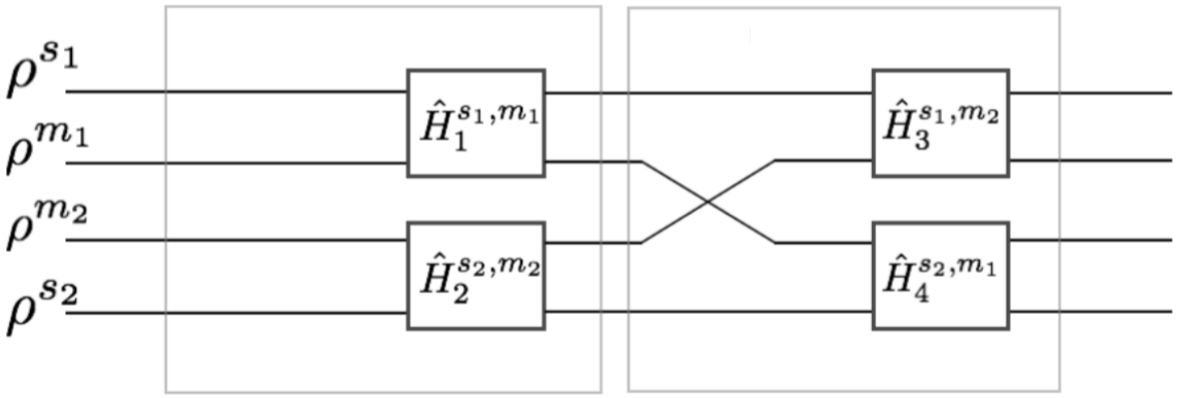

Figure 6.1: Composite system comprising subsystems s_1, s_2 prepared in the states ρ^{s_1}, ρ^{s_2} interacting with ancillae m_1, m_2, initially in the states ρ^{m_1}, ρ^{m_2}. If each ancilla interacts with only one subsystem at a time, the resulting effective interaction between the subsystems is always accompanied by decoherence.

with ancilla m_1 and subsystem s_2 interacts with ancilla m_2. In the second sub-step this is interchanged: s_1 interacts with m_2 and s_2 with m_1. Then the ancillae are discarded and the step repeats, a total of n times, each time with a pair of fresh ancillae. We can visualize the process through the circuit in Figure 6.1.

During each sub-step, the bipartite interaction between subsystem s_j, $j = 1, 2$ and ancilla m_k, $k = 1, 2$ is given by

$$\hat{H}_i^{s_j,m_k} = g_i(t)\hat{S}_i{}^{s_j} \otimes \hat{M}_i{}^{m_k}, \tag{6.2}$$

where $\hat{S}_i$ is an operator acting on subsystem s_j, $\hat{M}_i$ is an operator acting on the ancilla m_k and $g_i(t)$ the interaction strength. The index $i = 1, ..., 4$ labels the bipartite interactions, with $i = 1$ corresponding to the interaction between s_1 and m_1 and $i = 2$ between s_2 and m_2, both happening during the first sub-step. Likewise, $i = 3$ corresponds to an interaction between s_1 and m_2 and $i = 4$ between s_2 and m_1, both happening during the second sub-step. For simplicity, we assume that the ancillae have trivial free evolution, since incorporating it would simply add terms analogous to those already found in Section 5.3. Therefore, the total Hamiltonian during the r^{th} step is

$$\begin{aligned} \hat{\mathcal{H}}_r^{(2)} &= \hat{S}_0 + g_1(t)\hat{S}_1{}^{s_1} \otimes \hat{M}_1{}^{m_1} + g_2(t)\hat{S}_2{}^{s_2} \otimes \hat{M}_2{}^{m_2} \\ &+ g_3(t)\hat{S}_3{}^{s_1} \otimes \hat{M}_3{}^{m_2} + g_4(t) \otimes \hat{S}_4{}^{s_2} \otimes \hat{M}_4{}^{m_1} \end{aligned} \tag{6.3}$$

where $\hat{S}_0$ is the system's free Hamiltonian and the exponent (2) indicates that it is a two sub-steps process. Notice that unlike in Equation (5.58), we have only explicitly written the non trivial interactions. Following the same derivation as in the previous chapter, the master equation describing the dynamics of the subsystems at time T is

$$\begin{aligned}
\dot{\rho}^{s_1,s_2}(T) &= -\frac{i}{\hbar}[\hat{S}_0 + \frac{\Xi_1^{m_1}}{2}\hat{S}_1^{s_1} + \frac{\Xi_3^{m_2}}{2}\hat{S}_3^{s_1} + \frac{\Xi_2^{m_2}}{2}\hat{S}_2^{s_2} + \frac{\Xi_4^{m_1}}{2}\hat{S}_4^{s_2}, \rho^{s_1,s_2}] \\
&+ \frac{i}{\hbar}\left(\tilde{M}_{32}^{m2}[\hat{S}_3^{s_1}, \hat{S}_2^{s_2}\rho^{s_1,s_2} + \rho^{s_1,s_2}\hat{S}_2^{s_2}] + \tilde{M}_{41}^{m2}[\hat{S}_4^{s_2}, \hat{S}_1^{s_1}\rho^{s_1,s_2} + \rho^{s_1,s_2}\hat{S}_1^{s_1}]\right) \\
&- \frac{1}{2\hbar^2}\Big(\Gamma_{11}^{m_1}[\hat{S}_1^{s_1}, [\hat{S}_1^{s_1}, \rho^{s_1,s_2}]] + \Gamma_{33}^{m_2}[\hat{S}_3^{s_1}, [\hat{S}_3^{s_1}, \rho^{s_1,s_2}]] \\
&\qquad + \Gamma_{22}^{m_2}[\hat{S}_2^{s_2}, [\hat{S}_2^{s_2}, \rho^{s_1,s_2}]] + \Gamma_{44}^{m_1}[\hat{S}_4^{s_2}, [\hat{S}_4^{s_2}, \rho^{s_1,s_2}]]\Big) \\
&- \frac{1}{\hbar^2}\left(\Gamma_{23}^{m_2}[\hat{S}_3^{s_1}, [\hat{S}_2^{s_2}, \rho^{s_1,s_2}]] + \Gamma_{14}^{m_1}[\hat{S}_4^{s_2}, [\hat{S}_1^{s_1}, \rho^{s_1,s_2}]]\right) \qquad (6.4)
\end{aligned}$$

with ρ^{s_1,s_2} the joint state of both subsystems and where we have suppressed the redundant identity operators. The definitions for the finite constants $\Xi_i^{m_k}$, $\tilde{M}_{ij}^{m_k}$ and $\Gamma_{ij}^{m_k}$ are the same as in the previous chapter, but we present them again here for convenience

$$\begin{aligned}
\Xi_i^{m_k} &= \lim_{\tau'\to 0} g_i \langle \hat{M}_i^{m_k} \rangle \\
\Gamma_{ij}^{m_k} &= \lim_{\tau'\to 0} \frac{1}{4}\tau' g_i g_j \langle \{\hat{M}_i^{m_k}, \hat{M}_j^{m_k}\} \rangle \\
\tilde{M}_{ij}^{m_k} &= \lim_{\tau'\to 0} \frac{1}{4\hbar}\tau' g_i g_j \langle i[\hat{M}_i^{m_k}, \hat{M}_j^{m_k}] \rangle \qquad (6.5)
\end{aligned}$$

The analysis of the terms in the master equation (6.4) is the same as the one presented for Equation (5.59). The first line contains terms that yield effective unitary evolution. The third and fourth lines are decoherence terms for each subsystem, and the final line contains terms that introduce 'cross-decoherence' between the subsystems. The second line contains the terms

$$\tilde{M}_{32}^{m_2}[\hat{S}_3^{s_1}, \hat{S}_2^{s_2}\rho^{s_1,s_2} + \rho^{s_1,s_2}\hat{S}_2^{s_2}] + \tilde{M}_{41}^{m_2}[\hat{S}_4^{s_2}, \hat{S}_1^{s_1}\rho^{s_1,s_2} + \rho^{s_1,s_2}\hat{S}_1^{s_1}] \qquad (6.6)$$

Remember that these terms connect the two subsystems and thus introduce effective interactions that can generate forces between them. Consequently, two systems interacting only with common ancillae develop an effective interaction with each other. Here, the discussion about the magnitude of the induced decoherence applies as well: the magnitude

of the above effective interactions is at most of the same order as that of the induced decoherence, which follows from the inequality (5.50). If more general interactions are allowed, the induced terms could entangle the subsystems. Therefore, the assumption of bipartite interactions for the gravitational example as presented in [67, 68, 124] is essential.

Since our main aim was to keep the terms in Equation (6.6), we need the commutators $\langle[\hat{M_4}^{m_1}, \hat{M_1}^{m_1}]\rangle$ and $\langle[\hat{M_3}^{m_2}, \hat{M_2}^{m_2}]\rangle$ to be non vanishing. For simplicity, we choose the ancillae operators to be the momentum operators during the first sub-step and the position operators during the second sub-step, so

$$\hat{M_1}^{m_1} = \hat{p}^{m_1} \quad \hat{M_2}^{m_2} = \hat{p}^{m_2} \quad \hat{M_3}^{m_2} = \hat{x}^{m_2} \quad \hat{M_4}^{m_1} = \hat{x}^{m_1} \tag{6.7}$$

We assume that the ancillae are prepared in a Gaussian state as in Equation (5.38), with $\mu = 0$ for simplicity. Using Equations (5.51) and assuming instantaneous interactions for $\bar{g}_2$ and $\bar{g}_1$ (such that $\bar{g}_i = \frac{1}{\tau'}$ for $i = 1, 2$) and constant interactions for $\bar{g}_3$ and $\bar{g}_4$ (such that $\bar{g}_i = \chi_i$ for $i = 3, 4$), then we get the following master equation

$$\begin{aligned}
\dot{\rho}^{s_1,s_2} =& -\frac{i}{\hbar}[\hat{S}_0, \rho^{s_1,s_2}] - \frac{i}{4\hbar}\left(\chi_3[\hat{S}_3^{s_1}, \hat{S}_2^{s_2}\rho^{s_1,s_2} + \rho^{s_1,s_2}\hat{S}_2^{s_2}] + \chi_4[\hat{S}_4^{s_2}, \hat{S}_1^{s_1}\rho^{s_1,s_2} + \rho^{s_1,s_2}\hat{S}_1^{s_1}]\right) \\
&- \frac{D}{4\hbar^2}\left(\chi_3^2[\hat{S}_3^{s_1}, [\hat{S}_3^{s_1}, \rho^{s_1,s_2}]] + \chi_4^2[\hat{S}_4^{s_2}, [\hat{S}_4^{s_2}, \rho^{s_1,s_2}]]\right) \\
&- \frac{1}{16D}\left([\hat{S}_1^{s_1}, [\hat{S}_1^{s_1}, \rho^{s_1,s_2}]] + [\hat{S}_2^{s_2}, [\hat{S}_2^{s_2}, \rho^{s_1,s_2}]]\right)
\end{aligned} \tag{6.8}$$

where σ^2 is chosen such that $D = \lim_{\tau' \to 0} \tau'\sigma^2$ remains finite. If we choose the subsystem operators $\hat{S}_1^{s_1} = 2\hat{S}_3^{s_1}$ and $\hat{S}_2^{s_2} = 2\hat{S}_4^{s_2}$ and set $\chi_3 = \chi_4 = K$, then this equation becomes

$$\begin{aligned}
\dot{\rho}^{s_1,s_2} =& -\frac{i}{\hbar}[\hat{S}_0, \rho^{s_1,s_2}] - \frac{iK}{2\hbar}\left([\hat{S}_3^{s_1}, \hat{S}_4^{s_2}\rho^{s_1,s_2} + \rho^{s_1,s_2}\hat{S}_4^{s_2}] + [\hat{S}_4^{s_2}, \hat{S}_3^{s_1}\rho^{s_1,s_2} + \rho^{s_1,s_2}\hat{S}_3^{s_1}]\right) \\
&- \frac{K^2 D}{4\hbar^2}\left([\hat{S}_3^{s_1}, [\hat{S}_3^{s_1}, \rho^{s_1,s_2}]] + [\hat{S}_4^{s_2}, [\hat{S}_4^{s_2}, \rho^{s_1,s_2}]]\right) \\
&- \frac{1}{4D}\left([\hat{S}_3^{s_1}, [\hat{S}_3^{s_1}, \rho^{s_1,s_2}]] + [\hat{S}_4^{s_2}, [\hat{S}_4^{s_2}, \rho^{s_1,s_2}]]\right) \\
=& -\frac{i}{\hbar}[\hat{S}_0 + K\hat{S}_3^{s_1}\hat{S}_4^{s_2}, \rho^{s_1,s_2}] - \left(\frac{K^2 D}{4\hbar^2} + \frac{1}{4D}\right)\left([\hat{S}_3^{s_1}, [\hat{S}_3^{s_1}, \rho^{s_1,s_2}]] + [\hat{S}_4^{s_2}, [\hat{S}_4^{s_2}, \rho^{s_1,s_2}]]\right)
\end{aligned}$$

The process then induces a potential term $K\hat{S}_3^{s_1}\hat{S}_4^{s_2}$ that contributes to the unitary dynamics of the joint system. We now make a connection to the case of two interacting masses presented at the beginning of the chapter. We assign s_1 to be the mass m_1 and s_2

to be the mass m_2 and we choose $\hat{S}_3^{s_1} = \hat{x}_1$ and $\hat{S}_4^{s_2} = \hat{x}_2$, with $\hat{x}_i$ the operator associated with the displacement of mass m_i. The induced potential term is then $K\hat{x}_1\hat{x}_2$, so by setting K to be

$$K = 2G\frac{m_1 m_2}{d^3} \tag{6.9}$$

we recover the last term of Equation (6.1). Notice that $K = -\frac{\partial F}{\partial x}\big|_{x=d}$, with F the gravitational force between the masses. We also remember that an interaction of the form $\propto \hat{V} \otimes \hat{M}$, with $\hat{V}$ acting on the system and $\hat{M}$ acting on the ancillae, adds to the dynamics of the system an effective unitary term $\propto \langle \hat{M} \rangle \hat{V}$, with arbitrary low decoherence. Therefore, by adding during the second sub-step an interaction

$$-G\frac{m_1 m_2}{d}\left(1 + \frac{\hat{x}_1}{d} + \frac{\hat{x}_1^2}{d^2}\right) \otimes \hat{I}^{m_2} - G\frac{m_1 m_2}{d}\left(1 - \frac{\hat{x}_2}{d} + \frac{\hat{x}_2^2}{d^2}\right) \otimes \hat{I}^{m_1} \tag{6.10}$$

with $\hat{x}_i$ acting on subsystem s_i, the effective unitary term becomes $\hat{V}_N$ and we obtain an approximate Newtonian potential between the two subsystems. The dynamics of the joint system is given by

$$\dot{\rho}^{s_1,s_2} = -\frac{i}{\hbar}[\hat{S}_0 + \hat{V}_N, \rho^{s_1,s_2}] - \left(\frac{K^2 D}{4\hbar^2} + \frac{1}{4D}\right)([\hat{x}_1, [\hat{x}_1, \rho^{s_1,s_2}]] + [\hat{x}_2, [\hat{x}_2, \rho^{s_1,s_2}]]) \tag{6.11}$$

(with $\hat{V}_N$ as in Equation (6.1)) which yields the quadratic potential for an induced gravitational interaction (with noise) studied in [67], taking $\hat{S}_0$ to be the sum of harmonic oscillator Hamiltonians for each subsystem.

The diagonal elements of each particle decays at a rate $\Gamma_{\text{KTM}} = f(D)(\Delta x)^2$, with $\Delta x = (x_i - x_j)$ the superposition size of state of the particle and where $f(D)$ is given by

$$f(D) = \frac{1}{4}\left(\frac{1}{D} + \frac{K^2 D}{\hbar^2}\right) \tag{6.12}$$

We notice that Equation (6.12) has a minimum at $D = \frac{\hbar}{K}$ where $f = \frac{K}{2\hbar}$, so the minimum decay rate for the KTM model is

$$\Gamma_{\text{KTM}}^{min} = \frac{K}{2\hbar}(\Delta x)^2 \tag{6.13}$$

This minimum rate violates the condition in [124] and therefore the interaction is classical. It is important to highlight that if the decoherence was slightly smaller, the emerging

interaction would be quantum, in the sense that entanglement generation would be possible.

6.2 Extension to composite systems

We now extend the previous model to macroscopic systems, that is, where the subsystems are themselves composed of other elementary subsystems. We consider the interaction of two 3-dimensional composite systems s_1 and s_2 with total masses M_1 and M_2 respectively, with subsystem s_1 consisting of N_1 elementary subsystems and subsystem s_2 consisting of N_2 elementary subsystems. The classical Newtonian potential energy between any two constituents of masses m_i and m_j, with $i, j = 1, 2, ..., N_1 + N_2$ is given by

$$V_{ij} = -G\frac{m_i m_j}{|\vec{r}_{ij}|} \tag{6.14}$$

with $\vec{r}_{ij}$ the vector joining their positions. Similarly to what we did in the previous section, we write $\vec{r}_{ij} = \vec{d}_{ij} + \vec{x}_i + \vec{x}_j$, with $\vec{d}_{ij}$ the vector that joined their positions initially and $\vec{x}_i, \vec{x}_j$ the displacement of mass m_i, m_j respectively. We focus in the particular case where the subsystem s_1 is a test mass and the subsystem s_2 consists of a macroscopic mass interacting with the test mass and which we assume to be well localized. We also assume a) that the bodies are rigid, such that all the constituents of a subsystem are displaced in a way that preserves the distances between them and b) that there is a distinguished direction defined by the coherent displacements of the test mass. An illustration of this is presented in Figure 6.2.

It is convenient to decompose the vector $\vec{d}_{ij}$ along the orthogonal axes defined by the direction of the displacement of the test mass. Writing $\vec{x}_i = x_i\hat{e}$ with $\hat{e}$ the unit vector in the direction of such displacement, then we can write $\vec{d}_{ij} = d_{ij}^{\parallel}\hat{e} + d_{ij}^{\perp}\hat{e}^{\perp}$ where $\hat{e}^{\perp}$ is the unit vector in the orthogonal direction to $\hat{e}$. With this, the potential V_{ij} to second order in the displacement can be written as

$$\begin{aligned} V_{ij} &= \frac{-Gm_i m_j}{\sqrt{(d_{ij}^{\parallel} + x_i + x_j)^2 + (d_{ij}^{\perp})^2}} \\ &\approx -Gm_i m_j \times \left(\frac{1}{d_{ij}} - \frac{d_{ij}^{\parallel}}{d_{ij}^3}(x_i + x_j) + \frac{(d_{ij}^{\parallel})^2 - \frac{1}{2}(d_{ij}^{\perp})^2}{d_{ij}^5}(x_i + x_j)^2 \right) \end{aligned} \tag{6.15}$$

where $d_{ij} = \sqrt{(d_{ij}^{\parallel})^2 + (d_{ij}^{\perp})^2}$.

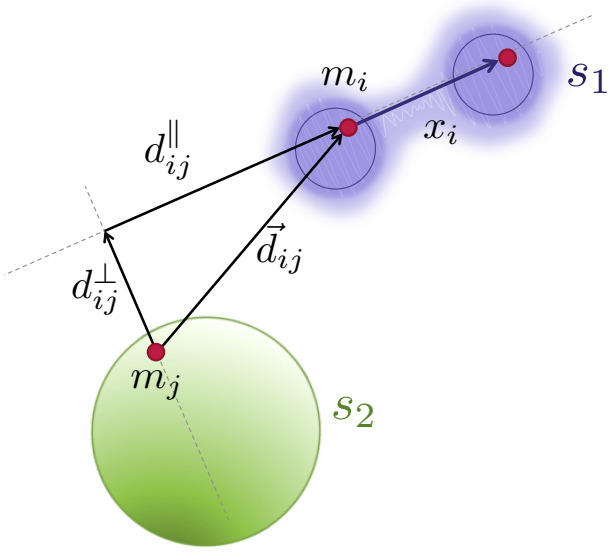

Figure 6.2: A pair of components m_i and m_j belonging to the test mass s_1 and the source mass s_2 respectively. The vector $\vec{d}_{ij}$ joining their positions is decomposed into two orthogonal vectors with components $d_{ij}^{\parallel}$ and $d_{ij}^{\perp}$, where $d_{ij}^{\parallel}$ lies along the direction of the spatial superposition of s_1. The displacement of the mass m_i from its initial position is x_i, whose values span all locations between which the particle can be superposed. Note that the assumption of rigidity implies that each constituent of s_1 is displaced by the same amount.

This potential has a similar form to the one given in Equation (6.1). We can therefore follow a procedure analogous to the one presented in the previous section: Each pair (i,j) interacts with a set of *gravitational* ancillae prepared in a Gaussian state as in Equation (5.38), in a two sub-step process, with the first sub-step $\propto \hat{x}_i \otimes \hat{p}_{m_i} + \hat{x}_j \otimes \hat{p}_{m_j}$ and the second sub-step given by $K_{ij}\hat{x}_i \otimes \hat{x}^{m_j} + K_{ij}\hat{x}_j \otimes \hat{x}^{m_i} + \hat{Y}_i \otimes \hat{I}^{m_j} + \hat{Y}_j \otimes \hat{I}^{m_i}$, with $\hat{Y}_{i(j)}$ a local interaction acting only on mass $m_{i(j)}$. Each pair would then evolve according to the master equation

$$\dot{\rho}_{ij} = -\frac{i}{\hbar}[\hat{S}_0 + \hat{Y}_i + \hat{Y}_j + K_{ij}\hat{x}_i\hat{x}_j, \rho_{ij}] - \Gamma_{ij}\left([\hat{x}_i, [\hat{x}_i, \rho_{ij}]] + [\hat{x}_j, [\hat{x}_j, \rho_{ij}]]\right) \tag{6.16}$$

where $\Gamma_{ij} \equiv \frac{1}{4D} + \frac{K_{ij}^2 D}{4\hbar^2}$. By defining K_{ij} and $\hat{Y}_i$ as

$$K_{ij} = 2Gm_i m_j \frac{(d_{ij}^{\parallel})^2 - \frac{1}{2}(d_{ij}^{\perp})^2}{d_{ij}^5} \tag{6.17}$$

$$\hat{Y}_i = -Gm_i m_j \left(\frac{1}{2d_{ij}} - \frac{d_{ij}^{\parallel}}{d_{ij}^3}\hat{x}_i + \frac{(d_{ij}^{\parallel})^2 - \frac{1}{2}(d_{ij}^{\perp})^2}{d_{ij}^5}\hat{x}_i^2 \right) \tag{6.18}$$

the unitary part of the evolution is approximately a Newtonian interaction between m_i and m_j. The master equation for the total system with $N_1 + N_2$ constituents is then given by

$$\dot{\rho}_{tot} = -\frac{i}{\hbar}[\hat{H}_0 + \sum_{i<j}^{N_1+N_2} V_{ij}, \rho_{tot}] \quad - \sum_{i<j}^{N_1+N_2} \Gamma_{ij}\Big([\hat{x}_i, [\hat{x}_i, \rho_{tot}]] + [\hat{x}_j, [\hat{x}_j, \rho_{tot}]] \Big). \tag{6.19}$$

with ρ_{tot} the density matrix of the total system.

In general, we can write the displacement of constituent i as $\hat{x}_i = \hat{r}_k + \hat{x}'_i$, with $\hat{x}'_i$ its displacement relative to the centre of mass of the system s_k to which it belongs and with $\hat{r}_k$ the displacement of that centre of mass. Figure 6.3 shows an illustration of this definition, for the case of rigid and non-rigid bodies. With this, we can write $[\hat{x}_i, [\hat{x}_i, \rho_{tot}]] = [\hat{r}_k, [\hat{r}_k, \rho_{tot}]] + [\hat{x}'_i, [\hat{x}'_i, \rho_{tot}]] + [\hat{r}_k, [\hat{x}'_i, \rho_{tot}]] + [\hat{x}'_i, [\hat{r}_k, \rho_{tot}]]$, with $k = 1$ for $i \leq N_1$ and $k = 2$ for $i > N_1$.

From our assumption of rigidity, all constituents of a body remain at the same fixed distance from its centre of mass and therefore the relative displacements are negligible (see Figure 6.3 a)). Furthermore, all the displacements x_i are the same as the displacement of the centre of mass of the body they belong to. We then trace over the relative degrees of freedom and keep the centres of mass positions of s_1 and s_2, resulting in the following master equation (in performing the trace, for simplicity one can assume that the centre of mass of s_i coincides with the position of one of its particles)

$$\begin{aligned} \dot{\rho}_{s_1 s_2} = &-\frac{i}{\hbar}[\hat{H}_0 + V, \rho_{s_1 s_2}] - 2\sum_{i<j=1}^{N_1} \Gamma_{ij}[\hat{r}_1, [\hat{r}_1, \rho_{s_1 s_2}]] - 2\sum_{N_1<i<j}^{N_1+N_2} \Gamma_{ij}[\hat{r}_2, [\hat{r}_2, \rho_{s_1 s_2}]] \\ &- \sum_{i=1}^{N_1}\sum_{j=N_1+1}^{N_1+N_2} \Gamma_{ij}\Big([\hat{r}_1, [\hat{r}_1, \rho_{s_1 s_2}]] + [\hat{r}_2, [\hat{r}_2, \rho_{s_1 s_2}]] \Big) \end{aligned} \tag{6.20}$$

where $V = \sum_{i<j}^{N_1+N_2} V_{ij} \approx -G\frac{M_1 M_2}{|d+r_1+r_2|}$ and M_1 and M_2 are the total masses of s_1 and s_2 respectively.

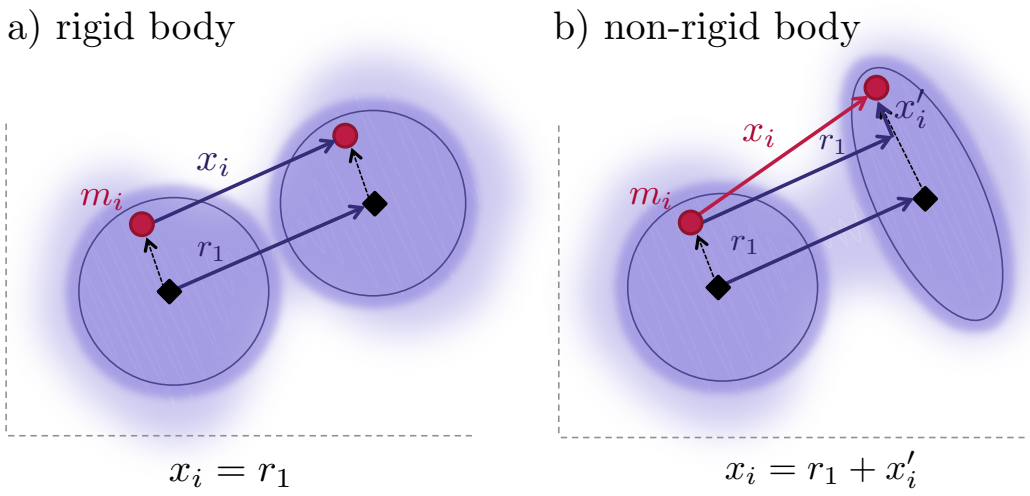

Figure 6.3: Displacement x_i of the i^{th} constituent of a) rigid body, b) non-rigid body. For a rigid body each constituent remains at the same distance (dashed arrow) from from the centre of mass (black diamond), and its displacement is the same as that of the centre of mass: $x_i = r_1$. For a non-rigid body, the displacement of a constituent can differ from that of the centre of mass: $x_i = r_1 + x_i'$. This work only considers case a).

Finally, tracing over the degrees of freedom of s_2, the dynamics of the centre of mass of s_1 are given by

$$\dot{\rho}_{s_1} = -\frac{i}{\hbar}[\hat{H}_0 + V, \rho_{s_1}] - \left(2\sum_{i<j=1}^{N_1}\Gamma_{ij} + \sum_{i=1}^{N_1}\sum_{j=N_1+1}^{N_1+N_2}\Gamma_{ij}\right)[\hat{r}_1, [\hat{r}_1, \rho_{s_1}]], \tag{6.21}$$

The unitary term approximates the Newtonian potential between two point masses M_1 and M_2 as in Equation (6.11). However the non unitary term now contains contributions from all the constituents of the systems. Each pair of elementary constituents contributes to the total decoherence. This includes pairs belonging to the same system (first sum in coefficient of the non unitary term) and pairs belonging to different systems (second two sums in coefficient of the non unitary term).

We note that Γ_{ij} is the decoherence rate for a pair (i, j) evolving under Equation (6.16), so it is natural to take the minimum decoherence rate for each pair (as in Equation (6.13)). We note that these gravitational ancillae could work such as to minimize noise with some other mechanism, but we consider this pairwise minimization to be the natural

minimization when extending the model to many such pairs and we will therefore work under this assumption. In this case, the master equation (6.21) becomes

$$\dot{\rho}_{s_1} = -\frac{i}{\hbar}[\hat{H}_0 + V, \rho_{s_1}] - \mathcal{D}_{min}[\hat{r}_1, [\hat{r}_1, \rho_{s_1}]], \tag{6.22}$$

where $\mathcal{D}_{min}$ is given by

$$\mathcal{D}_{min} := \frac{1}{2\hbar}\left(\sum_{i\neq j\in s_1} |K_{ij}| + \sum_{i\in s_1}\sum_{j\in s_2} |K_{ij}|\right), \tag{6.23}$$

with K_{ij} as defined in Equation (6.17). The total decay rate of subsystem s_1 is now given by

$$\tilde{\Gamma}^{min}_{\text{KTM}} = \mathcal{D}_{min}\Delta x^2. \tag{6.24}$$

with Δx the superposition size.

Finally, we note that in general we cannot approximate the mass distribution to be continuous, since doing so would introduce divergences coming from pairs belonging to the same body. To keep this contributions finite, we need to introduce a definition for the *fundamental* constituents of the system. Since we assumed that the total mass of the body is the sum of the masses of its constituents, a natural proposal for this fundamental constituents is that they are defined as the smallest constituents between which the binding energy contribution to the total mass can be neglected. We will consider atoms as such fundamental constituents when discussing macroscopic objects.

6.3 Test mass in Earth's gravitational field

We now apply this model to a pair of systems, where s_1 is an atom in an interferometer and s_2 is the Earth. The atom will therefore be in a superposition of different distances to the Earth, which is well localized, and the assumptions of our model are valid in this scenario.

The dynamics of the atom are given by

$$\dot{\rho}_{s_1} = -\frac{i}{\hbar}[\hat{H}_0 + V, \rho_{s_1}] - \mathcal{D}_{min}[\hat{r}, [\hat{r}, \rho_{s_1}]], \tag{6.25}$$

with V as defined before and where we now use $\hat{r}$ to describe the operator associated to the displacement of the atom.

Since $N_1 = 1$, in calculating $\mathcal{D}_{min}$ we do not have contributions connecting s_1 with itself, but only terms connecting s_1 with s_2. These are given by pairs $(1, j)$, each contributing a term K_{1j}, with j the total number of atoms in the Earth. Equation (6.23) in this case is then

$$\mathcal{D}_{min} = \sum_{j \in \text{Earth}} \frac{K_{1j}}{2\hbar} \tag{6.26}$$

In specifying the function K_{1j} we defined the distances $d^{\parallel}_{1j}$ and $d^{\perp}_{1j}$ as $\vec{d}_{1j} = d^{\parallel}_{1j}\hat{e} + d^{\perp}_{1j}\hat{e}^{\perp}$. We can furthermore decompose $\hat{e}^{\perp}$ in terms of the fixed orthogonal unit vectors $\hat{e}^{\perp}_1$ and $\hat{e}^{\perp}_2$ as $\hat{e}^{\perp} = \frac{1}{\sqrt{2}}(\hat{e}^{\perp}_1 + \hat{e}^{\perp}_2)$, so that $\vec{d}_{1j} = d^{\parallel}_{1j}\hat{e} + d^{\perp_1}_{1j}\hat{e}^{\perp}_1 + d^{\perp_2}_{1j}\hat{e}^{\perp}_2$, with $d^{\perp 2}_{1j} = d^{\perp_1 2}_{1j} + d^{\perp_2 2}_{1j}$. The function K_{1j} can be expressed as

$$K_{1j} = m_j f\left(d^{\parallel}_{1j}, d^{\perp_1}_{1j}, d^{\perp_2}_{1j}\right) \tag{6.27}$$

with f defined as

$$f\left(d^{\parallel}_{1j}, d^{\perp_1}_{1j}, d^{\perp_2}_{1j}\right) := 2Gm_1 \frac{d^{\parallel 2}_{1j} - \frac{1}{2}(d^{\perp_1 2}_{1j} + d^{\perp_2 2}_{1j})}{(d^{\parallel 2}_{1j} + d^{\perp_1 2}_{1j} + d^{\perp_2 2}_{1j})^{\frac{5}{2}}} \tag{6.28}$$

Calculating this quantity would involve calculating a function of approximately 10^{50} distances (one for each atom) in a specific configuration and summing them all. We therefore try to avoid this calculation and instead give it a lower bound.

6.3.1 Lower bound of total decoherence

To calculate the lower bound, we note that the contribution from each atom of the Earth will increase the decoherence rate of the test mass, so the decoherence coming from considering only a portion of the Earth will be less than the total decoherence. Moreover, in a region $\mathcal{C}$ where f (defined above) as a function of the distance variables $(d^{\parallel}_{1j}, d^{\perp_1}_{1j}, d^{\perp_2}_{1j})$ is convex, the following inequalities hold

$$\begin{aligned}\sum_{j\in\text{earth}} K_{1j} \geq \sum_{j\in\mathcal{C}} K_{1j} &= m_{\mathcal{C}} \sum_{j\in\mathcal{C}} \frac{m_j}{m_{\mathcal{C}}} f\left(d_{1j}^{\parallel}, d_{1j}^{\perp_1}, d_{1j}^{\perp_2}\right) \\ &\geq m_{\mathcal{C}} f\left(\sum_{j\in\mathcal{C}} \frac{m_j}{m_{\mathcal{C}}}\left(d_{1j}^{\parallel}, d_{1j}^{\perp_1}, d_{1j}^{\perp_2}\right)\right) \\ &= m_{\mathcal{C}} f\left(d_{CM_{\mathcal{C}}}^{\parallel}, d_{CM_{\mathcal{C}}}^{\perp_1}, d_{CM_{\mathcal{C}}}^{\perp_2}\right) \end{aligned} \tag{6.29}$$

where $m_{\mathcal{C}}$ is the mass of the region $\mathcal{C}$ and $(d_{CM_{\mathcal{C}}}^{\parallel}, d_{CM_{\mathcal{C}}}^{\perp_1}, d_{CM_{\mathcal{C}}}^{\perp_2})$ are its centre of mass coordinates. This centre of mass can therefore be used to give a lower bound on the total decoherence.

The function $f(d_{CM_{\mathcal{C}}}^{\parallel}, d_{CM_{\mathcal{C}}}^{\perp_1}, d_{CM_{\mathcal{C}}}^{\perp_2})$ is convex only in the region where $|d_{1j}^{\parallel}| < |d_{1j}^{\perp}|/2$. For simplicity, we take $\mathcal{C}$ to be the portion of the Earth where $|d_{1j}^{\parallel}| < |d_{1j}^{\perp}|$, which lies within the volume where f is convex (since $|d_{1j}^{\perp}|/2 < |d_{1j}^{\perp}|$). This region is a cone of height R and support of area πR^2 together with a half ball of radius R as shown in Figure 6.4.

Assuming a constant mass density, the mass $m_{\mathcal{C}}$ is equal to $\frac{3}{4}m_E$ and its centre of mass lies within the axis defined by the superposition, at a distance of $\frac{7}{6}R$ from the top surface, with m_E and R the mass and radius of the Earth respectively. Using these quantities, and Equations (6.24), (6.26) and (6.29), we get

$$\tilde{\Gamma}_{\text{KTM}}^{min} \geq \frac{\Delta x}{2\hbar}\left(2G\frac{(\frac{3}{4}m_E)m_1}{(\frac{7}{6}R)^3}\right) = \left(\frac{3}{4}\right)\left(\frac{6}{7}\right)^3 \frac{\Delta x}{2\hbar}\left(2G\frac{m_1 m_E}{R^3}\right) = \Gamma_{\text{KTM}}^{\text{LB}} \tag{6.30}$$

with $\Gamma_{\text{KTM}}^{\text{LB}}$ defined as

$$\Gamma_{\text{KTM}}^{\text{LB}} := \left(\frac{3}{4}\right)\left(\frac{6}{7}\right)^3 \Gamma_{\text{KTM}}^{min} \tag{6.31}$$

The decoherence rate $\Gamma_{\text{KTM}}^{\text{LB}}$ is a lower bound on $\tilde{\Gamma}_{\text{KTM}}^{min}$, the total decoherence rate of an atom due to the presence of the Earth, and is proportional to the decoherence rate of the original KTM model applied to the centres of mass of the systems, with the proportionality (in this case $\approx .47$) related to the geometry of the bodies.

For convenience, we define the decoherence rate Γ_{KTM}^{C} as

$$\Gamma_{\text{KTM}}^{C} := C\frac{Gm_1 m_2}{\hbar R^3}\Delta x^2 \tag{6.32}$$

for $C = 1$, we recover the original KTM minimum decoherence rate and for $C = 0.47$ we recover the lower bound for the macroscopic extension.

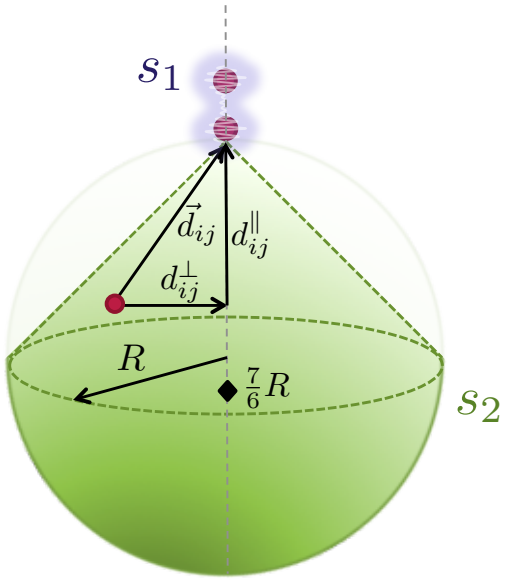

Figure 6.4: Region $\mathcal{C}$ (coloured in green) used to give a lower bound on the total decoherence rate of the atom, defined by the portion of the Earth where its constituents of mass m_j obey the inequality $|d_{1j}^{\parallel}| < |d_{1j}^{\perp}|$. It is formed by a cone and a half ball, with total mass $\frac{3}{4}m_E$, and with a centre of mass located a distance $\frac{7}{6}R$ from the top surface, where m_E and R are the mass and radius of the Earth respectively.

6.3.2 Atomic fountain tests of the KTM model

Using the results obtained in the previous subsection, we now use atomic fountain experiments to test the KTM model. From Equation (6.25), the magnitude of the off-diagonal elements of the atom is

$$V(t) := |\langle r_1 |\rho_{s_1}| r_2\rangle(t)| = |\langle r_1 |\rho_{s_1}| r_2\rangle(0)| e^{-\int_0^t dt' \mathcal{D}_{min} \Delta x^2(t')} \tag{6.33}$$

with Δx the atom superposition size. Note that the larger the superposition size, the smaller the magnitude of V is. Here r_1 and r_2 have a different meaning than in the previous section; in this case they represent different radial displacements of the atom.

We use recent results using large momentum transfer (LMT) interferometers [5, 6] that allow the realization of large wave packet separations. In LMT interferometers, an atomic cloud is vertically lunched and subject to a sequence of N $\frac{\pi}{2}$-optical pulses implementing a

beam splitter that places the atoms in a superposition of wave packets with a momentum difference of $2N\hbar k$, where k is the laser wave-number. The wave packets are allowed to separate vertically during a time T, at which point a sequence of π-pulses reverses their momentum and at time $2T$ the packets physically overlap and interfere in a final beam splitter, implemented by N $\frac{\pi}{2}$-pulses. The spatial separation of the wave packets in the interferometer is $\Delta x(t) = 2N\hbar kt/m$ for $t < T$, reaching a maximum separation of $2N\hbar kT/m$ and then symmetrically decreasing for $t > T$ until they overlap at $t = 2T$.

The interferometric visibility is defined as the magnitude of the off diagonal elements of the state of the atom after the interferometric sequence, so from Equation (6.33), it is given by $V(2T)$. From our discussion in Subsection 6.3.1, the maximum visibility allowed by the KTM model is therefore

$$V_{\text{KTM}}^{max} = e^{-\int_0^{2T} dt \Gamma_{\text{KTM}}^C} = e^{-\frac{2}{3}C\frac{G\hbar m_E}{mR^3}(2Nk)^2T^3} \tag{6.34}$$

with Γ_{KTM}^C as defined in Equation (6.32), where $C = 1$ for the original model and $C = 0.47$ for the multi particle extension.

We calculate V_{KTM}^{max} for both the original KTM model ($C = 1$) and for the multi particle extension ($C = 0.47$) as well as for an arbitrary downscaling of the decoherence rate ($C = 0.1$) using the parameters of the atomic fountain experiments with ^{87}Rb atoms reported in [5] and [6]. The values of these parameters are $m_E = 6 \cdot 10^{24}$ kg; $R = 6 \cdot 10^3$ km, $\frac{\hbar k}{m} = 5.8\ \frac{\text{mm}}{\text{s}}$, $m = 1.4 \cdot 10^{-25}$ kg (^{87}Rb); $T = 1.15$ s and $N = \{1, 3, 4, 5, 6\}$ in Ref. [6] and $T = 1.04$ s and $N = \{1, 8, 15, 30, 45\}$ in Ref. [5], resulting in superposition sizes of up to 8.2 cm and 54 cm respectively.

In Figure 6.5 we present the predicted maximum visibility together with the visibilities measured in their experiments. The plots show the visibility in a logarithmic scale in the vertical axes and the LMT order ($2\hbar k$) in the horizontal axes. We notice that their reported visibilities are larger than those predicted by the KTM model in all LMT orders. Even if the downscale correction is taken into account, the predicted visibilities are smaller than the ones reported by factors ranging from ~ 2.5 to $\sim 10^{18}$. Notice that this difference grows with the LMT order or equivalently, with larger spatial superpositions. The model of gravity as a classical channel is therefore incompatible with the experimental data.

6.4 Application to torsion balance experiments

We now apply the KTM model to torsion balance experiments. These experiments measure the gravitational constant G by detecting the torque produced by the gravitational

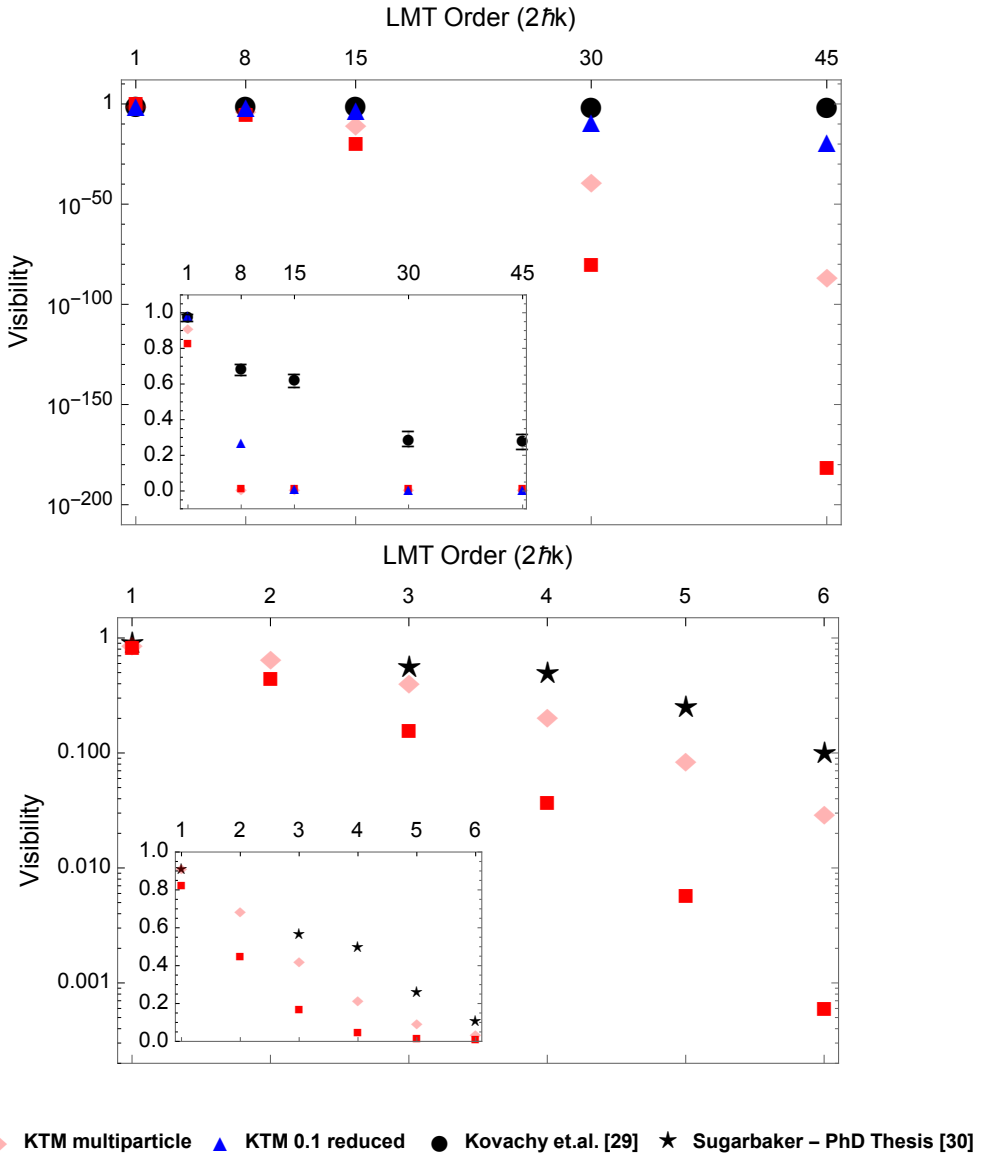

Figure 6.5: Comparison of the visibility predicted by the original KTM model (red squares), its multi particle extension (pink diamonds), and a reduced KTM correction (blue triangles) with the visibilities measured in two atom fountain experiments: [5] (black dots) in the top figure and [6] (black stars) in the bottom figure, both in a logarithmic scale and as a function of the LMT order. The insets shows the data in a linear scale, where in the case of [5], the reported errors are included.

attraction between massive objects on the balance. The experimental setup (see [144, 145]) consists of a set of small test masses of mass m in a 4-fold configuration, suspended by a thin strip and a set of large source masses of mass M, also in a 4-fold configuration as illustrated in Figure 6.6.

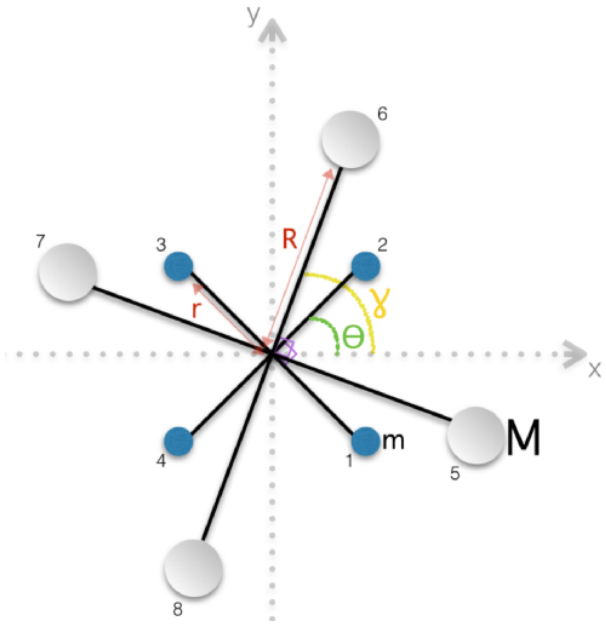

Figure 6.6: Setup of the torsion balance experiment: 4 small test masses m and 4 large source masses M in a 4-fold configuration. The gravitational attraction between them produces a torque that is measured to calculate the gravitational constant G.

We first show how the gravitational potential in this setup can emerge from the repeated interactions model. The Hamiltonian of the system is

$$H = \sum_i \frac{1}{2} m_i \left(\dot{x}_i^2 + \dot{y}_i^2\right) + \sum_{i,j} V_{ij} \,, \tag{6.35}$$

where i runs over all the masses in the experiment and V_{ij} denotes the Newtonian gravitational potential between pairs of bodies, with each body regarded as a pointlike object located at its centre of mass.

Since all bodies in the balance are in the same plane, we can write the above Hamiltonian

in polar coordinates as

$$\begin{aligned} H &= 2m\left(\dot{r}^2 + r^2\dot{\theta}^2\right) + 2M\left(\dot{R}^2 + R^2\dot{\gamma}^2\right) + \sum_{i,j} V_{ij} \\ &= 2mr^2\dot{\theta}^2 + 2MR^2\dot{\gamma}^2 + \sum_{i<j} V_{ij} \end{aligned} \tag{6.36}$$

where the second line follows from the rigidity of the balance arms. Here (r, θ) and (R, γ) are the distance to the axis of rotation and the angle that a mass makes to an arbitrary fixed axis in the plane of the masses, for the small and large bodies respectively (see Figure 6.6). Since the potential V_{ij} depends only on the variable $\alpha = \gamma - \theta$, the Hamiltonian can be written as

$$\begin{aligned} H =& \frac{mr^2 + MR^2}{4mr^2MR^2}p_\alpha^2 + \frac{p_\xi^2}{4(mr^2 + MR^2)} + \frac{4GmM}{\sqrt{r^2 + R^2 + 2rR\cos\alpha}} + \frac{4GmM}{\sqrt{r^2 + R^2 + 2rR\sin\alpha}} \\ &+ \frac{4GmM}{\sqrt{r^2 + R^2 - 2rR\cos\alpha}} + \frac{4GmM}{\sqrt{r^2 + R^2 - 2rR\sin\alpha}} + \frac{4Gm^2}{\sqrt{2}r} + \frac{4GM^2}{\sqrt{2}R} + \frac{Gm^2}{r} + \frac{GM^2}{R} \end{aligned} \tag{6.37}$$

where p_α is the conjugate momentum to α and p_ξ is the conjugate momentum to the variable $\xi \equiv \frac{mr^2\theta + MR^2\gamma}{mr^2 + MR^2}$.

The relevant variable is the small deviations of the angle α away from its equilibrium value α_0. Writing $\alpha = \alpha_0 + \delta\alpha$, where $\delta\alpha \ll \alpha_0$, the Hamiltonian can be approximated as

$$H = \frac{p_\alpha^2}{2I_{\text{eff}}} + \frac{p_\xi^2}{4(mr^2 + MR^2)} + B\delta\alpha + C(\delta\alpha)^2 + \cdots \tag{6.38}$$

where $I_{\text{eff}} = \frac{2mr^2MR^2}{mr^2 + MR^2}$ is the reduced moment of inertia and

$$\begin{aligned} B &= \sum_{n=1}^{3} \frac{4GmMrR\sin(\alpha_0 + (n+1)\pi/2)}{(r^2 + R^2 - 2rR\sin(\alpha_0 + n\pi/2))^{\frac{3}{2}}} \\ C &= -\sum_{n=1}^{3} \frac{2GmMrR\sin(\alpha_0 + n\pi/2)}{(r^2 + R^2 - 2rR\sin(\alpha_0 + n\pi/2))^{\frac{3}{2}}} + \sum_{n=1}^{3} \frac{6GmMr^2R^2\sin^2(\alpha_0 + (n+1)\pi/2)}{(r^2 + R^2 - 2rR\sin(\alpha_0 + n\pi/2))^{\frac{5}{2}}} \end{aligned} \tag{6.39}$$

and we have dropped the irrelevant constant terms from (6.37).

Since $(\delta\alpha)^2 = \delta\gamma^2 + \delta\theta^2 - 2\delta\gamma\delta\theta$, the master equation for this setup is obtained from Equation (6.11), with $\hat{x} \to \delta\hat{\alpha}$, and $K = -2C$. Writing $D = \frac{\hbar}{2C\epsilon}$, we obtain

$$\dot{\rho} = -\frac{i}{\hbar}\left[\frac{\hat{p}_\alpha^2}{2I_{\text{eff}}} + \frac{\hat{p}_\xi^2}{4(mr^2+MR^2)} + B\delta\hat{\alpha} + C\delta\hat{\alpha}^2, \rho\right] - \frac{C}{2\hbar}\left(\epsilon + \frac{1}{\epsilon}\right)[\delta\hat{\alpha}, [\delta\hat{\alpha}, \rho]] \tag{6.40}$$

The continuous interaction process would introduce additional noise to the measurement of G. Indeed, from Equation (6.40), the time averaged variance of $\delta\alpha$ is

$$\text{var}(\delta\hat{\alpha}) = \frac{\hbar}{8I_{\text{eff}}} T\left(\epsilon + \frac{1}{\epsilon}\right) \text{s}^{-1} \tag{6.41}$$

with $\text{var}(\delta\hat{\alpha}) = \langle(\delta\hat{\alpha})^2\rangle - \langle\delta\hat{\alpha}\rangle^2$ and T the timescale over which the experiment takes place. For example, the total error in G for the Cavendish experiment would now given by

$$\frac{\Delta G}{G} = \frac{\delta(\Delta\alpha)}{\Delta\alpha} + \frac{\delta k}{k} - \left(\frac{\delta M}{M} + \frac{\delta m}{m} + 4\frac{\delta r_a}{r_a} + 4\frac{\delta r_b}{r_b} - 5\frac{\delta R_{ac}}{R_{ac}} - 5\frac{\delta R_b}{R_b} + \alpha_{CT}\right) + \frac{\delta\tau_c}{\tau_c} \tag{6.42}$$

where $\Delta\alpha := |\langle(\delta\hat{\alpha})\rangle|$ the mean, and $\delta(\Delta\alpha) := \sqrt{\text{var}(\delta\hat{\alpha})}$ the standard deviation. The meaning of the various quantities in the previous equation is explained in [144] (see Equation (11.10) of [144])

We can therefore use the error in the measurement of G to constrain the effect introduced by the KTM model. From Equation (6.42), the minimal constraint is given by

$$\left|\frac{\delta(\Delta\alpha)}{\Delta\alpha}\right| \leq \left|\frac{\Delta G}{G}\right| \tag{6.43}$$

We use the parameters reported in [145] to estimate the size of $\delta(\Delta\alpha)$. These parameters are $m = 1.2$ kg, $M = 11$ kg, $r = 120$ mm, $R = 214$ mm, and $\alpha_0 = 18.9^o$, yielding $I_{\text{eff}} = 8.35 \times 10^{-3}$ kg m^2. Upon substituting these values on Equation (6.41), we get

$$\text{var}(\delta\hat{\alpha}) = 1.58 \times 10^{-33} T\left(\epsilon + \frac{1}{\epsilon}\right) \text{s}^{-1} \tag{6.44}$$

which upon substitution into Equation (6.43), gives

$$\begin{aligned} \left|\frac{\delta(\Delta\alpha)}{\Delta\alpha}\right| &= \sqrt{1.58 \times 10^{-33} T\left(\epsilon + \frac{1}{\epsilon}\right)} \leq \left|\frac{\Delta G}{G}\right| \sim 10^{-6} \\ &\Rightarrow T\left(\epsilon + \frac{1}{\epsilon}\right) \leq\sim 6 \times 10^{20} \end{aligned} \tag{6.45}$$

for $\Delta\alpha \sim 1$ radian. For an experiment on the order of 1 day $= 3600 \times 24 = 86400$ seconds, then

$$\left(\epsilon + \frac{1}{\epsilon}\right) \leq\sim 7 \times 10^{15}$$

and the decoherence rate satisfies

$$\frac{C}{2\hbar}\left(\epsilon + \frac{1}{\epsilon}\right) \leq\sim 3.7 \times 10^{40}.$$

To get this bound, we assumed for simplicity that the masses were pointlike, but similarly to the previous sections, a calculation involving the compositeness of the bodies in the torsion balance will add a geometrical factor of order unity to the decoherence rate. Since the above constraint is much weaker than that provided by the atomic fountain experiments we will not pursue this any further.

6.5 Conclusions

We have demonstrated how by choosing specific parameters of the model of continuous repeated interactions presented in Chapter 5 the KTM model of gravitational Newtonian interactions is recovered [67, 68]. We furthermore show an extension of the model to consider the contributions stemming from the constituents of massive bodies.

In the KTM model, gravity is therefore modelled as a channel connecting pairwise constituents of massive bodies, with arising decoherence of just the right magnitude so that the resulting dynamics are classical, where the classical regime is understood as an incapability of interactions to entangle systems. The importance of this model is that its minimum noise saturates the condition for having only classical communication [124]. In other words the limit that separates theories where interactions are mediated by a channel that can or cannot generate entanglement coincides with the minimum noise limit of the KTM model.

We discussed the observable implications the model would have on interferometric experiments and show that the visibilities attained in recent experiments using atom interferometers with large momentum transfer [5, 6] are larger than the maximum visibilities predicted by the model, or equivalently, the measured decoherence rate is smaller than the minimum rate of the KTM model.

Our results strongly suggest that if gravitational interactions are mediated by a pairwise channel, then they can in principle entangle particles. While the experiments analyzed

do not prove that gravity is capable of conveying entanglement, they provide a strong argument against the hypothesis that it is fundamentally incapable of doing so.

Chapter 7

Outlook

In the first part of this thesis we discussed how circuit quantum electrodynamics technologies can provide analogue-simulators of physical systems where relativistic regimes are achievable. In particular, we take advantage of the setup used for the detection of the dynamical Casimir effect [79, 80, 4], where fast modulation of a boundary was realized, in contrast with other experimental systems where relativistic regimes are hard to attain. We show that the simulation of different periodic boundary trajectories is experimentally feasible with state-of-the-art technology, yielding a particle creation spectra that allows for their differentiation.

For future work it would be interesting to analyze if the setup can be modified to allow for the simulation of Neumann boundary conditions and how this modifies the results, comparing the observations with theoretical predictions [146, 147]. Another possible future direction is to analyze the concrete experimental feasibility of simulating moving cavities. This could be achieved by terminating the CPW with two SQUIDs and subjecting both of them to the same flux so that they move in synchrony and the length of the cavity remains fixed. Once these experimental testbeds are developed, they can be applied to theoretical proposals such as the ones discussed in [148, 149, 150].

In the second part of this thesis we discussed how a model of continuous repeated interactions can be used to describe an extensive range of phenomena, including effective potentials in the evolution of a system, feedback-control over it and the emergence of non-local interactions between systems mediated by ancillae. We also spelled out the assumptions and conditions required to recover different dynamics of a system, providing particular examples to illustrate each regime.

For future investigations it would be interesting to analyze the consequences of the model beyond the Markovian approximation [151, 152]. For example, interactions between

the ancillae could be incorporated [153] or one could consider the effect of having initial correlations, either between the ancillae [154] or between the system and the ancillae [155].

We also explained how the KTM model of Newtonian gravity is recovered from the continuous interactions model and derived its minimum decoherence rate. Such rate is below the decoherence observed in recent interferometric experiments, suggesting that gravity is not a pairwise classical channel. We point out that one of the experimental results we base our conclusions on [5] has been a source of controversy (although our conclusions still hold considering [6]). It is therefore important to perform additional tests of the KTM model. For example, to relax our assumption of uniform mass distribution of the Earth, one could perform interferometric tests in the presence of high density masses acting as a source of the gravitational field, utilizing setups as the ones already used in [156, 157, 158] with minimal modifications. It would also be interesting to probe the model in other non interferometric systems.

Another important investigation would be to explore if the model of continuous interactions can generate an exact Newtonian potential. To recover the second order approximation, we considered ancillae prepared in a Gaussian distribution where the first and second order moments contributed to the dynamics but where all higher order moments vanished. To get an exact potential, one would need to retain terms higher than second order. This could be achieved by for example, analyzing if there exists a preparation of the ancillae with non vanishing higher order terms contributing to the effective unitary evolution that sum up to reproduce the Newtonian potential.

Additional explorations would contemplate the possibility of generating general relativistic gravity as an effective interaction with ancillae. Some first steps in this direction were already taken in [159], where the model results in decoherence of the state of a Friedman-Robertson-Walker universe, manifesting itself as a time-dependent dark energy fluid filing spacetime. Further studies of the effects of a collisional model in cosmological scenarios would be intriguing, for example, one could ask if it modifies the inflationary model.

Even though in this thesis we explore the implications of the continuous measurement model in the gravitational sector, the model itself has varying applications in different areas like quantum control [160] and quantum thermodynamics. Recent studies have suggested that energy transport in photosynthetic organisms could be assisted by noise [161, 162, 163]. It would be interesting to explore the implications of the model in this type of systems.

Bibliography

[1] P. Corona-Ugalde, E. Martín-Martínez, C. Wilson and R. B. Mann, "Dynamical Casimir effect in circuit QED for nonuniform trajectories", *Physical Review A* **93** (1), 012519 (2016).

[2] N. Altamirano, P. Corona-Ugalde, R. B. Mann and M. Zych, "Unitarity, feedback, interactions– Dynamics emergent from repeated measurements", *New Journal of Physics* **19** (1), 013035 (2017).

[3] N. Altamirano, P. Corona-Ugalde, R. B. Mann and M. Zych, "Gravity is not a pairwise local classical channel", *arXiv preprint arXiv:1612.07735* (2016).

[4] J. R. Johansson, G. Johansson, C. M. Wilson and F. Nori, "Dynamical Casimir effect in superconducting microwave circuits", *Physical Review A* **82**, 052509 (2010).

[5] T. Kovachy, P. Asenbaum, C. Overstreet, C. Donnelly, S. Dickerson, A. Sugarbaker, J. Hogan and M. Kasevich, "Quantum superposition at the half-metre scale", *Nature* **528**, 530–533 (2015).

[6] A. Sugarbaker, "Atom interferometry in a 10 m fountain", Ph.D. thesis, Stanford (2014).

[7] S. Eibenberger, S. Gerlich, M. Arndt, M. Mayor and J. Tüxen, "Matter–wave interference of particles selected from a molecular library with masses exceeding 10000 amu", *Physical Chemistry Chemical Physics* **15** (35), 14696–14700 (2013).

[8] R. M. Wald, *General relativity*, University of Chicago Press (2010).

[9] M. S. Grewal, L. R. Weill and A. P. Andrews, *Global Positioning Systems, Inertial Navigation, and Integration*, Wiley-Interscience (2007), ISBN 0470041900.

[10] S. W. Hawking, "Black hole explosions", *Nature* **248** (5443), 30–31 (1974).

[11] S. W. Hawking, "Particle creation by black holes", *Communications in mathematical physics* **43** (3), 199–220 (1975).

[12] V. Mukhanov and S. Winitzki, *Introduction to Quantum Effects in Gravity*, Cambridge University Press (2007).

[13] W. Unruh, "Notes on black-hole evaporation", *Physical Review D* **14** (4), 870 (1976).

[14] R. Penrose, "On gravity's role in quantum state reduction", *General Relativity and Gravitation* **28** (5), 581–600 (1996), ISSN 1572-9532.

[15] L. Diósi, "Models for universal reduction of macroscopic quantum fluctuations", *Physical Review A* **40** (3), 1165 (1989).

[16] B. L. Hu, "Gravitational decoherence, alternative quantum theories and semiclassical gravity", *Journal of Physics: Conference Series* **504** (1), 012021 (2014).

[17] L. Diosi, "Gravitation and quantum-mechanical localization of macro-objects", *Physics letters A* **105** (4-5), 199–202 (1984).

[18] R. Gambini and J. Pullin, "Free will, undecidability, and the problem of time in quantum gravity", *arXiv preprint arXiv:0903.1859* (2009).

[19] D. N. Page and W. K. Wootters, "Evolution without evolution: Dynamics described by stationary observables", *Physical Review D* **27**, 2885–2892 (1983).

[20] M. J. Hall and M. Reginatto, "Interacting classical and quantum ensembles", *Physical Review A* **72**, 062109 (2005).

[21] M. Albers, C. Kiefer and M. Reginatto, "Measurement analysis and quantum gravity", *Physical Review D* **78**, 064051 (2008).

[22] M. J. Hall and M. Reginatto, *Ensembles on Configuration Space: Classical, Quantum, and Beyond*, volume 184, Springer (2016).

[23] L. Diosi, "Notes on certain Newton gravity mechanisms of wavefunction localization and decoherence", *Journal of Physics A: Mathematical and Theoretical* **40**, 2989 (2007).

[24] A. Tilloy and L. Diosi, "Sourcing semiclassical gravity from spontaneously localized quantum matter", *Physical Review D* **93**, 024026 (2016).

[25] R. Penrose, "On the gravitization of quantum mechanics 1: Quantum state reduction", *Foundations of Physics* **44**, 557–575 (2014).

[26] T. Jacobson, "Thermodynamics of spacetime: the Einstein equation of state", *Physical Review Letters* **75**, 1260 (1995).

[27] M. A. Nielsen and I. L. Chuang, *Quantum Computation and Quantum Information*, Cambridge University Press (2000).

[28] T. D. Ladd, F. Jelezko, R. Laflamme, Y. Nakamura, C. Monroe and J. L. O'Brien, "Quantum computers", *Nature* **464** (7285), 45–53 (2010).

[29] A. Steane, "Quantum computing", *Reports on Progress in Physics* **61** (2), 117 (1998).

[30] I. Fuentes-Schuller and R. B. Mann, "Alice falls into a black hole: Entanglement in noninertial frames", *Physical Review Letters* **95**, 120404 (2005).

[31] P. M. Alsing, I. Fuentes-Schuller, R. B. Mann and T. E. Tessier, "Entanglement of dirac fields in noninertial frames", *Physical Review A* **74** (3), 032326 (2006).

[32] A. Kent, "A no-summoning theorem in relativistic quantum theory", *Quantum information processing* (1–10) (2013).

[33] A. Kent, "Quantum tasks in minkowski space", *Classical and Quantum Gravity* **29** (22), 224013 (2012).

[34] E. Martín-Martínez, D. Aasen and A. Kempf, "Processing quantum information with relativistic motion of atoms", *Physical Review Letters* **110**, 160501 (2013).

[35] H. Terashima and M. Ueda, "Einstein-podolsky-rosen correlation in a gravitational field", *Physical Review A* **69** (3), 032113 (2004).

[36] J. L. Ball, I. Fuentes-Schuller and F. P. Schuller, "Entanglement in an expanding spacetime", *Physics Letters A* **359** (6), 550–554 (2006).

[37] G. Ver Steeg and N. C. Menicucci, "Entangling power of an expanding universe", *Physical Review D* **79** (4), 044027 (2009).

[38] E. Martín-Martínez, L. J. Garay and J. León, "The fate of non-trivial entanglement under a gravitational collapse", *Classical and Quantum Gravity* **29** (22), 224006 (2012).

[39] Q. Pan and J. Jing, "Hawking radiation, entanglement, and teleportation in the background of an asymptotically flat static black hole", *Physical Review D* **78** (6), 065015 (2008).

[40] D. Ahn, Y. Moon, R. Mann and I. Fuentes-Schuller, "The black hole final state for the dirac fields in Schwarzschild spacetime", *Journal of High Energy Physics* **2008** (06), 062 (2008).

[41] E. Martín-Martínez, L. J. Garay and J. León, "Unveiling quantum entanglement degradation near a Schwarzschild black hole", *Physical review D* **82** (6), 064006 (2010).

[42] E. Martín-Martínez and J. León, "Fermionic entanglement that survives a black hole", *Physical Review A* **80**, 042318 (2009).

[43] E. Martín-Martínez and J. Louko, "Particle detectors and the zero mode of a quantum field", *Physical Review D* **90**, 024015 (2014).

[44] W. Brenna, R. B. Mann and E. Martín-Martínez, "The anti-Unruh effect", *arXiv preprint quantph/1504.02468* **33**.

[45] E. G. Brown, E. Martín-Martínez, N. C. Menicucci and R. B. Mann, "Detectors for probing relativistic quantum physics beyond perturbation theory", *Physical Review D* **87**, 084062 (2013).

[46] D. E. Bruschi, A. R. Lee and I. Fuentes, "Time evolution techniques for detectors in relativistic quantum information", *Journal of Physics A: Mathematical and Theoretical* **46** (16), 165303 (2013).

[47] J. Doukas, S.-Y. Lin, B. Hu and R. B. Mann, "Unruh Effect under Non-equilibrium conditions: Oscillatory motion of an Unruh-DeWitt detector", *Journal of High Energy Physics* **1311**, 119 (2013).

[48] D. E. Bruschi, J. Louko and D. Faccio, "Entanglement generation in relativistic cavity motion", in "Journal of Physics: Conference Series", IOP Publishing (2013), volume 442, (012024).

[49] N. Friis, D. E. Bruschi, J. Louko and I. Fuentes, "Motion generates entanglement", *Physical Review D* **85** (8), 081701 (2012).

[50] N. Friis and I. Fuentes, "Entanglement generation in relativistic quantum fields", *Journal of Modern Optics* **60** (1), 22–27 (2013).

[51] P. M. Alsing and G. J. Milburn, "Teleportation with a uniformly accelerated partner", *Physical Review Letters* **91** (18), 180404 (2003).

[52] N. Friis, A. R. Lee, K. Truong, C. Sabín, E. Solano, G. Johansson and I. Fuentes, "Relativistic quantum teleportation with superconducting circuits", *Physical Review Letters* **110** (11), 113602 (2013).

[53] P. M. Alsing, D. McMahon and G. Milburn, "Teleportation in a non-inertial frame", *Journal of Optics B: Quantum and Semiclassical Optics* **6** (8), S834 (2004).

[54] D. Hosler, "Relativistic quantum communication", *arXiv preprint arXiv:1306.4853* (2013).

[55] M. Cliche and A. Kempf, "Relativistic quantum channel of communication through field quanta", *Physical Review A* **81**, 012330 (2010).

[56] T. G. Downes, T. C. Ralph and N. Walk, "Quantum communication with an accelerated partner", *Physical Review A* **87**, 012327 (2013).

[57] R. H. Jonsson, E. Martín-Martínez and A. Kempf, "Information transmission without energy exchange", *Physical Review Letters* **114**, 110505 (2015).

[58] N. Friis, M. Huber, I. Fuentes and D. E. Bruschi, "Quantum gates and multipartite entanglement resonances realized by nonuniform cavity motion", *Physical Review D* **86**, 105003 (2012).

[59] E. Martín-Martínez and C. Sutherland, "Quantum gates via relativistic remote control", *Physics Letters B* **739**, 74–82 (2014).

[60] T. C. Ralph and N. Walk, "Quantum key distribution without sending a quantum signal", *New Journal of Physics* **17** (6), 063008 (2015).

[61] G. Salton, R. B. Mann and N. C. Menicucci, "Acceleration-assisted entanglement harvesting and rangefinding", *New Journal of Physics* **17** (3), 035001 (2015).

[62] A. Pozas-Kerstjens and E. Martín-Martínez, "Harvesting correlations from the quantum vacuum", *Physical Review D* **92** (6), 064042 (2015).

[63] M. Ahmadi, D. E. Bruschi and I. Fuentes, "Quantum metrology for relativistic quantum fields", *Physical Review D* **89**, 065028 (2014).

[64] M. Ahmadi, D. E. Bruschi, C. Sabín, G. Adesso and I. Fuentes, "Relativistic quantum metrology: Exploiting relativity to improve quantum measurement technologies", *Scientific reports* **4**, 4996 (2014).

[65] Z. Tian, J. Wang, J. Jing and A. Dragan, "Entanglement enhanced thermometry in the detection of the Unruh effect", *Annals of Physics* **377**, 1 – 9 (2017), ISSN 0003-4916.

[66] E. G. Brown, W. Donnelly, A. Kempf, R. B. Mann, E. Martín-Martínez and N. C. Menicucci, "Quantum seismology", *New Journal of Physics* **16** (10), 105020 (2014).

[67] D. Kafri, J. M. Taylor and G. J. Milburn, "A classical channel model for gravitational decoherence", *New Journal of Physics* **16**, 065020 (2014).

[68] D. Kafri, G. J. Milburn and J. M. Taylor, "Bounds on quantum communication via Newtonian gravity", *New Journal of Physics* **17**, 015006 (2015).

[69] I. Pikovski, M. Zych, F. Costa and Č. Brukner, "Universal decoherence due to gravitational time dilation", *Nature Physics* **11** (8), 668–672 (2015).

[70] M. Zych, F. Costa, I. Pikovski, T. C. Ralph and Č. Brukner, "General relativistic effects in quantum interference of photons", *Classical and Quantum Gravity* **29** (22), 224010 (2012).

[71] I. Pikovski, M. Zych, F. Costa and Č. Brukner, "Time dilation in quantum systems and decoherence", *New Journal of Physics* **19** (2), 025011 (2017).

[72] M. Zych, *Quantum systems under gravitational time dilation*, Springer (2017).

[73] E. Castro-Ruiz, F. Giacomini and Č. Brukner, "Entanglement of quantum clocks through gravity", *Proceedings of the National Academy of Sciences* **114** (12) E2303-E2309 (2017).

[74] P. J. Orlando, R. B. Mann, K. Modi and F. A. Pollock, "A test of the equivalence principle (s) for quantum superpositions", *Classical and Quantum Gravity* **33** (19), 19LT01 (2016).

[75] T. Damour, "Theoretical aspects of the equivalence principle", *Classical and Quantum Gravity* **29** (18), 184001 (2012).

[76] M. Zych, F. Costa, I. Pikovski and Č. Brukner, "Quantum interferometric visibility as a witness of general relativistic proper time", *Nature communications* **2**, 505 (2011).

[77] W. G. Unruh, "Experimental black-hole evaporation?", *Physical Review Letters* **46** (21), 1351 (1981).

[78] P. Nation, M. Blencowe, A. Rimberg and E. Buks, "Analogue Hawking radiation in a dc-SQUID array transmission line", *Physical Review Letters* **103** (8), 087004 (2009).

[79] C. M. Wilson, G. Johansson, A. Pourkabirian, M. Simoen, J. R. Johansson, T. Duty, F. Nori and P. Delsing, "Observation of the dynamical Casimir effect in a superconducting circuit", *Nature* **479**, 376–379 (2011).

[80] J. R. Johansson, G. Johansson, C. M. Wilson and F. Nori, "Dynamical Casimir effect in a superconducting coplanar waveguide", *Physical Review Letters* **103**, 147003 (2009).

[81] N. Birrell and P. Davies, *Quantum fields in curved space*, Cambridge University Press (1984).

[82] R. B. Mann and V. M. Villalba, "Speeding up Entanglement Degradation", *Physical Review A* **80** (2), 022305 (2009).

[83] D. C. Ostapchuk, S.-Y. Lin, R. B. Mann and B. Hu, "Entanglement Dynamics between Inertial and Non-uniformly Accelerated Detectors", *Journal of High Energy Physics* **1207**, 072 (2012).

[84] W. G. Brenna, E. G. Brown, R. B. Mann and E. Martín-Martínez, "Universality and thermalization in the Unruh effect", *Physical Review D* **88**, 064031 (2013).

[85] B. Hu and P. R. Johnson, "Beyond Unruh effect: nonequilibrium quantum dynamics of moving charges", *arXiv preprint quant-ph/0012132* (2000).

[86] A. M. Tsvelik, *Quantum field theory in condensed matter physics*, Cambridge University Press (2007).

[87] B. D. Serot and J. D. Walecka, "Recent progress in quantum hadrodynamics", *International Journal of Modern Physics E* **6** (04), 515–631 (1997).

[88] M. E. Peskin and D. V. Schroeder, *An introduction to quantum field theory*, Westview Press (1995).

[89] S. Weinberg, *The quantum theory of fields*, volume 2, Cambridge University Press (1995).

[90] G. T. Moore, "Quantum theory of the electromagnetic field in a variable length one dimensional cavity", *J. Math. Phys.* **11**, 2679 (1970).

[91] M. H. Devoret and R. J. Schoelkopf, "Superconducting circuits for quantum information: an outlook", *Science* **339** (6124), 1169–1174 (2013).

[92] D. Vion, A. Aassime, A. Cottet, P. Joyez, H. Pothier, C. Urbina, D. Esteve and M. H. Devoret, "Manipulating the quantum state of an electrical circuit", *Science* **296** (5569), 886–889 (2002).

[93] M. H. Devoret and J. M. Martinis, "Implementing qubits with superconducting integrated circuits", in "Experimental Aspects of Quantum Computing", Springer, (163–203) (2005).

[94] M. H. Devoret *et al.*, "Quantum fluctuations in electrical circuits", *Les Houches, Session LXIII* **7** (8) (1995).

[95] L. N. Cooper, "Bound electron pairs in a degenerate fermi gas", *Physical Review* **104** (4), 1189 (1956).

[96] B. D. Josephson, "Possible new effects in superconductive tunnelling", *Physics letters* **1** (7), 251–253 (1962).

[97] A. Lupascu, "Nanoelectronics for quantum computing, course QIC880, University of Waterloo".

[98] V. Ambegaokar and A. Baratoff, "Tunneling between superconductors", *Physical Review Letters* **10** (11), 486 (1963).

[99] R. C. Jaklevic, J. Lambe, A. H. Silver and J. E. Mercereau, "Quantum interference effects in Josephson tunneling", *Physical Review Letters* **12**, 159–160 (1964).

[100] P. W. Anderson and J. M. Rowell, "Probable observation of the Josephson superconducting tunneling effect", *Physical Review Letters* **10**, 230–232 (1963).

[101] J. Clarke and A. I. Braginski, *The SQUID handbook: Applications of SQUIDs and SQUID systems*, John Wiley & Sons (2006).

[102] R. E. Collin, *Foundations for microwave engineering*, John Wiley & Sons (2007).

[103] C. P. Wen, "Coplanar waveguide: A surface strip transmission line suitable for nonreciprocal gyromagnetic device applications", *IEEE Transactions on Microwave Theory and Techniques* **17** (12), 1087–1090 (1969).

[104] P. Chen and T. Tajima, "Testing Unruh radiation with ultraintense lasers", *Physical Review Letters* **83**, 256–259 (1999).

[105] S. A. Fulling and P. C. W. Davies, "Radiation from a moving mirror in two dimensional space-time: Conformal anomaly", *Proc. R. Soc. London, Ser. A* **348**, 393 (1976).

[106] V. V. Dodonov, "Nonstationary Casimir effect and analytical solutions for quantum fields in cavities with moving boundaries", *Adv. Chem. Phys.* **119**, 309–394 (2001).

[107] P. Corona-Ugalde, J. Louko and R. B. Mann, "Private correspondance".

[108] V. V. Dodonov, "Current status of the dynamical Casimir effect", *Physica Scripta* **82** (3), 038105 (2010).

[109] J. Doukas and J. Louko, "Superconducting circuit boundary conditions beyond the dynamical Casimir effect", *Physical Review D* **91**, 044010 (2015).

[110] C. M. Will, *Theory and experiment in gravitational physics*, Cambridge University Press (1993).

[111] A. Aspect, P. Grangier and G. Roger, "Experimental test of local hidden-variable theories via Bell's theorem", *Physical Review Letters* **47**, 460–463 (1981).

[112] M. Giustina, A. Mech, S. Ramelow, B. Wittmann, J. Kofler, J. Beyer, A. Lita, B. Calkins, T. Gerrits, S. W. Nam, R. Ursin and A. Zeilinger, "Bell violation using entangled photons without the fair-sampling assumption", *Nature* **497**, 227–230 (2013).

[113] B. Hensen, H. Bernien, A. Dréau, A. Reiserer, N. Kalb, M. Blok, J. Ruitenberg, R. Vermeulen, R. Schouten, C. Abellán, W. Amaya, V. Pruneri, M. W. Mitchell, M. Markham, D. J. Twitchen, D. Elkouss, S. Wehner, T. H. Taminiau and R. Hanson, "Loophole-free Bell inequality violation using electron spins separated by 1.3 kilometres", *Nature* **526**, 682–686 (2015).

[114] M. Giustina, M. A. M. Versteegh, S. Wengerowsky, J. Handsteiner, A. Hochrainer, K. Phelan, F. Steinlechner, J. Kofler, J.-A. Larsson, C. Abellán, W. Amaya, V. Pruneri, M. W. Mitchell, J. Beyer, T. Gerrits, A. E. Lita, L. K. Shalm, S. W. Nam, T. Scheidl, R. Ursin, B. Wittmann and A. Zeilinger, "Significant-loophole-free test of Bell's theorem with entangled photons", *Physical Review Letters* **115**, 250401 (2015).

[115] L. K. Shalm, E. Meyer-Scott, B. G. Christensen, P. Bierhorst, M. A. Wayne, M. J. Stevens, T. Gerrits, S. Glancy, D. R. Hamel, M. S. Allman, K. J. Coakley, S. D. Dyer, C. Hodge, A. E. Lita, V. B. Verma, C. Lambrocco, E. Tortorici, A. L. Migdall, Y. Zhang, D. R. Kumor, W. H. Farr, F. Marsili, M. D. Shaw, J. A. Stern, C. Abellán, W. Amaya, V. Pruneri, T. Jennewein, M. W. Mitchell, P. G. Kwiat, J. C. Bienfang, R. P. Mirin, E. Knill and S. W. Nam, "Strong loophole-free test of local realism", *Physical Review Letters* **115**, 250402 (2015).

[116] G. Kirchmair, F. Zähringer, R. Gerritsma, M. Kleinmann, O. Gühne, A. Cabello, R. Blatt and C. F. Roos, "State-independent experimental test of quantum contextuality", *Nature* **460**, 494–497 (2009).

[117] R. Lapkiewicz, P. Li, C. Schaeff, N. K. Langford, S. Ramelow, M. Wieśniak and A. Zeilinger, "Experimental non-classicality of an indivisible quantum system", *Nature* **474**, 490–493 (2011).

[118] X.-M. Hu, J.-S. Chen, B.-H. Liu, Y. Guo, Y.-F. Huang, Z.-Q. Zhou, Y.-J. Han, C.-F. Li and G.-C. Guo, "Experimental test of compatibility-loophole-free contextuality with spatially separated entangled qutrits", *Physical Review Letters* **117**, 170403 (2016).

[119] D. N. Page and C. D. Geilker, "Indirect evidence for quantum gravity", *Physical Review Letters* **47**, 979–982 (1981).

[120] C. Kiefer, *Springer Handbook of Spacetime*, Springer, chapter "Quantum Gravity", (709–722) (2014).

[121] F. Karolyhazy, "Gravitation and quantum mechanics of macroscopic objects", *Il Nuovo Cimento A* **42**, 390–402 (1966).

[122] C. Anastopoulos and B. Hu, "A master equation for gravitational decoherence: probing the textures of spacetime", *Classical and Quantum Gravity* **30**, 165007 (2013).

[123] A. Bassi, K. Lochan, S. Satin, T. P. Singh and H. Ulbricht, "Models of wave-function collapse, underlying theories, and experimental tests", *Reviews of Modern Physics* **85**, 471–527 (2013).

[124] D. Kafri and J. M. Taylor, "A noise inequality for classical forces", *arXiv preprint arXiv:1311.4558* (2013).

[125] J. Rau, "Relaxation phenomena in spin and harmonic oscillator systems", *Physical Review* **129**, 1880–1888 (1963).

[126] R. Alicki and K. Lendi, *Quantum Dynamical Semigroups and Applications*, volume 717 of *Lecture Notes in Physics*, Springer-Verlag, Berlin Heidelberg (1987).

[127] M. Ziman and V. Bužek, "All (qubit) decoherences: Complete characterization and physical implementation", *Physical Review A* **72**, 022110 (2005).

[128] M. Ziman, P. Štelmachovič and V. Bužek, "Description of quantum dynamics of open systems based on collision-like models", *Open Syst. Inf. Dyn.* **12** (1), 81–91 (2005), ISSN 1573-1324.

[129] D. Layden, E. Martín-Martínez and A. Kempf, "Universal scheme for indirect quantum control", *Physical Review A* **93** (4), 040301 (2016).

[130] D. Layden, E. Martín-Martínez and A. Kempf, "Perfect Zeno-like effect through imperfect measurements at a finite frequency", *Physical Review A* **91** (2), 022106 (2015).

[131] H.-P. Breuer and F. Petruccione, *The theory of open quantum systems*, Oxford University Press on Demand (2002).

[132] A. Rivas and S. F. Huelga, *Open Quantum Systems*, Springer (2012).

[133] A. Isar, A. Sandulescu, H. Scutaru, E. Stefanescu and W. Scheid, "Open quantum systems", *International Journal of Modern Physics E* **3** (02), 635–714 (1994).

[134] L. Viola, E. Knill and S. Lloyd, "Dynamical decoupling of open quantum systems", *Physical Review Letters* **82** (12), 2417 (1999).

[135] L. Viola, S. Lloyd and E. Knill, "Universal control of decoupled quantum systems", *Physical Review Letters* **83**, 4888–4891 (1999).

[136] J. Von Neumann, *Mathematical foundations of quantum mechanics*, 2, Princeton University Press (1955).

[137] K. Kraus, *States, Effects and Operations: Fundamental Notions of Quantum Theory*, Lecture Notes in Physics (190), Spring-Verlag, Berlin (1983).

[138] H. M. Wiseman and G. J. Milburn, *Quantum measurement and control*, Cambridge University Press (2009).

[139] Y. Aharonov, D. Z. Albert and L. Vaidman, "How the result of a measurement of a component of the spin of a spin-1/2 particle can turn out to be 100", *Physical Review Letters* **60** (14), 1351 (1988).

[140] C. M. Caves and G. J. Milburn, "Quantum-mechanical model for continuous position measurements", *Physical Review A* **36**, 5543–5555 (1987).

[141] S. Lloyd, "Coherent quantum feedback", *Physical Review A* **62**, 022108 (2000).

[142] J. Zhang, Y.-x. Liu, R.-B. Wu, K. Jacobs and F. Nori, "Quantum feedback: theory, experiments, and applications", *arXiv preprint arXiv:1407.8536* (2014).

[143] K. Jacobs, *Quantum measurement theory and its applications*, Cambridge University Press (2014).

[144] T. Quinn, C. Speake, H. Parks and R. Davis, "The BIMP measurements of the newtonian constant of gravitation, g", *Phil. Trans. R. Soc. A* **372** (2026), 20140032 (2014).

[145] T. Quinn, H. Parks, C. Speake and R. Davis, "Improved determination of g using two methods", *Physical Review Letters* **111**, 101102 (2013).

[146] D. T. Alves, C. Farina and P. A. M. Neto, "Dynamical Casimir effect with Dirichlet and Neumann boundary conditions", *Journal of Physics A: Mathematical and General* **36** (44), 11333 (2003).

[147] D. T. Alves, E. R. Granhen and M. G. Lima, "Quantum radiation force on a moving mirror with Dirichlet and Neumann boundary conditions for a vacuum, finite temperature, and a coherent state", *Physical Review Letters* **77**, 125001 (2008).

[148] N. Friis, A. R. Lee, K. Truong, C. Sabín, E. Solano, G. Johansson and I. Fuentes, "Relativistic quantum teleportation with superconducting circuits", *Physical Review Letters* **110**, 113602 (2013).

[149] J. Lindkvist, C. Sabín, I. Fuentes, A. Dragan, I.-M. Svensson, P. Delsing and G. Johansson, "Twin paradox with macroscopic clocks in superconducting circuits", *Physical Review A* **90** (5), 052113 (2014).

[150] D. E. Bruschi, A. Dragan, A. R. Lee, I. Fuentes and J. Louko, "Relativistic motion generates quantum gates and entanglement resonances", *Physical Review Letters* **111**, 090504 (2013).

[151] F. A. Pollock, C. Rodríguez-Rosario, T. Frauenheim, M. Paternostro and K. Modi, "Complete framework for efficient characterisation of non-Markovian processes", *arXiv preprint arXiv:1512.00589* (2015).

[152] H.-P. Breuer, E.-M. Laine, J. Piilo and B. Physical Review DVacchini, "*Colloquium* : Non-Markovian dynamics in open quantum systems", *Reviews of Modern Physics* **88**, 021002 (2016).

[153] F. Ciccarello, G. M. Palma and V. Giovannetti, "Collision-model-based approach to non-Markovian quantum dynamics", *Physical Review A* **87**, 040103 (2013).

[154] T. Rybár, M. Ziman, P. Štelmachovič and V. Bužek, "Simulation of indivisible qubit channels in collision models", *J. Phys. B: At. Mol. Opt. Phys.* **45** (15), 154006 (2012).

[155] K. Modi, "Operational approach to open dynamics and quantifying initial correlations", *Sci. Rep.* **2**, 581 (2012).

[156] G. Rosi, F. Sorrentino, L. Cacciapuoti, M. Prevedelli and G. Tino, "Precision measurement of the Newtonian gravitational constant using cold atoms", *Nature* **510**, 518–521 (2014).

[157] G. Rosi, L. Cacciapuoti, F. Sorrentino, M. Menchetti, M. Prevedelli and G. M. Tino, "Measurement of the gravity-field curvature by atom interferometry", *Physical Review Letters* **114**, 013001 (2015).

[158] P. Asenbaum, C. Overstreet, T. Kovachy, D. D. Brown, J. M. Hogan and M. A. Kasevich, "Phase shift in atom interferometry due to spacetime curvature", *Bulletin of the American Physical Society* (2017).

[159] N. Altamirano, P. Corona-Ugalde, K. E. Khosla, G. J. Milburn and R. B. Mann, "Emergent dark energy via decoherence in quantum interactions", *Classical and Quantum Gravity* **34** (11), 115007 (2017).

[160] D. Grimmer, D. Layden, R. Mann and E. Martín-Martínez, "Open Dynamics under Rapid Repeated Interaction", *Physical Review A* **94**, 032126 (2016).

[161] M. B. Plenio and S. F. Huelga, "Dephasing-assisted transport: quantum networks and biomolecules", *New Journal of Physics* **10** (11), 113019 (2008).

[162] P. Rebentrost, M. Mohseni, I. Kassal, S. Lloyd and A. Aspuru-Guzik, "Environment-assisted quantum transport", *New Journal of Physics* **11** (3), 033003 (2009).

[163] F. Caruso, A. W. Chin, A. Datta, S. F. Huelga and M. B. Plenio, "Highly efficient energy excitation transfer in light-harvesting complexes: The fundamental role of noise-assisted transport", *The Journal of Chemical Physics* **131** (10), 09B612 (2009).

Appendices

Appendix A

Magnus expansion and higher order corrections

In this Appendix we discuss the condition on the terms in the total Hamiltonian and the switching function $g(t)$ under which Equation (5.27) holds. To do so, we make use of the Magnus expansion, an elegant method introduced by Wilhelm Magnus that gives an exponential representation of the solution of a first order homogeneous linear ordinary differential equation, as presented below.

A.0.1 Magnus expansion

Magnus proposal was to write the evolution operator in Equation (5.23) as an exponential

$$\hat{U}(\tau) = \exp(\Omega(\tau)) = 1 + \sum_{k=1}^{\infty} \frac{1}{k!} \Omega^k(\tau)\,, \tag{A.1}$$

with $\Omega(\tau)$ as a series expansion

$$\Omega(\tau) = \sum_{m=1}^{\infty} \left(-\frac{i}{\hbar} \right)^m \Omega_m(\tau)\,, \tag{A.2}$$

This last expression is the so called Magnus expansion. The first three elements of the series are

$$
\begin{aligned}
\Omega_1 &= \int_0^\tau \mathcal{H}_{sm_r}(t_1)dt_1\,, \\
\Omega_2 &= \frac{1}{2}\int_0^\tau dt_1 \int_0^{t_1} dt_2[\mathcal{H}_{sm_r}(t_1), \mathcal{H}_{sm_r}(t_2)]\,, \\
\Omega_3 &= \frac{1}{6}\int_0^\tau dt_1 \int_0^{t_1} dt_2 \int_0^{t_2} dt_3([\mathcal{H}_{sm_r}(t_1), [\mathcal{H}_{sm_r}(t_2), \mathcal{H}_{sm_r}(t_3)]] \\
&\qquad\qquad +[\mathcal{H}_{sm_r}(t_3), [\mathcal{H}_{sm_r}(t_2), \mathcal{H}_{sm_r}(t_1)]])
\end{aligned}
\tag{A.3}
$$

Note that Ω_k is of order τ^k. Substituting Equation (A.2) into Equation (A.1) gives, including only up to second order terms in τ

$$
\hat{U}(\tau) = 1 - \frac{i}{\hbar}\Omega_1 - \frac{1}{\hbar^2}\Omega_2 - \frac{1}{2!\hbar^2}\Omega_1^2\,. \tag{A.4}
$$

If we now define

$$
\tilde{\Omega}_1 = \frac{1}{\tau}\Omega_1\,, \qquad \tilde{\Omega}_2 = \frac{1}{\tau^2}\Omega_2\,, \tag{A.5}
$$

the evolution operator can be written as

$$
\hat{U}(\tau) = 1 - \frac{i\tau}{\hbar}\tilde{\Omega}_1 - \frac{\tau^2}{\hbar^2}\tilde{\Omega}_2 - \frac{\tau^2}{2!\hbar^2}\tilde{\Omega}_1^2 + \mathcal{O}(\tau^3)\,. \tag{A.6}
$$

We use Equation (5.26) to write an explicit form of the operator $\tilde{\Omega}_1$ as

$$
\tilde{\Omega}_1 = \frac{1}{\tau}\int_0^\tau \mathcal{H}_{sm_r}(t)dt = \hat{\mathcal{H}}_0 + \bar{g}\hat{\mathcal{H}}_I = \hat{\mathcal{H}}\,, \tag{A.7}
$$

where $\hat{\mathcal{H}}$ is the Hamiltonian in Equation (5.28).

Equations (5.27) and (5.28) are equivalent to an expansion of Equation (A.6) in powers of τ that neglects terms $\tilde{\Omega}_k$ relative to the terms $\tilde{\Omega}_1^k$.

The terms $\tilde{\Omega}_k$ will contribute if the Hamiltonian does not commute with itself at different times or for specific forms of the switching function. For example, the term $\tilde{\Omega}_2$ is given by

$$
\begin{aligned}
\tilde{\Omega}_2 &\propto \frac{1}{2}\int_0^\tau dt_1 \int_0^{t_1} dt_2[\mathcal{H}_{sm_r}(t_1), \mathcal{H}_{sm_r}(t_2)]\,, &\text{(A.8)}\\
&= [\hat{\mathcal{H}}_0, \hat{\mathcal{H}}_I]\int_0^\tau dt_1 \int_0^{t_1} dt_2[g(t_2) - g(t_1)] &\text{(A.9)}
\end{aligned}
$$

which vanishes if the free Hamiltonian and the interaction Hamiltonian commute. It will also vanish if the integrals of the switching functions are zero (if $g(t) = g(\tau - t)$ in one cycle, at this order) which is the case in all the cases considered in this work, where the interaction strength is either constant or a highly peaked Gaussian symmetric in the duration of the cycle.

A.0.2 Higher order corrections

In our work, we are considering scenarios where the parameter $\bar{g}$ and the preparation of the ancillae can depend on τ. Therefore, we need to examine whether higher order terms in the expansion of the evolution superoperator (5.28) can give contributions of order τ to the master equation (5.30).

The term of order τ^k in the series in Equation (5.28) is

$$\frac{1}{k!}\left(-\frac{i\tau}{\hbar}\right)^k \langle[\hat{\mathcal{H}}, [\hat{\mathcal{H}}, [..., [\hat{\mathcal{H}}, \hat{\rho}_s]]]]\rangle_{\mathcal{M}} \tag{A.10}$$

It contains terms with up to k commutators of $\hat{S}$ and $\hat{S}_0$ with ρ_s. The power of $\bar{g}$ in each term is given by the number of $\hat{S}$ operators in the commutator. Consequently, no terms with only $\hat{S}_0$ operators will contribute beyond the lowest order $k = 1$.

For example, let us consider potentially relevant terms of order τ^3

$$\left(-\frac{i\tau}{\hbar}\right)^3 \bar{g}^3 \langle[\hat{H}_I, [\hat{H}_I, [\hat{H}_I, \hat{\rho}]]]\rangle = \left(-\frac{i\tau}{\hbar}\right)^3 \bar{g}^3 \langle\hat{M}^3\rangle [\hat{S}, [\hat{S}, [\hat{S}, \hat{\rho}_s]]]\,, \tag{A.11}$$

$$\left(-\frac{i\tau}{\hbar}\right)^3 \bar{g}^2 \langle[\hat{H}_I, [\hat{H}_I, [\hat{M}_0, \hat{\rho}]]]\rangle = \left(-\frac{i\tau}{\hbar}\right)^3 \bar{g}^2 \langle[\hat{M}^2, \hat{M}_0]\rangle [\hat{S}, [\hat{S}, \hat{\rho}_s]]\,, \tag{A.12}$$

$$\left(-\frac{i\tau}{\hbar}\right)^3 \bar{g} \langle[\hat{S}_0, [\hat{H}_I, [\hat{M}_0, \hat{\rho}]]]\rangle = \left(-\frac{i\tau}{\hbar}\right)^3 \bar{g} \langle[\hat{M}, \hat{M}_0]\rangle [\hat{S}_0, [\hat{S}, \hat{\rho}_s]]\,, \tag{A.13}$$

$$\left(-\frac{i\tau}{\hbar}\right)^3 \bar{g} \langle[\hat{H}_I, [\hat{M}_0, [\hat{M}_0, \hat{\rho}]]]\rangle = \left(-\frac{i\tau}{\hbar}\right)^3 \bar{g} \langle[\hat{M}_0, [\hat{M}_0, \hat{M}]]\rangle [\hat{S}, \hat{\rho}_s]\,, \tag{A.14}$$

Equation (5.36) guarantees that terms of the form (A.13) will not contribute. Also, terms with k commutators as in Equation (A.11) will be of order

$$\tau^k \bar{g}^m \langle\hat{M}^m\rangle\,, \tag{A.15}$$

where $0 \leq m \leq k$ and m is the number of $\hat{S}$ operators in the commutator. If the condition in Equation (5.32) is met, the terms $\tau^k \bar{g}^k \langle \hat{M}^k \rangle$ vanish in the considered limit. Terms as in Equation (A.14) for an arbitrary order k are

$$\bar{g}\tau^k \langle [\hat{M}_0, [\hat{M}_0, ...[\hat{M}_0, \hat{M}]]] \rangle [\hat{S}, \hat{\rho}_s] \,, \tag{A.16}$$

which have $(k-1)$ commutators between $\hat{M}_0$ and $\hat{M}$. These terms vanish in the strong coupling limit ($\lim_{\tau \to 0} \tau \bar{g} = 1$) but could survive for finite $\bar{g}$, for example, if $[\hat{M}_0, \hat{M}] = \lambda \hat{M}$. We shall not consider these cases in the present work.

Finally, let us note that in the gravitational interactions scenario presented in this work, expressions like the ones in Equations (A.12)-(A.14) and in particular all expressions in Equation (A.16) for $k \geq 2$ vanish.